

Supernova Nucleosynthesis in Population III 13 – 50 M_{\odot} Stars and Abundance Patterns of Extremely Metal-Poor Stars

Nozomu Tominaga¹, Hideyuki Umeda¹, and Ken'ichi Nomoto^{1,2}

ABSTRACT

We perform hydrodynamical and nucleosynthesis calculations of core-collapse supernovae (SNe) and hypernovae (HNe) of Population (Pop) III stars. We provide new yields for the main-sequence mass of $M_{\text{MS}} = 13 - 50 M_{\odot}$ and the explosion energy of $E = 1 - 40 \times 10^{51}$ ergs to apply for chemical evolution studies. Our HN yields based on the mixing-fallback model of explosions reproduce the observed abundance patterns of extremely metal-poor (EMP) stars ($-4 < [\text{Fe}/\text{H}] < -3$), while those of very metal-poor (VMP) stars ($-3 < [\text{Fe}/\text{H}] < -2$) are reproduced by the normal SN yields integrated over the Salpeter initial mass function. Moreover, the observed trends of abundance ratios $[\text{X}/\text{Fe}]$ against $[\text{Fe}/\text{H}]$ with small dispersions for the EMP stars can be reproduced as a sequence resulting from the various combination of M_{MS} and E . This is because we adopt the empirical relation that a larger amount of Fe is ejected by more massive HNe. Our results imply that the observed trends with small dispersions do not necessarily mean the rapid homogeneous mixing in the early galactic halo at $[\text{Fe}/\text{H}] < -3$, but can be reproduced by the “inhomogeneous” chemical evolution model. In addition, we examine how the modifications of the distributions of the electron mole fraction Y_e and the density in the presupernova models improve the agreement with observations. In this connection, we discuss possible contributions of nucleosynthesis in the neutrino-driven wind and the accretion disk.

Subject headings: Galaxy: halo — nuclear reactions, nucleosynthesis, abundances — stars: abundances — stars: Population III — supernovae: general

Accepted for publication in
the *Astrophysical Journal* (10 May 2007, v660n2 issue).

1. INTRODUCTION

The first metal enrichment in the universe was made by the supernova (SN) explosions of population (Pop) III stars. Despite the importance of Pop III stars in the evolution of the early universe, their properties are still uncovered. The main issues is the typical masses of Pop III stars. Some studies have suggested that the initial mass func-

tion (IMF) differs from the present day IMF (e.g., top-heavy IMF; Nakamura & Umemura 1999; Bromm & Larson 2004) and that a large number of stars might be so massive as to explode as pair-instability SNe (e.g., Wasserburg & Qian 2000). On the other hand, Tumlinson (2006) suggested an IMF that is peaked in the range of massive stars that exploded as core-collapse SNe.

In the early universe, the enrichment by a single SN can dominate the preexisting metal contents (e.g., Audouze & Silk 1995). The Pop III SN shock compresses the SN ejecta consisting of heavy elements, e.g., O, Mg, Si, and Fe, and the circumstellar materials consisting of H and He, and thus the abundance pattern of the enriched

¹Department of Astronomy, School of Science, University of Tokyo, Bunkyo-ku, Tokyo 113-0033, Japan; tominaga@astron.s.u-tokyo.ac.jp, umeda@astron.s.u-tokyo.ac.jp, nomoto@astron.s.u-tokyo.ac.jp

²Research Center for the Early Universe, School of Science, University of Tokyo, Bunkyo-ku, Tokyo 113-0033, Japan

gas may reflect nucleosynthesis in the SN. The SN compression will initiate a SN-induced star formation (e.g., Cioffi et al. 1988; Ryan et al. 1996; Shigeyama & Tsujimoto 1998) and the second-generation stars will be formed from the enriched gas. Among the second generation stars, low mass ($\sim 1M_{\odot}$) stars have long life-times and might be observed as extremely metal-poor (EMP) stars with $[\text{Fe}/\text{H}] < -3$ (Beers & Christlieb 2005). (Here $[\text{A}/\text{B}] = \log_{10}(N_{\text{A}}/N_{\text{B}}) - \log_{10}(N_{\text{A}}/N_{\text{B}})_{\odot}$, where the subscript \odot refers to the solar value and N_{A} and N_{B} are the abundances of elements A and B, respectively.) Therefore the EMP stars should conserve the nucleosynthetic results of the Pop III SN and can constrain the yields of the SN.

The elements ejected by various SNe are gradually mixed and the abundance patterns of the Galaxy becomes homogeneous with time. The abundance patterns of the newly formed stars reflect averaged nucleosynthesis over various SNe. It is important to know when the transition from inhomogeneous to homogeneous mixing occurs. The timing of this transition can be informed from chemical evolution calculations with hierarchical models; Argast et al. (2000) has suggested that a halo ISM is unmixed and inhomogeneous at $[\text{Fe}/\text{H}] < -3.0$, intermediate between unmixed and well mixed at $-3.0 < [\text{Fe}/\text{H}] < -2.0$, and well mixed at $[\text{Fe}/\text{H}] > -2.0$; Tumlinson (2006) has suggested that the mean number of reflected SNe is 10 at $[\text{Fe}/\text{H}] \sim -2.8$.

The previous observations (e.g., McWilliam et al. 1995a,b; Ryan et al. 1996; McWilliam 1997) provide the abundance patterns of the EMP stars that show interesting trends of elemental abundance ratios $[\text{Cr}/\text{Fe}]$, $[\text{Mn}/\text{Fe}]$, $[\text{Co}/\text{Fe}]$, $[\text{Zn}/\text{Fe}]$ with decreasing $[\text{Fe}/\text{H}]$, although dispersions are rather large. These trends, except for the absolute values of some elements, can be explained by the differences of the progenitors' masses and the explosion energies assuming the SN-induced star formation (Nakamura et al. 1999; Umeda & Nomoto 2002a, 2005, hereafter UN02a, UN05).

Recent observations for $-4 \lesssim [\text{Fe}/\text{H}] \lesssim -2$ by Cayrel et al. (2004, hereafter CA04) confirmed these trends shown by the previous studies with much smaller dispersions (see, however Honda et al. 2004, hereafter HO04, for the difference in $[\text{Cr}/\text{Fe}]$ at $-3 \lesssim [\text{Fe}/\text{H}] \lesssim -2$), except for much flatter trends of $[\text{Mg}/\text{Fe}]$ and $[\text{Mn}/\text{Fe}]$ than

the previous studies. CA04 and François et al. (2004) suggested the following interpretation of the observed small dispersions: the elements have been already mixed homogeneously in the halo even below $[\text{Fe}/\text{H}] < -3$ and the trends are due to the difference of the lifetime of progenitors with different masses. Homogeneous mixing is required because previous SN yields that have been used [e.g., Woosley & Weaver (1995, hereafter WW95); Nomoto et al. 1997; UN02a; and Chieffi & Limongi (2002, hereafter CL02)] show a large scatter in $[\alpha/\text{Fe}]$ (where α represents α -elements, for example, O, Ne, Mg, Si, e.g., Argast et al. 2002).

However, this interpretation may not be consistent with the Galactic chemical evolution models that suggest inhomogeneous mixing in such early phases (e.g., Argast et al. 2000; Tumlinson 2006). Also, r -process nuclei observed in the EMP stars show too large scatters (McWilliam 1998; Burris et al. 2000; Norris et al. 2001; HO04) to be reproduced by the homogeneous mixing model (Ishimaru et al. 2004), unless there exist a major site of r -process synthesis other than SN explosions (see Argast et al. 2004, who concluded core-collapse SNe are more preferable sites of r -process elements than neutron-star mergers).

In the regime of inhomogeneous mixing, UN05 have succeeded to reproduce the observed trends of the ratios, $[\text{Cr}/\text{Fe}]$, $[\text{Mn}/\text{Fe}]$, $[\text{Co}/\text{Fe}]$, and $[\text{Zn}/\text{Fe}]$, as a result of chemical enrichment of various SN models including hyper-energetic explosions ($E_{51} = E/10^{51}\text{ergs} \geq 10$: hypernovae, hereafter HNe). In their approach, variation of E and the mixing-fallback process are important (UN02a; UN05). The mixing-fallback model can solve the disagreement between $[\alpha/\text{Fe}]$ and $[(\text{Fe-peak element})/\text{Fe}]$ (e.g., WW95; Nakamura et al. 1999; CL02; Limongi & Chieffi 2003).

Traditionally, core-collapse SNe were considered to explode with $E_{51} \sim 1$ as SN 1987A (Blinnikov et al. 2000), SN 1993J (Nomoto et al. 1993), and SN 1994I (Nomoto et al. 1994) before the discoveries of HNe SN 1997ef (Iwamoto et al. 2000; Mazzali et al. 2000) and SN 1998bw (Patat et al. 2001; Nakamura et al. 2001a). After these discoveries, the number of Pop I HNe has been increasing, and the association with gamma-ray bursts (GRBs) has been established as GRB 980425/SN 1998bw (Galama et al. 1998;

Iwamoto et al. 1998; Woosley et al. 1999; Nakamura et al. 2001a), GRB 030329/SN 2003dh (Stanek et al. 2003; Hjorth et al. 2003; Matheson et al. 2003; Mazzali et al. 2003; Lipkin et al. 2004; Deng et al. 2005), and GRB 031203/SN 2003lw (Thomsen et al. 2004; Gal-Yam et al. 2004; Cobb et al. 2004; Malesani et al. 2004; Mazzali et al. 2006a). Though it is an interesting issue how much fraction of the core-collapse SNe explode as HNe (e.g., Podsiadlowski et al. 2004), non-negligible number of HNe occurred at least at present days.

Nucleosynthesis in HNe is characterized by the large amount of ^{56}Ni production ($M(^{56}\text{Ni}) \gtrsim 0.1$, e.g., Nakamura et al. 2001a). Two sites of ^{56}Ni synthesis have been suggested: the shocked stellar core (e.g., Nakamura et al. 2001a; Maeda & Nomoto 2003) and the accretion disk surrounding the central black hole (e.g., MacFadyen & Woosley 1999). We investigate the former site because the light curve and spectra of SN 1998bw favor the ^{56}Ni synthesis in the shocked stellar core (Maeda et al. 2006a,b; Maeda & Tominaga 2007).

In this paper, we construct core-collapse SNe models of the Pop III $13 - 50 M_{\odot}$ stars for various explosion energies of $E = 1 - 40 \times 10^{51}$ ergs. By applying the mixing-fallback model to the HN models, we show that the yields of these Pop III SNe and HNe are in good agreements with the observed abundance patterns and trends with reasonably small dispersions (CA04; HO04). We do not consider pair-instability SNe because previous studies (UN02a; Umeda & Nomoto 2003, hereafter UN03; UN05) found that there has been no evidence of the pair-instability SN abundance patterns in the EMP stars, although they might have existed before our galaxy become metal-rich-enough to form low-mass stars (see also Ohkubo et al. 2006 for core-collapse very massive stars).

In § 2, we describe our progenitor and explosion models. In § 3, we show that the abundance patterns of the EMP stars are reproduced by HN models and that the abundance patterns of the VMP stars are reproduced by normal SN models or an IMF-integrated model. In § 4, we show that the trends with small dispersions can be reproduced by Pop III SN models with various progenitors' masses and explosion energies assuming a SN-induce star formation. The scatters in our models are almost consistent with the observed

ones. In § 5, we examine how the agreements of Sc/Fe, Ti/Fe, Mn/Fe, and Co/Fe are improved by modifying the distributions of the neutron-proton (n/p) ratio and the density in the presupernova models. In § 6, summary and discussion are given.

2. EXPLOSION MODELS

The calculation method and other assumptions are the same as described in Umeda et al. (2000, hereafter UNN00), UN02a, and UN05. The isotopes in the reaction network for explosive nuclear burning include 280 species up to ^{79}Br as in UN05. We calculate the evolutions of Pop III progenitors, whose main-sequence masses are $M_{\text{MS}} = 13, 15, 18, 20, 25, 30, 40, 50 M_{\odot}$, and their SN explosions as summarized in Table 1. The mass loss rate from stars with metallicity Z is assumed to be proportional to $Z^{0.5}$ (Kudritzki 2000), so that Pop III $Z = 0$ models experience no mass loss. SN hydrodynamical calculations include nuclear energy generation with the α -network. The yields are obtained by detailed nucleosynthesis calculations as a post-processing.

2.1. Energy Injection

There are various ways to simulate the explosion. For example, CL02 assumed an approximate analytic formula to describe the radiation-dominated shock, although their recent modeling applied full hydrodynamics (Limongi & Chieffi 2003). WW95 and Limongi & Chieffi (2003) injected energy as a piston. Their piston model could mimic the time delay until the deposited energy by neutrino reaches a critical value. However, since the explosion mechanism of core-collapse SNe have not been well uncovered, one still does not know what is the most realistic way to inject explosion energy. Further, the yields do not strongly depend on how to generate the shock (Aufderheide et al. 1991). Therefore, in our calculation, the explosion is initiated as a thermal bomb with an arbitrary explosion energy, i.e., we elevate temperatures of an inner most region of the progenitor.

2.2. Normal Core-Collapse Supernovae and Hypernovae

We determine the explosion energy with referring to the relation between the main-sequence

mass and the explosion energy ($M_{\text{MS}} - E$) as obtained from observations and models of SNe (Fig. 1a). This relation is obtained from Pop I SNe, but we assume that the same $M_{\text{MS}} - E$ relation holds for Pop III SNe because the Fe core masses are roughly the same between Pop I and Pop III stars (UNN00). According to the observed relation, the massive stars with $M_{\text{MS}} \geq 20M_{\odot}$ are assumed to explode as hypernovae (HNe), which are hyper-energetic explosions and expected to leave black holes behind (Nomoto et al. 2004a), and the explosion energies of the models for $M_{\text{MS}} = 20, 25, 30, 40, 50 M_{\odot}$ are $E_{51} = 10, 10, 20, 30, 40$, respectively. The stars smaller than $20 M_{\odot}$ are considered to explode as normal SNe with $E_{51} = 1$. The explosion energy of normal SN models ($E_{51} = 1$) is consistent with that of SN 1987A ($E_{51} = 1.1 \pm 0.3$, Blinnikov et al. 2000).

Figures 2a and 2b show the abundance distributions in the ejecta of the $25M_{\odot}$ normal SN ($E_{51} = 1$) and HN ($E_{51} = 10$) models, respectively. Nucleosynthesis in HNe with large explosion energies takes place under high entropies and show the following characteristics (Nakamura et al. 2001b; Nomoto et al. 2001, 2004b, 2006; UN02a; UN05).

(1) Both complete and incomplete Si-burning regions shift outward in mass compared with normal supernovae. As seen in Figures 2a and 2b, the mass in the complete Si-burning region becomes larger, while the incomplete Si-burning region does not change much. As a result, higher energy explosions produce larger $[(\text{Zn}, \text{Co}, \text{V})/\text{Fe}]$ and smaller $[(\text{Mn}, \text{Cr})/\text{Fe}]$.

(2) In the complete Si-burning region of hypernovae, elements produced by α -rich freezeout are enhanced because of high entropies. Hence, elements synthesized through the α -capture process, such as ^{44}Ti , ^{48}Cr , and ^{64}Ge are more abundant. These species decay into ^{44}Ca , ^{48}Ti , and ^{64}Zn , respectively.

(3) Oxygen burning takes place in more extended regions for the larger explosion energy. Then more O, C, Al are burned to produce a larger amount of burning products such as Si, S, and Ar. As a result, hypernova nucleosynthesis is characterized by large abundance ratios of $[(\text{Si}, \text{S})/\text{O}]$ (Umeda et al. 2002b).

2.3. Mass Cut

The mass cut is defined to be a boundary between the central remnant and the SN ejecta and thus corresponds to the mass of the compact star remnant. The SN yield is an integration over the ejecta outside the mass cut. In 1D spherically symmetric models, the mass cut can be determined hydrodynamically as a function of the explosion energy (WW95). However, such 1D hydrodynamical determinations may not be relevant because SN explosions are found to be aspherical (e.g., Kawabata et al. 2002; Leonard et al. 2002; Wang et al. 2002, 2003; Maeda et al. 2002, 2006a,b; Mazzali et al. 2005; Chugai et al. 2005).

We take into account approximately the aspherical effects with a mixing-fallback model (see Appendix for detail) parameterising the aspherical SN explosions with three parameters, i.e., the initial mass cut $M_{\text{cut}}(\text{ini})$, the outer boundary of the mixing region $M_{\text{mix}}(\text{out})$ and the ejection factor f . The initial mass of the central remnant is represented by $M_{\text{cut}}(\text{ini})$. During the explosion, an inversion of the abundance distribution and a fallback of the materials above $M_{\text{cut}}(\text{ini})$ onto the central remnant might occur in the aspherical explosions (e.g., Maeda & Nomoto 2003; Nagataki et al. 2006; Tominaga et al. 2007), in contrast to the spherical explosions. The inversion is represented by the mixing of the materials between $M_{\text{cut}}(\text{ini})$ and $M_{\text{mix}}(\text{out})$ and the fraction of materials ejected from the mixing region is parameterized by the ejection factor f . As a consequence, the final mass of the central remnant $M_{\text{cut}}(\text{fin})$ is derived with Equation (7) in Appendix.

The parameters of the mixing-fallback model should essentially be derived from the mechanisms of SN explosions, e.g., the rotation, the asphericity, and the way to inject energy from the central region. However, the explosion mechanisms of SNe have not been clarified. Thus the parameters are constrained from the observed Fe (^{56}Ni) mass or from the comparison between the yield and the observed abundance pattern.

For normal SN models, we determine the mass cuts to yield $M(^{56}\text{Ni}) = 0.07M_{\odot}$ because the ejected ^{56}Ni mass of the observed normal SNe are clustered around this value (Fig. 1b, e.g., SN 1987A, Shigeyama & Nomoto 1990;

SN 1993J, Shigeyama et al. 1994; SN 1994I, Nomoto et al. 1994). We also assume that the whole materials above the mass cut are ejected without the mixing-fallback process. This corresponds to the ejection factor $f = 1$ in the mixing-fallback model (see Appendix).

For HN models, we apply the mixing-fallback model and determine parameters to yield $[\text{O}/\text{Fe}] = 0.5$ (case A) for all HN models or $[\text{Mg}/\text{Fe}] = 0.2$ (case B) for massive HN models ($M_{\text{MS}} \geq 30M_{\odot}$) as described in Appendix. While case A is similar to UN05, case B is to reproduce $[\text{Mg}/\text{Fe}] \sim 0.2$ plateau for $[\text{Fe}/\text{H}] < -3.5$ in CA04. The plateau had not been observed by the previous studies. Since case B has larger amount of fallback, i.e., larger $M_{\text{mix(out)}}$ and smaller f than case A, both of small $[\text{Mg}/\text{Fe}]$ and $[\text{Fe}/\text{H}]$ is realized in case B. The applied mixing-fallback parameters are summarised in Tables 1, 9, and 15 and the final yields are summarised in Tables 3, 5, 11, 13, 17, and 19.

2.4. SN-induced star formation

We assume that $[\text{Fe}/\text{H}]$ of a star formed by the SN shock compression is determined by the ratio between the ejected Fe mass $M(\text{Fe})$ and the swept-up H mass $M(\text{H})$ (Cioffi et al. 1988; Ryan et al. 1996; Thornton et al. 1998; Shigeyama & Tsujimoto 1998). According to Thornton et al. (1998), the swept-up H mass is given as

$$M(\text{H}) = X(\text{H}) \cdot M_{\text{SW}} = 3.93 \times 10^4 E_{51}^{6/7} n^{-0.24} M_{\odot} \quad (1)$$

where $X(\text{H})$ is the mass fraction of H in the primordial gases, M_{SW} is the total amount of the swept-up materials, and n is the number density of the circumstellar medium. Here we adopt $X(\text{H}) = 0.752$ as obtained from *Wilkinson Microwave Anisotropy Probe* (Spergel et al. 2003) and standard big bang nucleosynthesis (Coc et al. 2004). $[\text{Fe}/\text{H}]$ of the star is approximated as

$$\begin{aligned} [\text{Fe}/\text{H}] &= \log_{10}(M(\text{Fe})/M(\text{H})) \\ &\quad - \log_{10}(X(\text{Fe})/X(\text{H}))_{\odot} \\ &\simeq \log_{10}\left(\frac{M(\text{Fe})/M_{\odot}}{E_{51}^{6/7}}\right) - C. \quad (2) \end{aligned}$$

Here $(X(\text{Fe})/X(\text{H}))_{\odot}$ is the solar abundance ratio in mass between Fe and H (Anders & Grevesse 1989) and C is assumed to be a constant value of

1.4, which corresponds to $n \sim 75 \text{ cm}^{-3}$. Resulting values of $[\text{Fe}/\text{H}]$ are summarised in Tables 1, 9, and 15. $[\text{Fe}/\text{H}]$ of stars formed from the ejecta of HNe and normal SNe can be consistent with the observed $[\text{Fe}/\text{H}]$ of the EMP and VMP stars, respectively.

3. COMPARISONS WITH INDIVIDUAL STARS

3.1. EMP stars

CA04 provided abundance patterns of 35 metal-poor stars with small error bars for $-4 \lesssim [\text{Fe}/\text{H}] \lesssim -2$. Each EMP star may be formed from the ejecta of a single Pop III SN, although some of them might be the second or later generation stars. The yields of SNe with the progenitors of $[\text{Fe}/\text{H}] < -3$ can be well-approximated by those of Pop III SNe since they are similar (WW95; UNN00). In this subsection, the theoretical yields are compared with the averaged abundance pattern of four EMP stars, CS 22189-009, CD-38:245, CS 22172-002 and CS 22885-096, which have low metallicities ($-4.2 < [\text{Fe}/\text{H}] < -3.5$) and normal $[\text{C}/\text{Fe}] \sim 0$. Stars with large $[\text{C}/\text{Fe}]$ ($\sim +1$), called C-rich EMP stars, are discussed in UN03, UN05, and Tominaga et al. 2007. The origin of some of those stars may be a faint SN, being different from those of $[\text{C}/\text{Fe}] \sim 0$ stars (see § 4.1). Also some of the C-rich EMP stars might be originated from the mass transfer from the C-rich companion in close binaries (e.g., Aoki et al. 2002; Beers & Christlieb 2005; Ryan et al. 2005; Cohen et al. 2006).

Comparisons between the HN yields and the abundance pattern of the EMP stars are made in Figures 3a-3e. In the mixing-fallback model, both $[(\text{Fe-peak elements})/\text{Fe}]$ and $[\alpha/\text{Fe}]$ give good agreements with the observations, except for some elements, e.g., K, Sc, Ti, Cr, Mn, and Co. Possible ways to improve these elements are discussed in § 5.

3.2. VMP Stars

CA04 also provided the abundance patterns of the VMP stars whose metallicities ($[\text{Fe}/\text{H}] \sim -2.5$) are higher than the EMP stars. The observed abundance pattern is represented by the averaged abundance pattern of five stars BD+17:3248, HD 2796, HD 186478, CS 22966-057 and CS 22896-154, which have relatively high

metallicities ($-2.7 < [\text{Fe}/\text{H}] < -2.0$). Since these metallicities correspond to those of normal SN models according to Equation (2) for the SN-induced star formation model, we first compare the observations with normal SN yields (Figs. 4abc). The mass cuts of normal SN models are determined so that the ejected Fe (^{56}Ni) mass is $M(\text{Fe}) = 0.07M_{\odot}$.

On the other hand, most VMP stars are considered to have the abundance pattern averaged over IMF and metallicity of the progenitors, thus we also compare with the IMF-integrated yield (Fig. 5). Since the yields of SNe with the progenitors of $[\text{Fe}/\text{H}] < -3$ are quite similar to those of Pop III SNe (WW95; UNN00), we use the Pop III yields for these stars as well. The IMF integration is performed from $10 M_{\odot}$ to $50 M_{\odot}$ with 8 models, 13, 15, 18, 20, 25, 30, 40, $50 M_{\odot}$ and the extrapolations. We make the power-law IMF integrations as follows:

$$\phi(M) = KM^{-(1+a)} \quad (3)$$

where $\phi(M)dM$ is the number of stars within the mass range of $[M, M + dM]$, K is a normalization constant, and a is an integration index (Salpeter IMF has $a = 1.35$). The integration is performed and normalized by the total amount of gases forming stars as follows:

$$X(A) = \frac{\int_{0.07M_{\odot}}^{50M_{\odot}} X_M(A)M_{\text{ej}}(M)\phi(M)dM}{\int_{0.07M_{\odot}}^{50M_{\odot}} M\phi(M)dM} \quad (4)$$

where $X(A)$ is an integrated mass fraction of an element, A , $X_M(A)$ is mass fraction of A in a model interpolated between the nearest models, and $M_{\text{ej}}(M)$ is an ejected mass interpolated between the nearest models or the nearest model and the edge of the IMF-integrated mass range. Here we assume $M \leq 10M_{\odot}$ and $M = 50M_{\odot}$ stars do not yield any materials as type II SNe or HNe, i.e., $M_{\text{ej}}(M \leq 10M_{\odot}) = M_{\text{ej}}(50M_{\odot}) = 0M_{\odot}$.

Comparing the integrated yield with the Salpeter's IMF with the abundance pattern of the VMP stars (Fig. 5), most elements show reasonable agreements, except for N, K, Sc, Ti, and Mn. The integrated yields are summarised in Table 7.

3.2.1. Nitrogen & Oxygen

Figures 4a-4c and 5 show that N is underproduced in our models. There are two possible ex-

planations (1) and (2) for this discrepancy:

(1) N was actually underproduced in the Pop III SN as in our models, but was enhanced as observed during the first dredge-up in the low-mass red-giant EMP stars (e.g., Weiss et al. 2004; Suda et al. 2004). Observationally, the EMP and VMP stars in CA04 are giants and some of them show evidences of the deep mixing, i.e., the dilution of Li and the low $^{12}\text{C}/^{13}\text{C}$ ratio (Spite et al. 2006). On the other hand, the EMP and VMP stars with no evidence of the deep mixing show relatively small $[\text{N}/\text{Fe}]$ (~ -1 , Spite et al. 2005). However, $[\text{N}/\text{Fe}]$ in our models are even smaller than the smallest $[\text{N}/\text{Fe}]$ observed in the EMP and VMP stars (Spite et al. 2005). Thus the following mechanism might be important.

(2) N was enhanced in massive progenitor stars before the SN explosion. N is mainly synthesized by the mixing between the He convective shell and the H-rich envelope (e.g., UNN00; IW05). The mixing can be enhanced by rotation (Langer 1992; Heger & Langer 2000; Maeder & Meynet 2000). Suppose that the Pop III SN progenitors were rotating faster than more metal-rich stars because of smaller mass loss, then $[\text{N}/\text{Fe}]$ was enhanced as observed in the EMP stars.

$[\text{O}/\text{Fe}]$ of the $18 M_{\odot}$ and the IMF-integrated model are in good agreement with the observations (Figs. 4c and 5), while $[\text{O}/\text{Fe}]$ of the 13 and $15 M_{\odot}$ models are lower than the observations (Figs. 4a and 4b). In the abundance determination of O, however, uncertain hydrodynamical (3D) effects are important (Nissen et al. 2002) and CA04 applied the 3D correction for dwarfs to the metal-deficient giants. If the observed values of $[\text{O}/\text{Fe}]$ in the figures are correct, this may indicate that the contribution of a single normal SN from a small-mass progenitor to the chemical enrichment in the VMP stars is small.

We assumed all massive stars with $M_{\text{MS}} \geq 20M_{\odot}$ explode as HNe. However, there is a suggestion that the fraction of HNe to whole SNe (ϵ_{HN}) is $\epsilon_{\text{HN}} \sim 0.5$ (Kobayashi et al. 2006). If $\epsilon_{\text{HN}} \sim 0.5$, $[(\text{C}, \text{N}, \text{O})/\text{Fe}]$ and $[\text{Zn}/\text{Fe}]$ are slightly larger and smaller, respectively, than the case with $\epsilon_{\text{HN}} \sim 1$, but these are still in good agreement with the observation (Fig. 12 in Nomoto et al. 2006). On the other hand, if the contribution of the faint SNe ($M_{\text{MS}} \geq 20M_{\odot}$) to reproduce the abundance patterns of the C-rich EMP stars is large enough (see

§ 4.1; UN03; UN05; Tominaga et al. 2007), $[(\text{C}, \text{N}, \text{O})/\text{Fe}]$ is enhanced. This is because the faint SNe produce large $[(\text{C}, \text{N}, \text{O})/\text{Fe}]$ due to a small amount of Fe ejection. The contribution of the faint SNe, however, might be small, since $[\text{Mg}/\text{Fe}]$ is close to the upper limit of the observations without the contribution of the faint SNe. In order to estimate the ratios of HNe and faint SNe relative to all core-collapse SNe, further investigations are necessary.

4. TRENDS WITH METALLICITY

In § 3.1 and 3.2, we show that the observed abundance patterns can be reasonably reproduced by the mixing-fallback model. CA04 showed not only the abundance patterns of individual stars but also the existence of certain trends of the abundance ratios with respect to $[\text{Fe}/\text{H}]$. In this section, we compare the observed trends with our models in Tables 1-5.

In Figure 6, the observed abundance ratios $[\text{X}/\text{Fe}]$ against $[\text{Fe}/\text{H}]$ are compared with yields of individual SN models in Table 1 and the IMF-integrated yield described in § 3.2. Here $[\text{Fe}/\text{H}]$ of individual SN models are determined by Equation (2), while $[\text{Fe}/\text{H}]$ of the IMF-integrated abundance ratios are assumed to be same as normal SN models ($[\text{Fe}/\text{H}] \sim -2.6$). We note that the observed abundance ratios of most elements are roughly constant for $-2.5 \lesssim [\text{Fe}/\text{H}] < -1$. This can be interpreted that the SN ejecta had been mixed homogeneously in the halo at $-2.5 \lesssim [\text{Fe}/\text{H}]$. This is consistent with the chemical evolution models in Ishimaru & Wanao (1999), Argast et al. (2000), Tumlinson (2006), Nomoto et al. (2006), and Kobayashi et al. (2006).

According to the SN-induced star formation model (Eq. 2), our models cluster around $[\text{Fe}/\text{H}] \sim -3.5$ and only a few model exists around $[\text{Fe}/\text{H}] \sim -3$, because we applied only one explosion energy for each mass. In reality, the explosion energies of HNe may depend, e.g., on the rotation of the progenitors, even if the progenitors' masses of HNe are similar. The progenitors of SNe 1997ef and 2003dh, for instance, have similar masses, but the explosion energies are 1×10^{52} ergs and 4×10^{52} ergs, respectively (Iwamoto et al. 2000; Mazzali et al. 2003; Deng et al. 2005). Variations

of the explosion energy for the same stellar mass lead to variations of $[\text{Fe}/\text{H}]$. In order to produce a model with $[\text{Fe}/\text{H}] \sim -3$, therefore, we add the $25M_{\odot}$ model with $E_{51} = 5$ (see Fig. 7 for its abundance pattern).

The trends of most elements can be well reproduced by our models, except for K, Sc, Ti, Cr, Mn, and Co. In the followings, we discuss the trend of each element in more detail.

4.1. Carbon

The ratio C/Fe in our models are clustered around $[\text{C}/\text{Fe}] \sim 0$, while the observed $[\text{C}/\text{Fe}]$ of the EMP stars are scattered (see Fig. 6). The large $[\text{C}/\text{Fe}]$ ($\gtrsim 0.5$) can be interpreted as originated from the faint SNe that are characterised by a small ejection factor f and the resultant large $[(\text{C}, \text{N}, \text{O})/\text{Fe}]$ (UN03; UN05). In fact, Figure 8 shows that the abundance pattern of the C-rich EMP stars (CS 29498-043: Aoki et al. 2004) can be reproduced by our $25 M_{\odot}$ faint SN model with a normal explosion energy $E_{51} = 1$ and small $f = 0.004$ (model 25F in Tables 1-5). In this faint SN model, N/Fe is too small but can be enhanced as described in § 3.2.1.

We should note that the large $[\text{Co}/\text{Fe}]$ of CS 29498-043 is difficult to be reproduced by the faint SN model of $E_{51} = 1$. The parent SN of CS 29498-043 might be a faint SN with high-entropy jets (UN05; Tominaga et al. 2007).

Alternative explanation is that the production of C in other sites is important, that is, C is produced not only from SNe but also from mass-losing Wolf-Rayet (WR) stars. Fast rotating stars may undergo strong mass-loss and enter the WR phase, even if their metallicities are considerably low (Meynet & Maeder 2005). Also, the C-enhancement can be realized by transferring mass from the C-rich binary companion (e.g., Aoki et al. 2002; Ryan et al. 2005; Cohen et al. 2006).

4.2. The Even-Z Elements: Mg, Si, Ca, and Ti

4.2.1. Magnesium, Silicon & Calcium

The ratio Mg/Fe in CA04 is less-scattered around $[\text{Mg}/\text{Fe}] \sim 0.2$ which is smaller than $[\text{Mg}/\text{Fe}] \sim 0.5$ obtained by HO04 and other previous studies. Case A models, whose ejection factor

f is set to produce $[O/Fe] = 0.5$, appear around $-3.5 < [Fe/H] < -2.6$ and $0.1 < [Mg/Fe] < 0.6$. These are larger by 0.1 dex than observed $[Mg/Fe]$ in CA04 but consistent with these in the previous studies. We also consider case B models to reproduce the $[Mg/Fe] \sim 0.2$ plateau in CA04 at $[Fe/H] < -3.5$, although the plateau had not been observed by the previous studies.

$[(Si, Ca)/Fe]$ in CA04 and HO04 are slightly less-scattered than in previous studies. $[(Si, Ca)/Fe]$ in our models are in good agreements with the observations and the widths of the scatter in our models are consistent with the observations.

The small scatters of $[(Mg, Si, Ca)/Fe]$ in our present model are different from previous yields (Nomoto & Hashimoto 1988; WW95; Thielemann et al. 1996). This difference stems from the following different assumption. The previous yields assumed the ejected Fe mass ($M(Fe) \sim 0.07M_{\odot}$) depends weakly on the progenitors' masses. Therefore $[\alpha/Fe]$ in massive star models depends mainly on the α -element abundances, which strongly depend on the stellar mass. This leads to the large scatters. In the present stars, the EMP stars with $[Fe/H] < -3$ are produced by HNe only ($M_{MS} \geq 20M_{\odot}$), and those HN models produce Fe much more than $\sim 0.07M_{\odot}$. Instead, we assume $[O/Fe] = 0.5$ or $[Mg/Fe] = 0.2$ for $M_{MS} \geq 20M_{\odot}$ models. Our approach suggests that the observed small scatter of $[\alpha/Fe]$ implies that larger amount of Fe is produced in more massive stars. This is consistent with the observations that typical HNe eject larger amount of Fe than normal SNe (Fig. 1b).

4.2.2. Titanium

$[Ti/Fe]$ in our models is smaller than the observations. There are no clear trend in $[Ti/Fe]$ in our models as in the observations and the scatter is similar to the observations. $[Ti/Fe]$ may be enhanced by nucleosynthesis in high-entropy environments as will be discussed in § 5 (a “low-density” modification, see also UN05) or in a jet-like explosion (Nagataki et al. 2003; Maeda & Nomoto 2003).

4.3. The Odd-Z Elements: Na, Al, K, and Sc

4.3.1. Sodium & Aluminum

The abundances of Na and Al in CA04 are different from previous studies. This is partly because CA04 took into account non-LTE (NLTE) effects ($\Delta X(Na) = -0.5$ dex and $\Delta X(Al) = +0.65$ dex).

The CA04 result shows a trend in $[Na/Fe]$ against $[Fe/H]$. In Figure 6, our results also show such a trend, although Na/Fe is slightly smaller than the observations in the HN models, especially in $M_{MS} = 40M_{\odot}$ models. Because all our models are Pop III models, the trend is not due to the metallicity effect but due to the combination of the progenitors' masses and the explosion energies. The trend stems from the fact that more massive stars produce smaller $X(Na)$ and that more energetic explosions burn more Na.

$[Al/Fe]$ is also smaller by 0.5 dex than in CA04, especially in the HN model. However our models are in good agreements with $[Al/Fe]$ in HO04. The difference in the observed $[Al/Fe]$ between CA04 and HO04 may be mainly because HO04 does not take into account NLTE effects. The larger $M_{mix(out)}$ in case B enhances Na/Fe but reduces Al/Fe . This is because Na and Al are mainly synthesized near the outer and the inner edges of the O-rich region, respectively. Only $[Al/Fe]$ of model 40B is in reasonable agreement with CA04 because the $40 M_{\odot}$ progenitor star produce large $X(Al)$.

Both Na and Al are mostly synthesized in C shell-burning, and the produced amount depends on the overshooting at the edge of the convective C-burning shell (IW05). In the present presupernova evolution models, no overshooting is included. If the NLTE correction of Al is correct, it might be needed to consider convective overshooting in the C-burning shell. This could enhance Na/Mg and Al/Mg , thus weakening the odd-even effect in the abundance patterns and leading to a better agreement with CA04.

4.3.2. Potassium & Scandium

$[K/Fe]$ and $[Sc/Fe]$ in our models are much smaller than in CA04 and HO04. Possible improvements are discussed in detail in § 5. K/Fe is slightly enhanced by the “low-density” modifica-

tion as described in § 5, but still not large enough. Iwamoto et al. (in preparation) suggests that the model with large Y_e (> 0.5) in the inner region can produce enough K.

Sc/Fe can be enhanced by the “low-density” modification (see § 5; UN05). Further enhancement can be realized if $Y_e > 0.5$. Recently, Pruet et al. (2004a, 2005) and Fröhlich et al. (2006b) calculated nucleosynthesis based on the core-collapse SN simulations with neutrino transport. In their models, neutrino absorption enhances Y_e near the mass cut of the ejecta. According to their results, Sc/Fe in the normal SN model is enhanced to $[\text{Sc}/\text{Fe}] \sim 0$ due to the large Y_e ($\gtrsim 0.5$) and high-entropy ($s/k_B \gtrsim 20$, where s denotes the entropy per nucleon and k_B is the Boltzmann constant).

4.4. The Iron-Peak Elements: Cr, Mn, Co, Ni, Zn

4.4.1. Chromium, Manganese, & Cobalt

[Cr/Fe] in our models is larger than CA04 but consistent with HO04. The difference between CA04 and HO04 stems from the use of the different Cr lines (Cr I: CA04 and Cr II: HO04) in obtaining [Cr/Fe]. It is still uncertain which line is better to use in estimating [Cr/Fe]. If Cr I gives reliable abundance, Cr in our models is overproduced, although the trend in our models is similar to the observations. Since Cr is mostly produced in the incomplete Si-burning region, the size of this region relative to the complete Si-burning region should be smaller than the present model in order to produce smaller Cr/Fe. We also need to examine the nuclear reaction rates related to the synthesis of ^{52}Fe that decays into ^{52}Cr .

[Mn/Fe] and [Co/Fe] in our models are smaller than the observations, although the trend of [Co/Fe] in our models is similar to the observations. The negligibly small dependence of [Mn/Fe] on [Fe/H] in CA04 is different from previous observations that [Mn/Fe] significantly decreases toward smaller [Fe/H] (McWilliam et al. 1995a,b). They can be improved by the n/p modification as discussed in § 5.1. Also, Mn can be efficiently enhanced by a neutrino process (see § 5.3; WW95; T. Yoshida et al., in preparation). Therefore the Mn/Fe ratio is important to constrain the physical processes during the explosion.

4.4.2. Nickel & Zinc

[Ni/Fe] and [Zn/Fe] in our models are in good agreement with the observations, although [Ni/Fe] is slightly smaller than the observation. Ni/Fe is higher if $M_{\text{cut}}(\text{ini})$ is smaller (i.e., the mass cut is deeper) because ^{58}Ni , a main isotope of stable Ni, is mainly synthesized in a deep region with $Y_e < 0.5$. However, a smaller $M_{\text{cut}}(\text{ini})$ tends to suppress Zn/Fe (see Appendix), thus requiring more energetic explosions to produce large enough Zn/Fe.

The good agreement of [Zn/Fe] with observations strongly supports the SN-induced star formation model and suggests that the EMP stars with smaller [Fe/H] are made from the ejecta of HNe with higher explosion energies and larger progenitor’s masses. This is because higher explosion energies lead to larger [Zn/Fe] and smaller [Fe/H].

Other possible production sites of Zn include the neutrino-driven wind from a proto-neutron star (e.g., Hoffman et al. 1996; Pruet et al. 2005; Fröhlich et al. 2006b; Wanajo 2006a,b) and the accretion disk of a black hole (e.g., Pruet et al. 2004a,b; Fröhlich et al. 2006a). Further studies are needed to see how large the contributions of these sites to the Zn production are. In order to reproduce the trend and small scatter of [Zn/Fe], there must be some “hidden” relations between the explosion energy and nucleosynthesis in the neutrino-driven wind or the accretion disk models.

If the VMP stars with [Fe/H] ~ -2.5 is made from normal SNe with $E_{51} = 1$, Zn is underproduced in our models. Nucleosynthesis studies with neutrino transport (Hoffman et al. 1996; Pruet et al. 2004a, 2005; Fröhlich et al. 2006b) suggested that Zn in the normal SN model is enhanced to [Zn/Fe] ~ 0 . However, the enhancement is not large enough to explain the large [Zn/Fe] ($\gtrsim 0.5$) in the EMP stars.

5. IMPROVED MODELS FOR Sc, Ti, Mn, & Co

In this section, we present the models based on the modified presupernova distributions of the “n/p ratio (i.e., Y_e)” and the “density”. We then discuss how these modifications improve Sc, Ti, Mn, and Co. The IMF-integrated yields, the parameters, and the yields of the individual SNe are

summarised in Tables 7-19.

5.1. Neutron-Proton Ratio

In the above discussion, we assume that Y_e in the presupernova model is kept almost constant during the explosion. However, recent studies (e.g., Rampp & Janka 2000; Liebendörfer et al. 2005; Fröhlich et al. 2006b; Buras et al. 2006a,b) have suggested that Y_e may be significantly varied by the neutrino process during explosion. Further, the region, where the neutrino absorption and Y_e variation occur, is Rayleigh-Taylor unstable because of neutrino heating, so that there exists a large uncertainty in Y_e and its distribution.

We apply the following Y_e profile that was found to produce reasonable results in UN05, i.e., $Y_e = 0.5001$ in the complete Si burning region and $Y_e = 0.4997$ in the incomplete Si burning region. The Y_e profile is modified by adjusting the isotope ratios of Si. According to the recent explosion calculations with the neutrino effect (e.g., Rampp & Janka 2000; Buras et al. 2006b), materials with large Y_e (~ 0.54) may be ejected. However, Y_e might be diluted by mixing, and our Y_e profile might mimic such dilution. The adopted high Y_e in the complete Si-burning region and low Y_e in the incomplete Si-burning region lead to large Co/Fe and Mn/Fe, respectively.

Figures 9a-9j show better agreements between the models and the observations. Here we applied the same $M_{\text{cut}}(\text{ini})$ as in the models without the Y_e modification. The IMF-integrated yield, the parameters, and the yields of the individual SNe are summarised in Tables 7-13. Since the variation of Y_e is considered to be due to the ν -process, the Y_e modification might be applied to any core-collapse SNe.

5.2. Low Density

In the “low-density” modification, the density of the presupernova progenitor is artificially reduced without changing the total mass. UN05 assumed that such a low density would be realized if the explosion is induced by multiple jets consisted of the primary weak jets and the main strong SNe jets. The primary weak jets expand the interior of the progenitor before the SN explosions driven by the main jets (as described in Appendix in UN05). Alternate explosion mechanism

that realizes “low-density” is a delayed explosion (e.g., Fryer et al. 2006, who investigated explosive nucleosynthesis induced by a black hole forming collapse comparing a direct collapse and a delayed collapse caused by fallback). The “low-density” is presumed to be realized in the jet-like or delayed explosions involving fallback, thus being applied only to the HN models but not to the normal SN models.

Other mechanism to realize “low-density” was suggested by CL02, i.e., the L model using “low” $^{12}\text{C}(\alpha, \gamma)^{16}\text{O}$ rate (Caughlan & Fowler 1988). They showed that the “low” $^{12}\text{C}(\alpha, \gamma)^{16}\text{O}$ rate leads the higher C abundance (i.e., larger C/O ratio) and more active C-shell burning. As a consequence, the average density in the complete and incomplete Si-burning region is lower than the “high” $^{12}\text{C}(\alpha, \gamma)^{16}\text{O}$ rate case (Caughlan et al. 1985). If this mechanism is valid, the “low-density” will be realized in whole SNe. However, the large C/O ratio leads to overproduce Ne and Na at the solar metallicity (Woosley & Weaver 1993; Nomoto et al. 1997; Imbriani et al. 2001).

Explosive nucleosynthesis in the model with the “low-density” modification takes place at higher entropy ($s/k_B \sim 30 - 40$) than in the model without modification ($s/k_B \sim 10 - 20$), thus enhancing the α -rich freeze-out compared with the standard model. As a result, the Sc/Fe and Ti/Fe ratios are particularly enhanced. Figure 10a shows that the Sc/Fe and Ti/Fe ratios in the EMP stars can be better reproduced by the model of $M_{\text{MS}} = 20M_{\odot}$ and $E_{51} = 10$ with the “low-density” modification, whose presupernova density is reduced by a factor of 2. Here we applied the Y_e modification and the same $M_{\text{cut}}(\text{ini})$ as in the models without the Y_e modification.

The other HN models with both the Y_e and “low-density” modifications are also in good agreement with the abundance pattern of the EMP stars (Figs. 10b-10g). Because the degree of “low-density” is likely to be different in each explosion, we assume the “low-density” factor so that each model reproduces [Sc/Fe] of the EMP stars as given in Table 15. The IMF-integrated yield, the parameters, and the yields of the individual SNe are summarised in Tables 7 and 15-19.

The good agreements suggest that the Y_e and “low-density” modifications might actually be realized in the SN explosions. In the present

study, we consider the global enhancement of entropy due to the jet-like or delayed explosion, but such high-entropy region is also realized locally in the neutrino-driven wind or the accretion disk. Neutrino-driven wind nucleosynthesis (Pruet et al. 2005) for $Y_e = 0.5245$ and $s/k_B = 26.9$ produces $[\text{Sc}/\text{Fe}]$ ($\sim +0.3$) being consistent with that of the EMP stars but smaller $[\text{Co}/\text{Fe}]$ and $[\text{Zn}/\text{Fe}]$ than those of the EMP stars; for $Y_e = 0.5$ and $s/k_B = 18.4$, smaller $[\text{Sc}/\text{Fe}]$ (~ -1) is produced than that of the EMP stars. Accretion disk nucleosynthesis ($s/k_B = 20$ and 40 , Pruet et al. 2004a) produces much larger $[\text{Sc}/\text{Fe}]$ ($\sim +1$) than that of the EMP stars and does not produce simultaneously $[\text{Co}/\text{Fe}] \sim 0.5$ and $[\text{Zn}/\text{Fe}] \sim 0.5$ as observed in the EMP stars.

The above models show that it seems difficult to reproduce the overall abundance pattern of the EMP stars only with nucleosynthesis in the neutrino-driven wind or the accretion disk. However, if some contributions from these sites can be added to our models, it could enhance Sc/Fe. In order to obtain $[\text{Sc}/\text{Fe}] \sim 0$, the SN ejecta should have $M(\text{Sc})/M(\text{Fe}) \sim (X(\text{Sc})/X(\text{Fe}))_{\odot} \sim 3 \times 10^{-5}$ (Anders & Grevesse 1989). When about $0.1M_{\odot}$ of Fe and little Sc are ejected as in our model of $M_{\text{MS}} = 25M_{\odot}$ and $E_{51} = 10$, $[\text{Sc}/\text{Fe}] \sim 0$ is obtained by the ejection of extra $M(\text{Sc}) \sim 3 \times 10^{-6}M_{\odot}$ from either the neutrino-driven wind or the accretion disk.

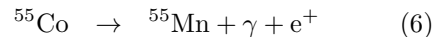
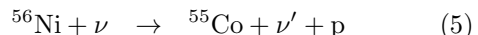
5.3. Trends

Figure 11 shows the trends resulting from the Y_e modification made for all models and the “low-density” modification applied only for HN models. Each comparison between the model and the observation is shown in Figures 9a-9c, and 10a-10g. While $[(\text{K}, \text{Cr})/\text{Fe}]$ still do not explain the observations well, the trends of $[(\text{Sc}, \text{Ti}, \text{Mn}, \text{Co})/\text{Fe}]$ are in much better agreement with the observations than the models without the modifications. Other elements also show good agreements and small scatters.

The Sc/Fe and Ti/Fe ratios in normal SN models are lower than the observations. This is partly because the “low-density” modification is not applied to normal SNe. To reproduce the observed high Sc/Fe and Ti/Fe ratios, there might be some mechanisms to realize the high entropy ($s/k_B \sim 30 - 40$) even for normal SNe. In this connec-

tion, it is interesting to note that the recent X-Ray Flash GRB 060218 was found to be associated with SN 2006aj (e.g., Pian et al. 2006). The properties of SN 2006aj are close to normal SNe; the progenitor’s main-sequence mass and the explosion energy were estimated to be $M_{\text{MS}} \sim 20M_{\odot}$ and $E_{51} \sim 2$ (Mazzali et al. 2006b). This suggests that the “low-density” modification could be realized in some normal SNe. Such explosions might contribute to enhance Sc/Fe and Ti/Fe.

$[\text{Cr}/\text{Fe}]$ and $[\text{Mn}/\text{Fe}]$ in our models are larger and smaller than CA04, respectively, while $[\text{Co}/\text{Fe}]$ is in good agreement with CA04. $[\text{Mn}/\text{Fe}]$ could also be enhanced by the following ν -process in the complete Si-burning region and the subsequent radioactive decay:



(WW95; T. Yoshida et al., in preparation).

6. SUMMARY & DISCUSSION

In this paper we performed the hydrodynamical and nucleosynthesis calculations of Pop III 13 – 50 M_{\odot} core-collapse SNe and provided the yields by adopting the mixing-fallback model. We show that our yields are consistent with the observed abundance patterns of the EMP and VMP stars (CA04; HO04). The trends of $[X/\text{Fe}]$ vs. $[\text{Fe}/\text{H}]$ with small scatters can be reproduced by our models as a sequence resulting from the combination of different progenitors’ masses (M_{MS}) and explosion energies (E). This is because we adopt the empirical relation that a larger amount of Fe is ejected by massive HNe ($M_{\text{MS}} \geq 20M_{\odot}$) than normal SNe. This indicates that the observed trends with small scatters do not necessarily mean the homogeneous mixing in the interstellar medium, but can be reproduced by the “inhomogeneous” chemical evolution model, in which the EMP stars are enriched by the individual SNe with different (M_{MS}, E).

In our model, yields of more massive HNe correspond to the EMP stars with smaller $[\text{Fe}/\text{H}]$ (< -3). We should stress that this is not because HNe were dominant among Pop III SNe, but because the second generation stars produced by Pop III core-collapse SNe with higher explosion energies tend to have smaller $[\text{Fe}/\text{H}]$ as $[\text{Fe}/\text{H}] \simeq$

$$\log_{10} \left(\frac{M(\text{Fe})}{M_{\odot}} / E_{51}^{6/7} \right) - C \text{ (Eq. 2)}.$$

Almost all stars in CA04 and HO04 can be reasonably well reproduced by core-collapse SNe yields, but none by the pure pair-instability SN yields (e.g., UN02a; Heger & Woosley 2002). In other words, the EMP stars in CA04 show no clear features of top-heavy IMF. Further, the VMP stars ($[\text{Fe}/\text{H}] \sim -2.5$) can be well-reproduced by integrating the yields of Pop III SNe over the Salpeter’s IMF. This also implies that the IMF of Pop III stars was not top-heavy, but approximately Salpeter’s. To constrain the IMF of Pop III stars, we need more complete set of the observed data as well as inhomogeneous chemical evolution models which properly take into account our model, especially the $M_{\text{MS}}\text{-}[\text{Fe}/\text{H}]$ relation (see, e.g., Argast et al. 2000, 2002; Tumlinson 2006).

We also investigate the yields of the models with the Y_e and “low-density” modifications suggested in UN05 and show that the yields are in better agreement with the observed abundance patterns than those without such modifications. The good agreements suggest that such modifications might be realized in the actual core-collapse SN explosions. We suggest that the Y_e and “low-density” modifications are actualized by the neutrino effects and the jet-like or delayed explosions, respectively.

The neutrino-driven wind and the accretion disk are other possible nucleosynthesis sites for Sc because they can actualize the Y_e ($\gtrsim 0.5$) and “low-density” modifications. However, nucleosynthesis in the neutrino-driven wind and the accretion disk might not be dominant sites of Fe synthesis because they can not reproduce the abundance ratios among the Fe-peak elements of the EMP stars. We thus suggest that the progenitor’s presupernova nucleosynthesis and explosive nucleosynthesis are predominant synthesis sites of most elements, while some elements (e.g., Sc, Ti, Mn, and Co) can be enhanced by the Y_e and “low-density” modifications.

We would like to thank C. Kobayashi for valuable discussion. The author N.T. is supported through the JSPS (Japan Society for the Promotion of Science) Research Fellowship for Young Scientists. This work has been supported in part by the Grant-in-Aid for Scientific Research

(17030005, 17033002, 18104003, 18540231) and the 21st Century COE Program (QUEST) from the JSPS and MEXT of Japan.

APPENDIX: MIXING-FALLBACK MODEL

The mixing-fallback model proposed by UN02a and UN03 can successfully reproduce the abundance patterns of the hyper metal-poor (HE0107–5240: Christlieb et al. 2002; UN03, HE1327–2326: Frebel et al. 2005; IW05) and EMP (UN02a; UN05) stars. The mixing-fallback model assumes the following situation: first, inner materials are mixed by some mixing process (e.g., Rayleigh-Taylor instabilities and/or aspherical explosions) during the shockwave propagations in the star (e.g., Hachisu et al. 1990; Kifonidis et al. 2003). Later, some fraction of materials in the mixing region undergoes fallback onto the central remnant by gravity (e.g., WW95; IW05), and the rests are ejected into interstellar space. The fallback mass depends on the explosion energy, the gravitational potential, and asphericity.

The mixing-fallback model can solve a problem associated with the ratios between the Fe-peak elements and Fe in the EMP stars, $[(\text{Fe-peak})/\text{Fe}]$. The large Zn/Fe ratio implies an energetic explosion as a HN and a deep mass cut, but these lead to eject too large amount of Fe to reproduce small $[\text{Fe}/\text{H}]$ and the large enough $[\alpha/\text{Fe}]$ ratio, if ones assume that the whole material above the mass cut are ejected. However, one can realize both the deep mass cut and the small amount of ejected Fe with the mixing-fallback model.

In the spherical models, IW05 found that the fallback takes place if the explosion energy is less than $E_{51} \sim 1$ for the $25 M_{\odot}$ star and obtained a relation between E_{51} and the final remnant mass, $M_{\text{cut}}(\text{fin})$, i.e., smaller E_{51} leads to a larger $M_{\text{cut}}(\text{fin})$. For example, $E_{51} = 0.74$ and 0.71 for the $25 M_{\odot}$ star lead to the final remnant mass $M_{\text{cut}}(\text{fin}) = 5.8M_{\odot}$ and $6.3M_{\odot}$, respectively. It is difficult for a spherical HN explosion to initiate a fallback, although for a larger star the fallback can occur even for a larger explosion energy because of a deeper gravitational potential. For instance, the fallback is found to occur for $E_{51} < 2$ in the $50 M_{\odot}$ star.

However, fallback can take place not only for relatively low energy explosions but for very energetic jet-like explosions (Maeda & Nomoto 2003; Tominaga et al. 2007). In fact, Tominaga et al. (2007) have simulated jet-induced explosions and showed that the resultant yields can reproduce the abundance patterns of the EMP stars as the mixing-fallback model. The mixing-fallback model mimics such aspherical explosions, although the spherical model tends to require larger explosion energies than the jet model to obtain similar yields (Maeda & Nomoto 2003; Tominaga et al. 2007).

In the mixing-fallback model, the physical process is explained by three parameters as follows:

- $M_{\text{cut}}(\text{ini})$: initial mass cut, which is corresponding to the inner boundary of the mixing region.
- $M_{\text{mix}}(\text{out})$: outer boundary of the mixing region.
- f : a fraction of matter ejected from the mixed region. It determines $[\alpha/\text{Fe}]$.

Figures 12ab illustrate these parameters for spherical and aspherical models. The final remnant mass, $M_{\text{cut}}(\text{fin})$, is determined by the above three parameters

$$M_{\text{cut}}(\text{fin}) = M_{\text{cut}}(\text{ini}) + (1 - f) \times (M_{\text{mix}}(\text{out}) - M_{\text{cut}}(\text{ini})). \quad (7)$$

In this paper, we determine these parameters as follows.

- $M_{\text{cut}}(\text{ini})$: the initial mass cut is adopted so that $[\text{Zn}/\text{Fe}]$ attains maximum, thus locates at the bottom of the $Y_e \simeq 0.5$ layer (Fig. 13) where is very close to the surface of Fe core of the progenitors. Figure 13 shows the abundance distribution of the $25 M_{\odot}$ star with $E_{51} = 10$ around the complete Si burning region. For Population III SNe, the dominant isotope of Zn is ^{64}Zn , which is the decay product of ^{64}Ge . ^{64}Zn is mostly produced in the complete Si burning region where $Y_e \simeq 0.5$ and the Zn/Fe ratio decreases for lower Y_e (see Fig. 4 in UN05). Therefore, as the mass cut decreases, $[\text{Zn}/\text{Fe}]$ in the ejecta first increases and then decreases. This choice of $M_{\text{cut}}(\text{ini})$ tends to give a smaller estimate of E_{51} to fit to the observed Zn/Fe, because Zn/Fe is larger for larger E_{51} .

- $M_{\text{mix}}(\text{out})$ and f : we study two cases as follows. Case B is an additional model for massive star models. The abundance distribution of the $30 M_{\odot}$, $E_{51} = 20$ model is shown in Figure 14 illustrating the mixing region in both cases.

Case “A” : We assume that the mixing occurs in the Si burning region and thus $M_{\text{mix}}(\text{out})$ is where $X(^{56}\text{Ni}) = 10^{-3}$. f is chosen to yield $[\text{O}/\text{Fe}] = 0.5$. For most cases, $f \sim 0.1$.

Case “B” : For the $M \geq 30M_{\odot}$ models, we consider another case. In this case, we assume that $M_{\text{mix}}(\text{out})$ is 2/3 of the O-rich layer, and determine f so that $[\text{Mg}/\text{Fe}] = 0.2$ to be consistent with the $[\text{Fe}/\text{H}] < -3.5$ stars in CA04.

In this paper, we consider two cases A and B for $M \geq 30M_{\odot}$ stars. $[\text{Mg}/\text{Fe}]$ in case B is smaller than in case A but the ejected Fe mass in case B is smaller than in case A (Tables 1, 9, and 15). This is because case B has a larger amount of fallback, i.e., larger $M_{\text{mix}}(\text{out})$ and smaller f , than case A. Such large fallback which reaches the Mg-rich layer decreases the amount of ejected Mg and leads to a smaller Mg/Fe for case B than case A in spite of a smaller amount of ejected Fe. The observed HNe have variations of the ejected Fe mass. Case A corresponds to typical HNe like SN 1998bw that ejected $M(^{56}\text{Ni}) \sim 0.4M_{\odot}$ (Nakamura et al. 2001a) and case B corresponds to HNe like SN 1997ef that ejected $M(^{56}\text{Ni}) \sim 0.15M_{\odot}$ (Iwamoto et al. 2000; Mazzali et al. 2000).

Alternative interpretation of $[\text{Mg}/\text{Fe}] \sim 0.2$ is to eject a larger amount of Fe than case A for the same amount of ejected Mg. In this case, because of larger Fe, larger explosion energies ($E_{51} \gtrsim 100$) are needed for this model to reproduce the small $[\text{Fe}/\text{H}]$ (~ -4), as long as $[\text{Fe}/\text{H}]$ is determined by Equation (2) (i.e., the same constant C) of the SN-induced star formation model. The explosion energies are considerably larger than those of Pop I SNe. We thus do not consider such a possibility in this paper.

REFERENCES

- Aoki, W., Norris, J. E., Ryan, S. G., Beers, T. C., & Ando, H. 2002, *PASJ*, 54, 933
- Aoki, W., Norris, J. E., Ryan, S. G., Beers, T. C., Christlieb, N., Tsangarides, S., & Ando, H. 2004, *ApJ*, 608, 971
- Anders, E., & Grevesse, N. 1989, *Geochim. Cosmochim. Acta*, 53, 197
- Argast, D., Samland, M., Gerhard, O. E., & Thielemann, F.-K. 2000, *A&A*, 356, 873
- Argast, D., Samland, M., Thielemann, F.-K., & Gerhard, O. E. 2002, *A&A*, 388, 842
- Argast, D., Samland, M., Thielemann, F.-K., & Qian, Y.-Z. 2004, *A&A*, 416, 997
- Aufferheide, M. B., Baron, E., & Thielemann, F.-K. 1991, *ApJ*, 370, 630
- Audouze, J., & Silk, J. 1995, *ApJ*, 451, L49
- Beers, T.C., & Christlieb, N. 2005, *ARA&A*, 43, 531
- Bensby T., Feltzing S., Lundström I. 2003, *A&A*, 410, 527
- Blinnikov, S., Lundqvist, P., Bartunov, O., Nomoto, K., & Iwamoto, K. 2000, *ApJ*, 532, 1132
- Bromm, V., & Larson, R. B. 2004, *ARA&A*, 42, 79
- Buras, R., Janka, H.-Th., Rampp, M., & Kifonidis, K. 2006a, *A&A*, 457, 281
- Buras, R., Rampp, M., Janka, H.-Th., & Kifonidis, K. 2006b, *A&A*, 447, 1049
- Burris, D. L., Pilachowski, C. A., Armandroff, T. E., Sneden, C., Cowan, J. J., & Roe, H. 2000, *ApJ*, 544, 302
- Carretta, E., Gratton, R. G., Sneden, C. 2000, *A&A*, 356, 238
- Caughlan, G. R., Fowler, W. A., Harris, M. J., & Zimmermann, B. A. 1985, *At Data Nucl. Data Tables*, 32, 197
- Caughlan, G. R., & Fowler, W. A. 1988, *At Data Nucl. Data Tables*, 40, 283
- Cayrel, R., et al. 2004, *A&A*, 416, 1117 (CA04)
- Chieffi, A., & Limongi, M. 2002, *ApJ*, 577, 281 (CL02)
- Christlieb, N., et al. 2002, *Nature*, 419, 904
- Chugai, N.N., Fabrika, S.N., Sholukhova, O.N., Goranskij, V.P., Abolmasov, P.K., & Vlasyuk, V.V. 2005, *Astron. Lett.*, 31, 792
- Cioffi, D. F., McKee, C. F., Bertschinger, E. 1988, *ApJ*, 334, 252
- Cobb, B. E., Baily, C. D., van Dokkum, P. G., Buxton, M. M., & Bloom, J. S. 2004, *ApJ*, 608, L93
- Coc, A., Vangioni-Flam, E., Descouvemont, P., Adahchour, A., & Angulo, C. 2004, *ApJ*, 600, 544
- Cohen, J.G., et al. 2006, *AJ*, 132, 137
- Deng, J., Tominaga, N., Mazzali, P.A., Maeda, K., & Nomoto, K. 2005, *ApJ*, 624, 898
- Edvardsson, B., Andersen, J., Gustafsson, B., Lambert, D. L., Nissen, P. E., & Tomkin, J. 1993, *A&A*, 275, 101
- François, P., Matteucci, F., Cayrel, R., Spite, M., Spite, F., & Chiappini, C. 2004, *A&A*, 421, 613
- Frebel, A., et al. 2005, *Nature*, 434, 871
- Fröhlich, C., Martínez-Pinedo, G., Liebendörfer, M., Thielemann, F.-K., Bravo, E., Hix, W. R., Langanke, K., & Zinner, N.T. 2006a, *Phys. Rev. Lett.*, 96, 142502
- Fröhlich, C., et al. 2006b, *ApJ*, 637, 415
- Fryer, C. L., Young, P. A., & Hungerford, A. L. 2006, *ApJ*, 650, 1028
- Galama, T. J., et al. 1998, *Nature*, 395, 670
- Gal-Yam, A., et al. 2004, *ApJ*, 609, L59
- Gratton, R. G. & Sneden, C. 1991, *A&A*, 241, 501
- Gratton, R. G. et al. 2003, *A&A*, 404, 187

- Hachisu, I., Matsuda, T., Nomoto, K., & Shigeyama, T. 1990, *ApJ*, 358, L57
- Heger, A., & Langer, N. 2000, *ApJ*, 544, 1016
- Heger, A., & Woosley, S.E. 2002, *ApJ*, 567, 532
- Hjorth, J., et al. 2003, *Nature*, 423, 847
- Hoffman, R.D., Woosley, S.E., Fuller, G.M., & Meyer, B.S. 1996, *ApJ*, 460, 478
- Honda, S., Aoki, W., Kajino, T., Ando, H., Beers, T. C., Izumiura, H., Sadakane, K., Takada-Hidai, M. 2004, *ApJ*, 607, 474 (HO04)
- Imbriani, G., Limongi, M., Gialanella, L., Terrasi, F., Straniero, O., & Chieffi, A. 2001, *ApJ*, 558, 903
- Ishimaru, Y., & Wanajo, S. 1999, *ApJ*, 511, L33
- Ishimaru, Y., Wanajo, S., Aoki, W., & Ryan, S.G. 2004, *ApJ*, 600, L47
- Iwamoto, K., et al. 1994, *ApJ*, 437, L115
- Iwamoto, K., et al. 1998, *Nature*, 395, 672
- Iwamoto, K., et al. 2000, *ApJ*, 534, 660
- Iwamoto, N., Umeda, H., Tominaga, N., Nomoto, K., & Maeda, K. 2005, *Science*, 309, 451 (IW05)
- Kawabata, K., et al. 2002, *ApJ*, 580, 39
- Kifonidis, K., Plewa, T., Janka, H.-Th., & Müller, E. 2003, *A&A*, 408, 621
- Kobayashi, C., Umeda, H., Nomoto, K., Tominaga, N., & Ohkubo, T. 2006, *ApJ*, 653, 1145
- Kudritzki, R.-P. 2000, in *The First Stars*. eds. Weiss, A., Abel, T. G., & Hill, V. (Berlin: Springer), 127
- Langer, N. 1992, *A&A*, 265, L17
- Leonard, D., et al. 2002, *Pub. Astron. Soc. Pacific*, 114, 1333
- Liebendörfer, M., Rampp, M., Janka, H.-Th., & Mezzacappa, A. 2005, *ApJ*, 620, 840
- Limongi, M., & Chieffi, A. 2003, *ApJ*, 592, 404
- Lipkin, Y. M., et al. 2004, *ApJ*, 606, 381
- MacFadyen, A., & Woosley, S.E. 1999, *ApJ*, 524, 262
- Maeda, K., Mazzali, P. A., & Nomoto, K. 2006a, *ApJ*, 645, 1331
- Maeda, K., Nakamura, T., Nomoto, K., Mazzali, P. A., Patat, F., & Hachisu, I. 2002, *ApJ*, 565, 405
- Maeda, K., & Nomoto, K. 2003, *ApJ*, 598, 1163
- Maeda, K., Nomoto, K., Mazzali, P. A., & Deng, J. 2006b, *ApJ*, 640, 854
- Maeda, K., & Tominaga, N. 2007, *ApJ*, submitted
- Maeder, A., & Meynet, G. 2000, *ARA&A*, 38, 143
- Malesani, D., et al. 2004, *ApJ*, 609, L5
- Matheson, T., et al. 2003, *ApJ*, 599, 394
- Mazzali, P. A., Iwamoto, K., & Nomoto, K. 2000, *ApJ*, 545, 407
- Mazzali, P. A., et al. 2002, *ApJ*, 572, L61
- Mazzali, P. A., et al. 2003, *ApJ*, 599, L95
- Mazzali, P. A., et al. 2005, *Science*, 308, 1284
- Mazzali, P. A., et al. 2006a, *ApJ*, 645, 1323
- Mazzali, P. A., et al. 2006b, *Nature*, 442, 1018
- Meynet, G., & Maeder, A. 2005, *A&A*, 429, 581
- McWilliam, A. 1997, *ARA&A*, 35, 503
- McWilliam, A. 1998, *AJ*, 115, 1640
- McWilliam, A., Preston, G. W., Sneden, C., & Searle, L. 1995a, *AJ*, 109, 2757
- McWilliam, A., Preston, G. W., Sneden, C., & Shectman, S. 1995b, *AJ*, 109, 2736
- Nagataki, S., Mizuta, A., & Sato, K. 2006, *ApJ*, 647, 1255
- Nagataki, S., Mizuta, A., Yamada, S., Takabe, H., & Sato, K. 2003, *ApJ*, 596, 401
- Nakamura, F., & Umemura, M. 1999, *ApJ*, 515, 239
- Nakamura, T., Mazzali, P.A., Nomoto, K., & Iwamoto, K. 2001a, *ApJ*, 550, 991

- Nakamura, T., Umeda, H., Nomoto, K., Thielemann, F.-K., & Burrows, A. 1999, *ApJ*, 517, 193
- Nakamura, T., et al. 2001b, *ApJ*, 555, 880
- Nissen, P.E., Primas, F., Asplund, M., & Lambert, D.L. 2002, *A&A*, 390, 235
- Nomoto, K., & Hashimoto, M. 1988, *Phys. Rep.*, 163, 13
- Nomoto, K., Hashimoto, M., Tsujimoto, T., Thielemann, F.-K., Kishimoto, M., Kubo, Y., & Nakasato, N. 1997, *Nucl. Phys. A*, 616, 79
- Nomoto, K., Maeda, K., Mazzali, P. A., Umeda, H., Deng, J., & Iwamoto, K. 2004a, in *Stellar Collapse*, ed. C. L. Fryer (Dordrecht: Kluwer), 277 (astro-ph/0308136)
- Nomoto, K., Maeda, K., Umeda, H., Tominaga, N., Ohkubo, T., Deng, J., & Mazzali, P.A. 2004b, *MmSAI*, 75, 312
- Nomoto, K., Mazzali, P.A., Nakamura, T., et al. 2001, in *Supernovae and Gamma Ray Bursts*, ed. M. Livio et al. (Cambridge: Cambridge Univ. Press), 144 (astro-ph/0003077)
- Nomoto, K., Suzuki, T., Shigeyama, T., Kumagai, S., Yamaoka, H., & Saio, H. 1993, *Nature*, 364, 507
- Nomoto, K., Tominaga, N., Umeda, H., Kobayashi, C., & Maeda, K. 2006, *Nucl. Phys. A*, 777, 424 (astro-ph/0605725)
- Nomoto, K., Yamaoka, H., Pols, O. R., van den Heuvel, E. P. J., Iwamoto, K., Kumagai, S., & Shigeyama, T. 1994, *Nature*, 371, 227
- Norris, J. E., Ryan, S. G., & Beers, T. C. 2001, *ApJ*, 561, 1034
- Ohkubo, T., Umeda, H., Maeda, K., Nomoto, K., Tsuruta, S., & Rees, M. J. 2006, *ApJ*, 645, 1352
- Patat, F., et al. 2001, *ApJ*, 555, 900
- Pian, E., et al. 2006, *Nature*, 442, 1011
- Podsiadlowski, Ph., Mazzali, P. A., Nomoto, K., Lazzati, D., & Cappellaro, E. 2004, *ApJ*, 607, L17
- Primas, F., Reimers, D., Wisotzki, L., Reetz, J., Gehren, T., & Beers, T. C. 2000, in *The First Stars*, ed. A. Weiss, T. Abel, & V. Hill (Berlin: Springer), 51
- Pruet, J., Surman, R., & McLaughlin, G.C. 2004a, *ApJ*, 602, L101
- Pruet, J., Thompson, T.A., & Hoffman, R.D. 2004b, *ApJ*, 606, 1006
- Pruet, J., Woosley, S. E., Buras, R., Janka, H.-T., & Hoffman, R. D. 2005, *ApJ*, 623, 325
- Rampp, M., & Janka, H.-Th. 2000, *ApJ*, 539, L33
- Ryan, S. G., Aoki, W., Norris, J. E., & Beers, T. C. 2005, *ApJ*, 635, 349
- Ryan, S. G., Norris, J. E., & Beers, T. C. 1996, *ApJ*, 471, 254
- Sauer, D. N., Mazzali, P. A., Deng, J., Valenti, S., Nomoto, K., & Filippenko, A. V. 2006, *MNRAS*, 369, 1939
- Shigeyama, T., & Nomoto, K. 1990, *ApJ*, 360, 242
- Shigeyama, T., Suzuki, T., Kumagai, S., Nomoto, K., Saio, H., & Yamaoka, H. 1994, *ApJ*, 420, 341
- Shigeyama, T., & Tsujimoto, T. 1998, *ApJ*, 507, L135
- Snedden, C., Gratton, R. G., & Crocker, D. A. 1991, *A&A*, 246, 354
- Spergel, D. N., et al. 2003, *ApJS*, 148, 175
- Spite, M., et al. 2005, *A&A*, 430, 655
- Spite, M., et al. 2006, *A&A*, 455, 291
- Stanek, K. Z., et al. 2003, *ApJ*, 591, L17
- Suda, T., Aikawa, M., Machida, M. N., Fujimoto, M. Y., & Iben, I., Jr. 2004, *ApJ*, 611, 476
- Taubenberger, S., et al. 2006, *MNRAS*, 371, 1459
- Thielemann, F.K., Nomoto, K., & Hashimoto, M. 1996, *ApJ*, 460, 408
- Thomsen, B., et al. 2004, *A&A*, 419, L21
- Thornton, K., Gaudlitz, M., Janka, H.-Th., & Steinmetz, M. 1998, *ApJ*, 500, 95

- Tominaga, N., Maeda, K., Umeda, H., Nomoto, K., Tanaka, M., Iwamoto, N., & Mazzali, P.A. 2007, ApJ, submitted
- Tominaga, N., et al. 2005, ApJ, 633, L97
- Tomita, H., et al. 2006, ApJ, 644, 400
- Turatto, M., et al. 1998, 498, L129
- Tumlinson, J. 2006, ApJ, 641, 1
- Umeda, H., & Nomoto, K. 2002a, ApJ, 565, 385 (UN02a)
- Umeda, H., & Nomoto, K. 2003, Nature, 422, 871 (UN03)
- Umeda, H., & Nomoto, K. 2005, ApJ, 619, 427 (UN05)
- Umeda, H., Nomoto, K., & Nakamura, T. 2000, in *The First Stars*. eds. Weiss, A., Abel, T. G., & Hill, V. (Berlin: Springer), 150 (astro-ph/9912248) (UNN00)
- Umeda, H., Nomoto, K., Tsuru, T., & Matsumoto, H. 2002b, ApJ, 578, 855
- Wanajo, S. 2006a, ApJ, 647, 1323
- Wanajo, S. 2006b, ApJ, 650, L79
- Wang, L., et al. 2002, ApJ, 579, 671
- Wang, L., et al. 2003, ApJ, 592, 457
- Wasserburg, G. J., & Qian, Y.-Z. 2000, ApJ, 529, L21
- Weiss, A., Schlattl, H., Salaris, M., & Cassisi, S. 2004, A&A, 422, 217
- Wosley, S. E., Eastman, R.G., & Schmidt, B.P. 1999, ApJ, 516, 788
- Wosley, S. E., & Weaver, T. A. 1993, Phys. Rep., 227, 65
- Wosley, S. E., & Weaver, T. A. 1995, ApJS, 101, 181 (WW95)
- Zampieri, L., Pastorello, A., Turatto, M., Cappellaro, E., Benetti, S., Altavilla, G., Mazzali, P., & Hamuy, M. 2003, MNRAS, 338, 711

TABLE 1
THE EXPLOSION MODELS

M_{MS}	E_{51}	$M(^{56}\text{Ni})$	$M(\text{Mg})$	$[\text{Fe}/\text{H}]^{\text{a}}$	$[\text{O}/\text{Fe}]$	$[\text{Mg}/\text{Fe}]$	$M_{\text{cut}}(\text{fin})$	$M_{\text{cut}}(\text{ini})$	$M_{\text{mix}}(\text{out})$	f^{b}	The abundance pattern
13	1	0.07	0.09	-2.55	-0.08	0.37	1.57			1	Fig. 4a
15	1	0.07	0.07	-2.55	0.15	0.27	1.48			1	Fig. 4b
18	1	0.07	0.16	-2.55	0.41	0.63	1.65			1	Fig. 4c
20	10	0.08	0.17	-3.34	0.50	0.58	1.90	1.52	2.05	0.28	Fig. 3a
25	5	0.11	0.14	-2.97	0.50	0.41	2.45	1.79	2.69	0.26	Fig. 7
25	10	0.10	0.15	-3.27	0.50	0.48	2.86	1.79	3.07	0.16	Fig. 3b
25F	1	0.0008	0.03	-4.50	2.40	1.81	4.20	1.79	4.21	0.004	Fig. 8
30A	20	0.16	0.22	-3.31	0.50	0.41	3.27	1.65	3.59	0.17	Fig. 3c
30B	20	0.05	0.04	-3.81	0.55	0.20	6.73	1.65	7.01	0.05	Fig. 3c
40A	30	0.26	0.34	-3.25	0.50	0.39	5.53	2.24	6.00	0.12	Fig. 3d
40B	30	0.11	0.09	-3.63	0.46	0.20	10.70	2.24	11.16	0.05	Fig. 3d
50A	40	0.36	0.57	-3.22	0.50	0.47	3.76	1.89	4.49	0.28	Fig. 3e
50B	40	0.23	0.20	-3.40	0.35	0.20	11.01	1.89	13.05	0.18	Fig. 3e

^a $[\text{Fe}/\text{H}]$ is determined as $[\text{Fe}/\text{H}] \simeq \log_{10}(M(\text{Fe})/E_{51}^{6/7}) - C$. Here we assume that C is a constant value, $C = 1.4$.

^b f is an ejection factor. $f = 1$ corresponds to normal SN models without the mixing-fallback model.

NOTE.—The numbers shown are the main-sequence mass, the explosion energy, the ejected ^{56}Ni mass, the ejected Mg mass, $[\text{Fe}/\text{H}]$, $[\text{O}/\text{Fe}]$, $[\text{Mg}/\text{Fe}]$, the final central remnant mass, the mass of inner boundary of the mixing region, the mass of outer boundary of the mixing region, the ejection factor and the figure number of the comparison with the EMP and VMP stars. The masses are in unit of M_{\odot} .

TABLE 3
YIELDS OF STABLE ISOTOPES.

Species Mass [M_{\odot}] E_{51}	Yields [M_{\odot}]												
	13 1	15 1	18 1	20 10	25 5	25 10	25F 1	30A 20	30B 20	40A 30	40B 30	50A 40	50B 40
p	6.59E+00	7.58E+00	8.43E+00	8.77E+00	1.06E+01	1.06E+01	1.06E+01	1.17E+01	1.17E+01	1.40E+01	1.40E+01	1.63E+01	1.63E+01
d	1.49E-16	1.69E-16	1.28E-16	8.66E-17	2.04E-16	2.06E-16	2.02E-16	1.09E-14	1.09E-14	1.66E-14	1.66E-14	1.24E-15	1.24E-15
³ He	4.12E-05	4.09E-05	3.33E-05	4.76E-05	2.11E-04	2.11E-04	2.11E-04	2.06E-04	2.06E-04	2.56E-05	2.56E-05	2.86E-05	2.86E-05
⁴ He	4.01E+00	4.40E+00	5.42E+00	5.96E+00	8.03E+00	8.03E+00	8.02E+00	8.03E+00	9.54E+00	9.51E+00	1.18E+01	1.18E+01	1.56E+01
⁶ Li	3.29E-23	1.28E-22	4.52E-23	1.36E-22	2.28E-20	4.26E-20	2.68E-21	3.50E-17	3.50E-17	5.39E-17	5.39E-17	2.02E-18	2.02E-18
⁷ Li	2.17E-10	2.94E-10	7.34E-11	2.79E-10	5.68E-09	5.68E-09	5.68E-09	2.36E-08	2.36E-08	3.42E-11	3.42E-11	8.78E-12	8.78E-12
⁹ Be	1.77E-20	3.22E-22	1.05E-22	4.83E-20	5.00E-17	3.69E-17	1.24E-17	3.09E-18	3.09E-18	9.03E-18	9.03E-18	6.04E-17	6.04E-17
¹⁰ B	3.16E-21	3.92E-20	2.86E-20	2.88E-19	2.79E-15	2.05E-13	2.67E-18	1.05E-14	1.05E-14	9.41E-15	9.41E-15	1.72E-17	7.85E-18
¹¹ B	2.89E-16	3.55E-16	1.59E-14	1.19E-15	6.09E-14	5.27E-13	1.90E-16	9.61E-14	9.16E-14	9.41E-13	9.40E-13	2.49E-11	1.62E-11
¹² C	7.41E-02	1.72E-01	2.18E-01	1.90E-01	2.79E-01	2.67E-01	2.74E-01	3.16E-01	2.86E-01	3.72E-01	3.51E-01	1.56E+00	1.17E+00
¹³ C	8.39E-08	6.21E-08	2.63E-09	1.18E-08	2.90E-08	6.94E-08	1.05E-08	6.32E-08	6.03E-08	8.18E-08	7.84E-08	2.38E-07	1.70E-07
¹⁴ N	1.83E-03	1.86E-03	1.89E-04	5.42E-05	5.92E-04	5.96E-04	5.91E-04	4.18E-05	4.17E-05	3.39E-06	3.33E-06	4.38E-04	4.37E-04
¹⁵ N	6.38E-08	6.86E-08	2.40E-08	2.96E-08	1.64E-07	1.75E-07	7.17E-08	2.20E-07	1.16E-07	6.54E-07	6.51E-07	3.33E-07	8.27E-08
¹⁶ O	4.50E-01	7.73E-01	1.38E+00	2.03E+00	2.60E+00	2.37E+00	1.52E+00	3.92E+00	1.37E+00	6.32E+00	2.40E+00	8.81E+00	4.02E+00
¹⁷ O	1.69E-06	1.57E-06	2.79E-07	7.13E-08	1.49E-06	1.49E-06	1.48E-06	3.81E-08	2.64E-08	1.23E-08	8.65E-09	8.60E-06	8.56E-06
¹⁸ O	5.79E-08	4.89E-06	4.63E-06	2.33E-08	4.66E-07	3.87E-07	6.73E-07	5.03E-07	5.02E-07	2.93E-07	2.92E-07	6.00E-06	5.99E-06
¹⁹ F	1.17E-10	1.97E-09	7.91E-09	2.12E-09	1.43E-09	1.67E-09	1.01E-09	7.88E-09	6.41E-09	1.17E-07	1.16E-07	8.49E-09	4.06E-09
²⁰ Ne	1.53E-02	3.27E-01	4.94E-01	7.49E-01	3.91E-01	2.85E-01	3.16E-01	5.20E-01	2.60E-01	2.64E-01	2.19E-01	2.48E+00	1.30E+00
²¹ Ne	5.42E-07	3.76E-05	9.12E-05	3.58E-05	1.47E-05	1.22E-05	3.05E-06	3.51E-05	2.26E-05	1.41E-05	1.07E-05	2.40E-04	1.14E-04
²² Ne	1.98E-07	1.61E-05	2.57E-05	5.51E-05	1.30E-05	8.62E-06	1.27E-05	3.52E-05	1.98E-05	1.66E-05	1.45E-05	2.10E-04	1.08E-04
²³ Na	1.44E-04	2.45E-03	2.08E-03	2.31E-03	6.74E-04	4.42E-04	6.61E-04	7.36E-04	3.24E-04	3.28E-04	1.66E-04	4.27E-03	1.99E-03
²⁴ Mg	8.62E-02	6.82E-02	1.57E-01	1.65E-01	1.43E-01	1.53E-01	2.70E-02	2.17E-01	4.20E-02	3.37E-01	8.99E-02	5.70E-01	1.97E-01
²⁵ Mg	1.56E-04	2.98E-04	5.83E-04	1.07E-04	4.52E-05	4.57E-05	1.29E-05	1.45E-04	9.00E-05	5.95E-04	4.11E-04	3.10E-04	1.16E-04
²⁶ Mg	7.07E-05	3.98E-04	8.73E-04	2.09E-04	4.31E-05	3.89E-05	1.48E-05	8.00E-05	2.62E-05	6.90E-05	1.22E-05	2.32E-04	9.70E-05
²⁶ Al	9.92E-07	1.11E-06	3.33E-06	1.02E-06	1.21E-06	1.28E-06	5.34E-09	2.92E-06	1.33E-06	3.80E-05	3.43E-05	5.46E-06	1.40E-06
²⁷ Al	3.78E-03	1.37E-03	3.14E-03	1.50E-03	8.59E-04	8.93E-04	9.78E-05	1.55E-03	1.59E-04	7.52E-03	1.34E-03	3.29E-03	8.07E-04
²⁸ Si	8.08E-02	7.18E-02	1.07E-01	9.15E-02	2.21E-01	1.97E-01	2.07E-03	2.44E-01	3.11E-02	7.17E-01	2.28E-01	3.61E-01	1.18E-01
²⁹ Si	7.50E-04	2.38E-04	4.36E-04	2.89E-04	5.12E-04	5.23E-04	3.96E-06	8.85E-04	4.89E-05	3.72E-03	1.29E-03	9.32E-04	1.80E-04
³⁰ Si	1.42E-03	1.49E-04	3.50E-04	1.12E-04	5.90E-05	6.13E-05	2.66E-06	1.47E-04	9.97E-06	2.82E-03	4.83E-04	2.10E-04	5.04E-05
³¹ P	4.88E-04	5.66E-05	1.31E-04	7.30E-05	5.44E-05	5.03E-05	1.68E-06	1.18E-04	7.87E-06	1.01E-03	2.24E-04	1.75E-04	4.26E-05
³² S	2.36E-02	3.24E-02	4.45E-02	3.71E-02	1.00E-01	7.52E-02	8.10E-04	8.49E-02	1.49E-02	2.60E-01	6.11E-02	1.41E-01	6.23E-02
³³ S	9.00E-05	7.48E-05	9.49E-05	1.31E-04	2.06E-04	1.99E-04	9.32E-07	3.02E-04	1.59E-05	8.44E-04	1.29E-04	3.89E-04	7.15E-05
³⁴ S	2.79E-04	2.01E-04	2.59E-04	1.46E-04	5.13E-05	2.47E-05	5.83E-07	2.70E-04	1.78E-05	2.08E-03	1.32E-04	6.60E-05	2.92E-05
³⁶ S	1.48E-08	1.43E-09	5.34E-09	8.33E-10	6.69E-11	5.25E-11	1.35E-12	1.41E-09	7.70E-11	5.04E-08	2.63E-09	4.52E-11	8.39E-12
³⁵ Cl	5.48E-05	1.44E-05	2.42E-05	3.28E-05	2.01E-05	1.68E-05	1.83E-07	4.51E-05	6.11E-06	1.80E-04	2.46E-05	6.89E-05	3.30E-05
³⁷ Cl	3.11E-06	5.62E-06	7.80E-06	1.52E-05	2.26E-05	2.02E-05	2.21E-07	2.37E-05	1.29E-06	7.92E-05	4.28E-06	3.29E-05	6.06E-06
³⁶ Ar	3.18E-03	5.53E-03	7.26E-03	6.04E-03	1.67E-02	1.15E-02	1.54E-04	1.18E-02	2.71E-03	3.62E-02	6.08E-03	2.29E-02	1.23E-02
³⁸ Ar	5.23E-05	6.18E-05	1.45E-04	6.35E-05	4.55E-05	8.35E-06	6.11E-07	9.06E-05	5.58E-06	7.83E-04	4.15E-05	1.81E-05	7.26E-06
⁴⁰ Ar	8.01E-11	1.78E-11	3.95E-11	3.77E-11	5.17E-12	3.77E-12	1.40E-13	1.87E-11	2.69E-12	2.68E-10	1.99E-11	1.38E-12	3.41E-13
³⁹ K	5.14E-06	7.23E-06	1.59E-05	1.06E-05	1.61E-05	8.69E-06	2.08E-07	2.05E-05	2.88E-06	1.31E-04	1.07E-05	2.52E-05	1.47E-05
⁴⁰ K	1.14E-09	9.07E-10	1.84E-09	3.95E-09	1.82E-09	4.46E-10	2.89E-11	2.52E-09	1.32E-10	1.18E-08	6.14E-10	7.09E-10	1.30E-10
⁴¹ K	3.72E-07	7.43E-07	1.51E-06	2.63E-06	5.94E-06	4.00E-06	7.98E-08	3.63E-06	2.04E-07	2.12E-05	1.14E-06	1.72E-06	4.78E-07
⁴⁰ Ca	2.82E-03	4.72E-03	6.14E-03	4.39E-03	1.43E-02	9.20E-03	1.36E-04	8.77E-03	2.45E-03	2.97E-02	5.60E-03	1.87E-02	1.20E-02

TABLE 3—*Continued*

Species Mass [M_{\odot}] E_{51}	Yields [M_{\odot}]												
	13 1	15 1	18 1	20 10	25 5	25 10	25F 1	30A 20	30B 20	40A 30	40B 30	50A 40	50B 40
⁴² Ca	9.80E-07	1.21E-06	3.15E-06	1.34E-06	1.11E-06	1.76E-07	1.65E-08	1.62E-06	8.48E-08	1.97E-05	1.02E-06	2.29E-07	7.46E-08
⁴³ Ca	6.66E-08	4.76E-08	3.48E-08	2.59E-07	4.68E-08	7.12E-08	3.33E-10	1.71E-07	5.33E-08	1.40E-07	5.32E-08	7.31E-07	4.75E-07
⁴⁴ Ca	1.70E-05	2.17E-05	1.40E-05	1.25E-04	4.26E-05	6.82E-05	1.82E-07	1.80E-04	5.67E-05	1.76E-04	7.16E-05	6.08E-04	3.95E-04
⁴⁶ Ca	1.07E-12	1.75E-12	9.26E-12	1.15E-11	2.61E-12	1.80E-11	1.18E-13	9.25E-12	7.64E-12	3.69E-11	2.45E-11	2.66E-13	6.72E-14
⁴⁸ Ca	1.99E-17	4.21E-14	4.21E-16	5.87E-16	8.89E-12	8.91E-12	9.58E-12	8.16E-13	8.15E-13	1.27E-11	1.27E-11	1.56E-13	5.63E-14
⁴⁵ Sc	2.16E-08	3.53E-08	4.82E-08	1.44E-07	1.77E-07	1.24E-07	2.44E-09	6.09E-08	1.06E-08	6.15E-07	4.34E-08	6.31E-08	3.69E-08
⁴⁶ Ti	6.21E-06	2.56E-06	3.41E-06	5.59E-06	2.21E-06	2.88E-06	8.20E-09	6.13E-06	1.80E-06	1.11E-05	1.99E-06	1.40E-05	9.07E-06
⁴⁷ Ti	8.72E-06	3.68E-06	4.68E-06	9.77E-06	8.14E-06	9.89E-06	2.42E-08	2.06E-05	6.47E-06	2.59E-05	1.08E-05	5.85E-05	3.80E-05
⁴⁸ Ti	6.32E-05	8.94E-05	9.35E-05	1.59E-04	1.37E-04	1.41E-04	1.09E-06	2.88E-04	9.07E-05	3.53E-04	1.47E-04	7.84E-04	5.09E-04
⁴⁹ Ti	2.24E-06	2.79E-06	9.83E-07	2.65E-06	1.89E-06	2.22E-06	1.02E-08	3.44E-06	1.08E-06	5.00E-06	1.89E-06	3.93E-06	2.55E-06
⁵⁰ Ti	1.18E-12	9.24E-13	1.62E-12	8.98E-13	1.92E-12	1.96E-12	5.20E-13	2.49E-12	2.09E-12	3.37E-11	2.94E-11	1.45E-12	5.46E-13
⁵⁰ V	1.36E-11	1.04E-11	3.08E-11	1.44E-11	7.71E-12	2.13E-12	2.17E-13	9.03E-12	7.15E-13	1.20E-10	2.76E-11	1.14E-12	2.83E-13
⁵¹ V	1.63E-05	8.53E-06	8.97E-06	2.36E-05	1.01E-05	1.59E-05	1.74E-08	3.24E-05	1.02E-05	3.06E-05	1.26E-05	7.13E-05	4.63E-05
⁵⁰ Cr	1.02E-05	7.43E-06	6.90E-06	8.43E-06	2.89E-06	2.79E-06	1.70E-08	5.18E-06	1.40E-06	2.57E-05	3.29E-06	9.36E-06	6.06E-06
⁵² Cr	8.66E-04	1.17E-03	1.35E-03	6.79E-04	1.55E-03	1.30E-03	1.47E-05	1.61E-03	5.06E-04	2.82E-03	1.18E-03	3.13E-03	2.03E-03
⁵³ Cr	4.97E-05	5.66E-05	1.87E-05	3.03E-05	3.18E-05	4.17E-05	1.60E-07	5.58E-05	1.76E-05	9.62E-05	3.94E-05	4.87E-05	3.16E-05
⁵⁴ Cr	2.38E-10	3.84E-10	7.70E-10	1.35E-10	2.15E-10	3.78E-11	1.45E-12	9.63E-11	1.16E-11	3.51E-09	2.09E-10	6.61E-12	1.72E-12
⁵⁵ Mn	1.39E-04	9.01E-05	3.74E-05	4.77E-05	3.70E-05	3.05E-05	1.44E-07	2.77E-05	8.68E-06	1.28E-04	4.80E-05	2.87E-05	1.86E-05
⁵⁴ Fe	7.23E-04	5.00E-04	2.70E-04	1.85E-04	2.14E-04	8.50E-05	4.48E-07	3.94E-05	1.17E-05	1.31E-03	2.42E-04	2.51E-05	1.63E-05
⁵⁶ Fe	7.00E-02	7.00E-02	7.00E-02	8.30E-02	1.07E-01	9.70E-02	7.93E-04	1.60E-01	5.04E-02	2.58E-01	1.08E-01	3.61E-01	2.34E-01
⁵⁷ Fe	1.01E-03	1.08E-03	7.98E-04	1.77E-03	1.54E-03	1.55E-03	9.27E-06	3.03E-03	9.53E-04	4.17E-03	1.74E-03	7.35E-03	4.77E-03
⁵⁸ Fe	5.96E-11	1.56E-10	2.76E-10	1.32E-10	5.82E-10	1.21E-10	3.68E-12	9.17E-11	6.18E-12	3.30E-09	2.33E-10	1.53E-11	4.52E-12
⁵⁹ Co	1.75E-04	1.30E-04	1.49E-04	3.72E-04	1.96E-04	2.42E-04	4.36E-07	5.14E-04	1.62E-04	5.19E-04	2.16E-04	1.34E-03	8.70E-04
⁵⁸ Ni	3.79E-04	3.55E-04	2.92E-04	8.45E-04	4.56E-04	5.44E-04	1.30E-06	1.15E-03	3.62E-04	1.28E-03	4.84E-04	2.76E-03	1.79E-03
⁶⁰ Ni	2.14E-03	1.56E-03	1.44E-03	2.99E-03	2.74E-03	2.78E-03	1.89E-05	5.43E-03	1.71E-03	8.37E-03	3.49E-03	1.31E-02	8.49E-03
⁶¹ Ni	3.68E-05	3.03E-05	1.95E-05	6.27E-05	3.66E-05	4.19E-05	2.33E-07	8.54E-05	2.69E-05	9.87E-05	4.12E-05	2.18E-04	1.42E-04
⁶² Ni	1.92E-05	1.47E-05	1.23E-05	4.24E-05	2.25E-05	2.86E-05	2.00E-07	5.68E-05	1.79E-05	6.74E-05	2.81E-05	1.43E-04	9.31E-05
⁶⁴ Ni	2.18E-15	2.67E-13	1.35E-14	8.70E-13	3.73E-12	9.60E-12	1.84E-12	3.38E-12	2.41E-12	2.46E-11	2.46E-11	6.72E-12	1.67E-12
⁶³ Cu	4.86E-06	3.45E-06	3.58E-06	1.19E-05	6.41E-06	8.18E-06	2.02E-08	1.70E-05	5.34E-06	2.06E-05	8.60E-06	4.44E-05	2.88E-05
⁶⁵ Cu	2.24E-07	2.33E-07	1.50E-07	7.21E-07	4.92E-07	5.77E-07	3.71E-09	1.37E-06	4.32E-07	1.86E-06	7.75E-07	4.37E-06	2.83E-06
⁶⁴ Zn	1.26E-04	1.18E-04	8.72E-05	3.79E-04	2.04E-04	2.58E-04	9.63E-07	5.77E-04	1.82E-04	6.88E-04	2.87E-04	1.56E-03	1.01E-03
⁶⁶ Zn	7.74E-07	1.03E-06	4.67E-07	5.05E-06	1.66E-06	2.44E-06	1.14E-08	6.98E-06	2.20E-06	6.90E-06	2.88E-06	2.29E-05	1.48E-05
⁶⁷ Zn	1.73E-08	2.30E-08	1.20E-08	1.94E-07	2.66E-08	5.83E-08	3.99E-11	1.89E-07	5.95E-08	1.18E-07	4.93E-08	5.60E-07	3.63E-07
⁶⁸ Zn	2.85E-08	3.16E-08	3.66E-08	8.93E-08	1.25E-07	1.21E-07	1.07E-09	2.67E-07	8.40E-08	4.86E-07	2.03E-07	8.45E-07	5.48E-07
⁷⁰ Zn	3.04E-16	3.03E-14	7.45E-15	1.08E-13	2.04E-13	2.90E-12	1.82E-16	8.49E-13	6.00E-13	1.95E-11	1.95E-11	1.00E-11	5.36E-12
⁶⁹ Ga	7.59E-09	5.50E-09	5.55E-09	1.77E-08	1.91E-08	2.12E-08	1.41E-10	4.04E-08	1.27E-08	8.95E-08	3.74E-08	1.08E-07	7.00E-08
⁷¹ Ga	1.00E-14	8.31E-14	3.35E-14	1.53E-12	1.60E-12	2.95E-11	1.05E-14	3.79E-12	2.38E-12	1.57E-10	1.57E-10	2.30E-11	1.06E-11
⁷⁰ Ge	8.90E-09	6.27E-09	4.35E-09	2.41E-08	1.04E-08	1.41E-08	6.21E-11	2.92E-08	9.20E-09	3.75E-08	1.57E-08	8.09E-08	5.23E-08
⁷² Ge	7.42E-15	7.63E-13	5.90E-13	5.95E-12	2.83E-12	2.09E-11	3.85E-14	7.43E-12	3.96E-12	7.11E-11	7.10E-11	4.76E-11	1.59E-11
⁷³ Ge	1.37E-14	1.84E-13	1.36E-13	3.73E-12	5.55E-12	3.95E-11	7.15E-15	6.59E-12	4.98E-12	9.15E-11	9.15E-11	3.12E-11	1.26E-11
⁷⁴ Ge	3.77E-15	5.05E-14	5.80E-14	2.14E-13	1.16E-12	1.45E-11	9.96E-14	2.47E-12	1.68E-12	4.28E-11	4.28E-11	6.22E-12	1.98E-12

TABLE 5
YIELDS OF UNSTABLE ISOTOPES.

Species Mass [M_{\odot}] E_{51}	Yields [M_{\odot}]												
	13	15	18	20	25	25	25F	30A	30B	40A	40B	50A	50B
	1	1	1	10	5	10	1	20	20	30	30	40	40
^{22}Na	1.51E-07	7.70E-06	1.68E-05	4.65E-05	9.97E-06	6.54E-06	8.98E-06	2.70E-05	1.34E-05	1.37E-05	1.19E-05	1.77E-04	9.12E-05
^{26}Al	9.80E-07	1.10E-06	3.32E-06	8.93E-07	1.21E-06	1.26E-06	5.34E-09	2.87E-06	1.32E-06	2.13E-05	1.76E-05	5.34E-06	1.32E-06
^{41}Ca	3.72E-07	7.42E-07	1.51E-06	2.63E-06	5.94E-06	4.00E-06	7.98E-08	3.63E-06	2.04E-07	2.12E-05	1.14E-06	1.72E-06	4.78E-07
^{44}Ti	1.70E-05	2.17E-05	1.40E-05	1.25E-04	4.26E-05	6.82E-05	1.82E-07	1.80E-04	5.67E-05	1.76E-04	7.16E-05	6.08E-04	3.95E-04
^{60}Fe	4.47E-16	2.44E-14	4.24E-15	1.10E-13	1.54E-13	1.10E-12	1.01E-15	2.10E-12	1.95E-12	2.44E-11	2.44E-11	1.11E-12	3.86E-13
^{56}Ni	7.00E-02	7.00E-02	7.00E-02	8.30E-02	1.07E-01	9.70E-02	7.93E-04	1.60E-01	5.04E-02	2.58E-01	1.08E-01	3.61E-01	2.34E-01
^{57}Ni	1.01E-03	1.08E-03	7.98E-04	1.77E-03	1.54E-03	1.55E-03	9.27E-06	3.03E-03	9.53E-04	4.17E-03	1.74E-03	7.35E-03	4.77E-03

TABLE 7
IMF-INTEGRATED YIELDS.

Species $M_{\text{MS}} \geq 30M_{\odot}$ models "n/p ratio" "low-density" The abundance pattern	A		B		Yields [Mass fractions]		A		B	
	No	No	No	No	Yes	Yes	Yes	Yes	Yes	Yes
	No	No	No	No	No	No	Yes	Yes	Yes	Yes
	Fig. 5		Fig. 9j		Fig. 10g					
p	3.28E-02	3.28E-02	3.27E-02	3.27E-02	3.28E-02	3.28E-02	3.28E-02	3.28E-02	3.28E-02	3.28E-02
d	8.97E-18	8.97E-18	8.97E-18	8.97E-18	8.97E-18	8.97E-18	1.22E-15	1.22E-15	1.22E-15	1.22E-15
³ He	2.72E-07	2.72E-07	2.72E-07	2.72E-07	2.72E-07	2.72E-07	2.72E-07	2.72E-07	2.72E-07	2.72E-07
⁴ He	2.31E-02	2.31E-02	2.30E-02	2.30E-02	2.33E-02	2.33E-02	2.33E-02	2.32E-02	2.32E-02	2.32E-02
⁶ Li	2.75E-20	2.75E-20	2.75E-20	2.75E-20	4.04E-18	4.04E-18	4.04E-18	4.04E-18	4.04E-18	4.04E-18
⁷ Li	1.14E-11	1.14E-11	1.12E-11	1.12E-11	1.14E-11	1.14E-11	1.14E-11	1.14E-11	1.14E-11	1.14E-11
⁹ Be	2.40E-20	2.40E-20	2.50E-20	2.50E-20	2.09E-19	2.09E-19	2.09E-19	2.09E-19	2.09E-19	2.09E-19
¹⁰ B	8.94E-17	8.94E-17	4.80E-17	4.80E-17	7.70E-18	7.70E-18	7.70E-18	7.70E-18	7.70E-18	7.70E-18
¹¹ B	2.74E-15	1.95E-15	7.68E-16	7.64E-16	4.17E-16	4.14E-16	4.17E-16	4.14E-16	4.17E-16	4.14E-16
¹² C	8.27E-04	7.76E-04	8.35E-04	7.84E-04	8.56E-04	8.07E-04	8.56E-04	8.07E-04	8.56E-04	8.07E-04
¹³ C	2.24E-10	2.15E-10	2.26E-10	2.18E-10	2.43E-10	2.36E-10	2.43E-10	2.36E-10	2.43E-10	2.36E-10
¹⁴ N	3.41E-06	3.41E-06	3.38E-06	3.38E-06	3.41E-06	3.41E-06	3.41E-06	3.41E-06	3.41E-06	3.41E-06
¹⁵ N	4.89E-10	4.28E-10	4.87E-10	4.27E-10	4.99E-10	4.40E-10	4.99E-10	4.40E-10	4.99E-10	4.40E-10
¹⁶ O	7.32E-03	4.91E-03	7.40E-03	4.98E-03	7.62E-03	5.23E-03	7.62E-03	5.23E-03	7.62E-03	5.23E-03
¹⁷ O	4.23E-09	4.22E-09	4.16E-09	4.15E-09	4.23E-09	4.22E-09	4.23E-09	4.22E-09	4.23E-09	4.22E-09
¹⁸ O	6.25E-09	6.24E-09	6.26E-09	6.26E-09	6.24E-09	6.24E-09	6.24E-09	6.24E-09	6.24E-09	6.24E-09
¹⁹ F	4.18E-11	4.08E-11	4.18E-11	4.09E-11	1.80E-11	1.70E-11	1.80E-11	1.70E-11	1.80E-11	1.70E-11
²⁰ Ne	1.37E-03	1.16E-03	1.38E-03	1.17E-03	1.41E-03	1.21E-03	1.41E-03	1.21E-03	1.41E-03	1.21E-03
²¹ Ne	1.24E-07	1.07E-07	1.25E-07	1.08E-07	1.22E-07	1.08E-07	1.22E-07	1.08E-07	1.22E-07	1.08E-07
²² Ne	8.56E-08	7.03E-08	8.59E-08	7.05E-08	8.53E-08	7.11E-08	8.53E-08	7.11E-08	8.53E-08	7.11E-08
²³ Na	4.57E-06	4.17E-06	4.58E-06	4.19E-06	4.55E-06	4.23E-06	4.55E-06	4.23E-06	4.55E-06	4.23E-06
²⁴ Mg	5.54E-04	3.91E-04	5.59E-04	3.95E-04	5.50E-04	3.87E-04	5.50E-04	3.87E-04	5.50E-04	3.87E-04
²⁵ Mg	9.14E-07	8.27E-07	9.16E-07	8.28E-07	8.23E-07	7.43E-07	8.23E-07	7.43E-07	8.23E-07	7.43E-07
²⁶ Mg	8.94E-07	8.47E-07	8.95E-07	8.48E-07	9.02E-07	8.54E-07	9.02E-07	8.54E-07	9.02E-07	8.54E-07
²⁶ Al	1.60E-08	1.41E-08	1.63E-08	1.43E-08	1.83E-08	1.15E-08	1.83E-08	1.15E-08	1.83E-08	1.15E-08
²⁷ Al	9.94E-06	7.54E-06	9.96E-06	7.56E-06	1.02E-05	7.49E-06	1.02E-05	7.49E-06	1.02E-05	7.49E-06
²⁸ Si	6.09E-04	3.78E-04	6.48E-04	4.06E-04	5.55E-04	3.49E-04	5.55E-04	3.49E-04	5.55E-04	3.49E-04
²⁹ Si	2.84E-06	1.81E-06	2.88E-06	1.84E-06	2.36E-06	1.50E-06	2.36E-06	1.50E-06	2.36E-06	1.50E-06
³⁰ Si	2.57E-06	1.87E-06	2.58E-06	1.88E-06	2.73E-06	1.85E-06	2.73E-06	1.85E-06	2.73E-06	1.85E-06
³¹ P	9.63E-07	6.98E-07	9.74E-07	7.06E-07	9.85E-07	6.83E-07	9.85E-07	6.83E-07	9.85E-07	6.83E-07
³² S	2.25E-04	1.38E-04	2.38E-04	1.46E-04	2.14E-04	1.35E-04	2.14E-04	1.35E-04	2.14E-04	1.35E-04
³³ S	6.90E-07	3.64E-07	7.33E-07	3.97E-07	6.16E-07	3.54E-07	6.16E-07	3.54E-07	6.16E-07	3.54E-07
³⁴ S	1.27E-06	6.41E-07	1.39E-06	7.29E-07	1.40E-06	7.13E-07	1.40E-06	7.13E-07	1.40E-06	7.13E-07
³⁶ S	3.25E-11	1.91E-11	3.25E-11	1.91E-11	3.25E-11	1.97E-11	3.25E-11	1.97E-11	3.25E-11	1.97E-11
³⁵ Cl	1.67E-07	1.07E-07	1.91E-07	1.25E-07	2.10E-07	1.31E-07	2.10E-07	1.31E-07	2.10E-07	1.31E-07
³⁷ Cl	5.80E-08	2.72E-08	6.86E-08	3.46E-08	7.43E-08	3.87E-08	7.43E-08	3.87E-08	7.43E-08	3.87E-08
³⁶ Ar	3.34E-05	2.10E-05	3.42E-05	2.12E-05	3.46E-05	2.19E-05	3.46E-05	2.19E-05	3.46E-05	2.19E-05
³⁸ Ar	4.35E-07	2.02E-07	6.24E-07	3.29E-07	6.09E-07	2.58E-07	6.09E-07	2.58E-07	6.09E-07	2.58E-07
⁴⁰ Ar	2.06E-13	1.33E-13	2.10E-13	1.37E-13	2.00E-13	1.33E-13	2.00E-13	1.33E-13	2.00E-13	1.33E-13
³⁹ K	7.01E-08	3.03E-08	1.08E-07	5.71E-08	1.02E-07	4.33E-08	1.02E-07	4.33E-08	1.02E-07	4.33E-08
⁴⁰ K	8.63E-12	4.66E-12	9.77E-12	5.44E-12	9.60E-12	5.28E-12	9.60E-12	5.28E-12	9.60E-12	5.28E-12
⁴¹ K	1.15E-08	4.72E-09	1.45E-08	6.74E-09	1.25E-08	5.65E-09	1.25E-08	5.65E-09	1.25E-08	5.65E-09
⁴⁰ Ca	2.71E-05	1.77E-05	2.66E-05	1.69E-05	2.92E-05	1.85E-05	2.92E-05	1.85E-05	2.92E-05	1.85E-05
⁴² Ca	9.76E-09	4.13E-09	1.55E-08	7.88E-09	1.60E-08	5.63E-09	1.60E-08	5.63E-09	1.60E-08	5.63E-09
⁴³ Ca	4.19E-10	3.30E-10	3.87E-10	3.05E-10	8.50E-10	5.80E-10	8.50E-10	5.80E-10	8.50E-10	5.80E-10
⁴⁴ Ca	2.86E-07	1.94E-07	2.33E-07	1.55E-07	6.98E-07	4.00E-07	6.98E-07	4.00E-07	6.98E-07	4.00E-07
⁴⁶ Ca	3.20E-14	2.80E-14	3.78E-14	3.38E-14	2.04E-14	1.77E-14	2.04E-14	1.77E-14	2.04E-14	1.77E-14
⁴⁸ Ca	7.40E-15	7.39E-15	6.30E-15	6.29E-15	3.85E-15	3.85E-15	3.85E-15	3.85E-15	3.85E-15	3.85E-15
⁴⁵ Sc	3.73E-10	1.98E-10	7.31E-10	5.15E-10	1.25E-08	6.35E-09	1.25E-08	6.35E-09	1.25E-08	6.35E-09
⁴⁶ Ti	1.94E-08	1.49E-08	3.08E-08	2.43E-08	3.11E-08	2.21E-08	3.11E-08	2.21E-08	3.11E-08	2.21E-08
⁴⁷ Ti	4.10E-08	3.00E-08	6.41E-08	4.86E-08	4.90E-08	3.88E-08	4.90E-08	3.88E-08	4.90E-08	3.88E-08
⁴⁸ Ti	5.58E-07	4.06E-07	4.62E-07	3.34E-07	9.10E-07	5.76E-07	9.10E-07	5.76E-07	9.10E-07	5.76E-07
⁴⁹ Ti	9.45E-09	7.63E-09	1.33E-08	1.05E-08	6.87E-08	3.94E-08	6.87E-08	3.94E-08	6.87E-08	3.94E-08
⁵⁰ Ti	1.38E-14	1.25E-14	1.33E-14	1.19E-14	7.05E-15	5.30E-15	7.05E-15	5.30E-15	7.05E-15	5.30E-15
⁵⁰ V	7.70E-14	4.89E-14	1.11E-13	7.21E-14	1.35E-13	6.19E-14	1.35E-13	6.19E-14	1.35E-13	6.19E-14

TABLE 7—*Continued*

Species $M_{\text{MS}} \geq 30M_{\odot}$ models “n/p ratio” “low-density” The abundance pattern	A		B		Yields [Mass fractions]	
	No	No	A	B	A	B
	No	No	Yes	Yes	Yes	Yes
	Fig. 5		Fig. 9j		Fig. 10g	
⁵¹ V	6.87E-08	5.36E-08	1.03E-07	8.07E-08	1.23E-07	9.00E-08
⁵⁰ Cr	3.25E-08	2.47E-08	7.81E-08	5.93E-08	1.03E-07	6.57E-08
⁵² Cr	4.66E-06	3.72E-06	4.45E-06	3.53E-06	5.28E-06	3.97E-06
⁵³ Cr	1.75E-07	1.44E-07	2.44E-07	1.96E-07	3.14E-07	2.33E-07
⁵⁴ Cr	1.89E-12	9.63E-13	9.03E-12	6.09E-12	1.14E-11	3.10E-12
⁵⁵ Mn	2.92E-07	2.63E-07	6.64E-07	5.29E-07	7.88E-07	5.88E-07
⁵⁴ Fe	1.64E-06	1.34E-06	5.10E-06	3.82E-06	5.31E-06	3.74E-06
⁵⁶ Fe	3.81E-04	2.89E-04	3.82E-04	2.92E-04	3.91E-04	2.95E-04
⁵⁷ Fe	6.33E-06	4.69E-06	4.98E-06	3.59E-06	5.25E-06	3.73E-06
⁵⁸ Fe	1.32E-12	4.56E-13	4.26E-12	2.48E-12	5.62E-12	1.24E-12
⁵⁹ Co	1.03E-06	7.78E-07	1.58E-06	1.25E-06	2.77E-06	1.94E-06
⁵⁸ Ni	2.33E-06	1.74E-06	2.81E-06	2.13E-06	5.35E-06	3.50E-06
⁶⁰ Ni	1.16E-05	8.52E-06	1.21E-05	8.96E-06	1.38E-05	9.82E-06
⁶¹ Ni	1.86E-07	1.42E-07	1.34E-07	1.01E-07	1.60E-07	1.14E-07
⁶² Ni	1.16E-07	8.64E-08	1.27E-07	9.99E-08	1.61E-07	1.12E-07
⁶⁴ Ni	1.30E-14	1.21E-14	9.99E-15	9.24E-15	7.71E-15	6.32E-15
⁶³ Cu	3.28E-08	2.40E-08	3.93E-08	2.97E-08	6.47E-08	4.41E-08
⁶⁵ Cu	2.38E-09	1.61E-09	1.76E-09	1.16E-09	3.46E-09	2.03E-09
⁶⁴ Zn	1.04E-06	7.43E-07	9.53E-07	6.75E-07	1.83E-06	1.15E-06
⁶⁶ Zn	1.13E-08	7.72E-09	7.09E-09	4.81E-09	2.32E-08	1.35E-08
⁶⁷ Zn	2.96E-10	2.13E-10	2.41E-10	1.73E-10	2.26E-09	1.28E-09
⁶⁸ Zn	4.57E-10	2.87E-10	5.14E-10	3.23E-10	2.75E-10	1.94E-10
⁷⁰ Zn	7.74E-15	7.23E-15	7.44E-15	7.20E-15	5.12E-15	4.64E-15
⁶⁹ Ga	7.83E-11	5.08E-11	8.78E-11	5.67E-11	8.48E-11	5.51E-11
⁷¹ Ga	5.87E-14	5.70E-14	5.44E-14	5.36E-14	1.85E-14	1.74E-14
⁷⁰ Ge	5.90E-11	4.33E-11	5.35E-11	3.90E-11	8.06E-11	5.34E-11
⁷² Ge	3.81E-14	3.40E-14	4.45E-14	4.05E-14	1.34E-14	1.01E-14
⁷³ Ge	4.78E-14	4.56E-14	4.46E-14	4.18E-14	2.23E-14	2.01E-14
⁷⁴ Ge	1.91E-14	1.84E-14	1.50E-14	1.45E-14	8.33E-15	7.80E-15

TABLE 9
THE EXPLOSION MODELS WITH THE Y_e MODIFICATION.

M_{MS}	E_{51}	$M(^{56}\text{Ni})$	$M(\text{Mg})$	$[\text{Fe}/\text{H}]^{\text{a}}$	$[\text{O}/\text{Fe}]$	$[\text{Mg}/\text{Fe}]$	$M_{\text{cut}}(\text{fin})$	$M_{\text{cut}}(\text{ini})$	$M_{\text{mix}}(\text{out})$	f^{b}	The abundance pattern
13	1	0.07	0.09	-2.55	-0.08	0.37	1.57			1	Fig. 9a
15	1	0.07	0.07	-2.55	0.15	0.27	1.48			1	Fig. 9b
18	1	0.07	0.16	-2.55	0.40	0.63	1.65			1	Fig. 9c
20	10	0.08	0.17	-3.34	0.50	0.58	1.88	1.52	2.02	0.28	Fig. 9d
25	5	0.10	0.14	-2.98	0.50	0.41	2.39	1.79	2.61	0.27	Fig. 9i
25	10	0.10	0.16	-3.25	0.50	0.48	2.90	1.79	2.99	0.07	Fig. 9e
30A	20	0.16	0.22	-3.31	0.50	0.41	3.27	1.65	3.59	0.17	Fig. 9f
30B	20	0.05	0.04	-3.82	0.55	0.20	6.73	1.65	7.01	0.05	Fig. 9f
40A	30	0.26	0.34	-3.26	0.50	0.39	5.53	2.24	6.00	0.12	Fig. 9g
40B	30	0.11	0.09	-3.63	0.46	0.20	10.70	2.24	11.16	0.05	Fig. 9g
50A	40	0.36	0.57	-3.22	0.50	0.47	3.51	1.89	4.15	0.28	Fig. 9h
50B	40	0.24	0.20	-3.40	0.35	0.20	10.99	1.89	13.05	0.18	Fig. 9h

^a $[\text{Fe}/\text{H}]$ is determined as $[\text{Fe}/\text{H}] \simeq \log_{10}(M(\text{Fe})/E_{51}^{6/7}) - C$. Here we assume that C is a constant value, $C = 1.4$.

^b f is an ejection factor. $f = 1$ corresponds to normal SN models without the mixing-fallback model.

NOTE.—Same as Table 1, but for models applied the Y_e modification described in § 5.

TABLE 11
YIELDS OF STABLE ISOTOPES FOR THE MODELS WITH THE Y_e MODIFICATION.

Species Mass [M_\odot] E_{51}	Yields [M_\odot]											
	13 1	15 1	18 1	20 10	25 5	25 10	30A 20	30B 20	40A 30	40B 30	50A 40	50B 40
p	6.59E+00	7.58E+00	8.43E+00	8.77E+00	1.06E+01	1.05E+01	1.17E+01	1.17E+01	1.40E+01	1.40E+01	1.63E+01	1.63E+01
d	1.49E-16	1.69E-16	1.28E-16	8.66E-17	2.04E-16	2.06E-16	1.09E-14	1.09E-14	1.66E-14	1.66E-14	1.24E-15	1.24E-15
³ He	4.12E-05	4.09E-05	3.33E-05	4.76E-05	2.11E-04	2.11E-04	2.06E-04	2.06E-04	2.56E-05	2.56E-05	2.86E-05	2.86E-05
⁴ He	4.01E+00	4.40E+00	5.42E+00	5.96E+00	8.03E+00	7.82E+00	9.54E+00	9.51E+00	1.18E+01	1.18E+01	1.56E+01	1.55E+01
⁶ Li	3.65E-23	1.11E-22	4.37E-23	1.36E-22	2.28E-20	2.72E-20	3.50E-17	3.50E-17	5.39E-17	5.39E-17	2.02E-18	2.02E-18
⁷ Li	2.17E-10	2.94E-10	7.34E-11	2.79E-10	5.68E-09	5.12E-09	2.36E-08	2.36E-08	3.42E-11	3.42E-11	8.78E-12	8.78E-12
⁹ Be	1.77E-20	3.22E-22	1.05E-22	4.83E-20	5.00E-17	3.96E-17	3.09E-18	3.09E-18	9.03E-18	9.03E-18	6.04E-17	6.04E-17
¹⁰ B	2.92E-21	8.30E-20	3.92E-21	2.88E-19	2.79E-15	8.28E-14	2.95E-14	2.95E-14	1.41E-14	1.41E-14	1.51E-17	5.27E-18
¹¹ B	2.94E-16	3.30E-16	7.14E-16	1.09E-15	5.91E-14	1.06E-12	6.84E-13	6.80E-13	3.25E-13	3.24E-13	2.98E-14	5.55E-15
¹² C	7.41E-02	1.72E-01	2.18E-01	1.90E-01	2.79E-01	2.86E-01	3.16E-01	2.86E-01	3.72E-01	3.51E-01	1.56E+00	1.17E+00
¹³ C	8.39E-08	6.21E-08	2.63E-09	1.18E-08	2.90E-08	7.43E-08	6.32E-08	6.03E-08	8.19E-08	7.85E-08	2.38E-07	1.70E-07
¹⁴ N	1.83E-03	1.86E-03	1.89E-04	5.42E-05	5.92E-04	5.29E-04	4.18E-05	4.17E-05	3.39E-06	3.33E-06	4.38E-04	4.37E-04
¹⁵ N	6.38E-08	6.86E-08	2.40E-08	2.95E-08	1.64E-07	1.73E-07	2.20E-07	1.16E-07	6.54E-07	6.51E-07	3.30E-07	8.15E-08
¹⁶ O	4.50E-01	7.73E-01	1.38E+00	2.03E+00	2.60E+00	2.55E+00	3.92E+00	1.37E+00	6.32E+00	2.40E+00	8.86E+00	4.04E+00
¹⁷ O	1.69E-06	1.57E-06	2.79E-07	7.13E-08	1.49E-06	1.33E-06	3.81E-08	2.64E-08	1.23E-08	8.65E-09	8.60E-06	8.56E-06
¹⁸ O	5.79E-08	4.89E-06	4.63E-06	2.33E-08	4.66E-07	4.15E-07	5.03E-07	5.02E-07	2.93E-07	2.92E-07	6.00E-06	5.99E-06
¹⁹ F	1.17E-10	1.97E-09	7.91E-09	2.12E-09	1.43E-09	1.77E-09	7.88E-09	6.41E-09	1.17E-07	1.16E-07	8.49E-09	4.07E-09
²⁰ Ne	1.53E-02	3.27E-01	4.94E-01	7.49E-01	3.91E-01	3.06E-01	5.20E-01	2.64E-01	2.64E-01	2.19E-01	2.48E+00	1.30E+00
²¹ Ne	5.42E-07	3.76E-05	9.12E-05	3.58E-05	1.47E-05	1.31E-05	3.51E-05	2.26E-05	1.41E-05	1.07E-05	2.40E-04	1.15E-04
²² Ne	1.98E-07	1.61E-05	2.57E-05	5.51E-05	1.30E-05	9.24E-06	3.52E-05	1.98E-05	1.66E-05	1.45E-05	2.10E-04	1.08E-04
²³ Na	1.44E-04	2.45E-03	2.08E-03	2.31E-03	6.74E-04	4.74E-04	7.36E-04	3.24E-04	3.28E-04	1.66E-04	4.27E-03	1.99E-03
²⁴ Mg	8.62E-02	6.82E-02	1.57E-01	1.65E-01	1.43E-01	1.64E-01	2.17E-01	4.20E-02	3.37E-01	9.00E-02	5.70E-01	1.97E-01
²⁵ Mg	1.56E-04	2.98E-04	5.83E-04	1.07E-04	4.52E-05	4.90E-05	1.45E-04	9.00E-05	5.95E-04	4.11E-04	3.10E-04	1.17E-04
²⁶ Mg	7.07E-05	3.98E-04	8.73E-04	2.09E-04	4.31E-05	4.17E-05	8.00E-05	2.62E-05	6.90E-05	1.23E-05	2.32E-04	9.73E-05
²⁶ Al	1.01E-06	1.14E-06	3.34E-06	1.32E-06	1.22E-06	1.40E-06	3.01E-06	1.36E-06	3.80E-05	3.43E-05	5.37E-06	1.34E-06
²⁷ Al	3.78E-03	1.37E-03	3.14E-03	1.50E-03	8.59E-04	9.58E-04	1.55E-03	1.59E-04	7.52E-03	1.34E-03	3.29E-03	8.12E-04
²⁸ Si	8.04E-02	7.32E-02	1.16E-01	1.03E-01	2.62E-01	2.41E-01	2.47E-01	3.17E-02	7.20E-01	2.29E-01	4.77E-01	1.25E-01
²⁹ Si	7.50E-04	2.39E-04	4.42E-04	2.95E-04	5.15E-04	5.77E-04	8.85E-04	4.90E-05	3.72E-03	1.29E-03	9.96E-04	1.91E-04
³⁰ Si	1.42E-03	1.50E-04	3.45E-04	1.15E-04	5.88E-05	6.90E-05	1.49E-04	1.06E-05	2.82E-03	4.84E-04	2.20E-04	5.21E-05
³¹ P	4.88E-04	5.65E-05	1.32E-04	7.79E-05	5.34E-05	6.38E-05	1.17E-04	7.55E-06	1.01E-03	2.24E-04	2.13E-04	4.61E-05
³² S	2.37E-02	3.20E-02	4.07E-02	4.27E-02	1.18E-01	9.43E-02	8.49E-02	1.48E-02	2.59E-01	6.11E-02	2.00E-01	6.03E-02
³³ S	8.98E-05	7.55E-05	1.03E-04	1.44E-04	2.15E-04	2.47E-04	3.02E-04	1.61E-05	8.45E-04	1.29E-04	5.42E-04	1.02E-04
³⁴ S	2.81E-04	2.03E-04	2.85E-04	1.89E-04	5.43E-05	1.37E-04	2.75E-04	1.92E-05	2.09E-03	1.34E-04	5.94E-04	1.32E-04
³⁶ S	1.48E-08	1.43E-09	5.34E-09	8.33E-10	6.69E-11	5.77E-11	1.41E-09	7.84E-11	5.04E-08	2.66E-09	5.58E-11	1.04E-11
³⁵ Cl	5.54E-05	1.56E-05	2.69E-05	4.28E-05	2.33E-05	3.70E-05	4.98E-05	7.51E-06	1.82E-04	2.58E-05	1.50E-04	5.16E-05
³⁷ Cl	3.04E-06	5.83E-06	9.12E-06	1.89E-05	2.54E-05	3.10E-05	2.39E-05	1.35E-06	7.96E-05	4.48E-06	7.61E-05	1.46E-05
³⁶ Ar	3.24E-03	5.28E-03	5.67E-03	6.79E-03	1.86E-02	1.38E-02	1.15E-02	2.59E-03	3.55E-02	5.86E-03	3.06E-02	1.05E-02
³⁸ Ar	5.30E-05	6.32E-05	1.70E-04	1.28E-04	4.98E-05	1.84E-04	9.20E-05	6.00E-06	7.84E-04	4.22E-05	8.75E-04	1.67E-04
⁴⁰ Ar	8.01E-11	1.78E-11	3.96E-11	3.79E-11	5.17E-12	6.41E-12	1.95E-11	3.51E-12	2.77E-10	2.93E-11	3.64E-12	6.74E-13
³⁹ K	5.74E-06	8.88E-06	1.98E-05	2.54E-05	2.27E-05	4.25E-05	2.38E-05	3.90E-06	1.33E-04	1.17E-05	1.71E-04	4.44E-05
⁴⁰ K	1.14E-09	9.10E-10	1.96E-09	4.40E-09	1.84E-09	1.51E-09	2.52E-09	1.34E-10	1.18E-08	6.21E-10	5.89E-09	1.09E-09
⁴¹ K	3.54E-07	8.05E-07	1.72E-06	3.73E-06	6.75E-06	6.94E-06	3.66E-06	2.15E-07	2.13E-05	1.20E-06	1.43E-05	2.82E-06
⁴⁰ Ca	2.92E-03	4.41E-03	4.40E-03	4.77E-03	1.49E-02	1.02E-02	8.22E-03	2.25E-03	2.86E-02	5.18E-03	2.22E-02	8.98E-03

TABLE 11—*Continued*

Species Mass [M_{\odot}]	Yields [M_{\odot}]											
	13 1	15 1	18 1	20 10	25 5	25 10	30A 20	30B 20	40A 30	40B 30	50A 40	50B 40
⁴² Ca	9.77E-07	1.23E-06	3.62E-06	3.41E-06	1.29E-06	5.53E-06	1.62E-06	8.49E-08	1.97E-05	1.03E-06	2.75E-05	5.08E-06
⁴³ Ca	6.75E-08	4.58E-08	3.65E-08	2.06E-07	5.54E-08	9.96E-08	1.68E-07	5.18E-08	1.50E-07	5.83E-08	4.79E-07	3.10E-07
⁴⁴ Ca	9.55E-06	1.19E-05	8.75E-06	1.09E-04	2.86E-05	5.25E-05	1.49E-04	4.63E-05	1.53E-04	6.28E-05	5.37E-04	3.51E-04
⁴⁶ Ca	1.07E-12	1.76E-12	9.27E-12	1.15E-11	2.61E-12	2.66E-11	8.42E-12	6.77E-12	4.61E-11	3.37E-11	1.04E-12	1.93E-13
⁴⁸ Ca	1.14E-17	4.21E-14	4.17E-16	5.74E-16	8.89E-12	1.08E-11	5.76E-13	5.72E-13	6.20E-12	6.20E-12	7.67E-14	1.42E-14
⁴⁵ Sc	2.09E-08	4.00E-08	5.52E-08	7.30E-07	2.51E-07	2.32E-07	6.85E-08	1.29E-08	6.27E-07	4.89E-08	5.89E-07	1.59E-07
⁴⁶ Ti	8.17E-06	4.97E-06	4.96E-06	1.09E-05	3.38E-06	7.57E-06	8.92E-06	2.65E-06	1.21E-05	2.42E-06	3.38E-05	1.58E-05
⁴⁷ Ti	1.22E-05	8.51E-06	7.79E-06	1.86E-05	1.27E-05	1.82E-05	3.21E-05	9.99E-06	3.18E-05	1.34E-05	8.35E-05	5.47E-05
⁴⁸ Ti	5.66E-05	7.32E-05	7.18E-05	1.23E-04	1.06E-04	1.13E-04	2.36E-04	7.36E-05	3.13E-04	1.31E-04	6.41E-04	4.20E-04
⁴⁹ Ti	2.26E-06	3.30E-06	2.99E-06	3.80E-06	4.13E-06	3.30E-06	5.62E-06	1.75E-06	6.87E-06	2.70E-06	8.37E-06	5.26E-06
⁵⁰ Ti	1.18E-12	9.55E-13	1.72E-12	9.35E-13	1.92E-12	3.02E-12	1.61E-12	1.26E-12	3.10E-11	2.68E-11	1.10E-12	2.03E-13
⁵⁰ V	1.35E-11	1.05E-11	4.60E-11	2.62E-11	8.16E-12	2.88E-11	9.04E-12	7.27E-13	1.13E-10	2.06E-11	1.42E-10	2.63E-11
⁵¹ V	2.00E-05	1.60E-05	1.41E-05	4.05E-05	1.63E-05	2.55E-05	4.90E-05	1.53E-05	3.91E-05	1.63E-05	1.11E-04	7.21E-05
⁵⁰ Cr	1.07E-05	1.61E-05	2.64E-05	1.98E-05	3.29E-05	2.60E-05	1.96E-05	5.88E-06	4.13E-05	9.90E-06	8.80E-05	2.88E-05
⁵² Cr	8.84E-04	1.09E-03	1.13E-03	6.89E-04	1.31E-03	1.17E-03	1.57E-03	4.89E-04	2.75E-03	1.16E-03	3.17E-03	2.07E-03
⁵³ Cr	4.96E-05	6.76E-05	6.43E-05	3.34E-05	7.78E-05	6.64E-05	9.04E-05	2.82E-05	1.31E-04	5.46E-05	1.43E-04	8.85E-05
⁵⁴ Cr	2.35E-10	4.13E-10	3.25E-09	2.61E-09	4.15E-10	6.12E-09	9.16E-11	7.16E-12	3.52E-09	2.17E-10	2.76E-08	5.11E-09
⁵⁵ Mn	1.33E-04	1.86E-04	1.74E-04	8.17E-05	2.22E-04	1.86E-04	2.47E-04	7.70E-05	3.69E-04	1.50E-04	3.88E-04	2.25E-04
⁵⁴ Fe	7.29E-04	1.24E-03	1.40E-03	7.18E-04	2.79E-03	1.73E-03	1.74E-03	5.41E-04	3.30E-03	1.09E-03	4.66E-03	1.93E-03
⁵⁶ Fe	7.00E-02	7.00E-02	7.00E-02	8.27E-02	1.04E-01	1.03E-01	1.60E-01	4.97E-02	2.56E-01	1.08E-01	3.59E-01	2.35E-01
⁵⁷ Fe	7.33E-04	6.88E-04	6.60E-04	1.13E-03	1.26E-03	1.40E-03	2.43E-03	7.57E-04	3.80E-03	1.60E-03	6.10E-03	3.99E-03
⁵⁸ Fe	5.67E-11	1.76E-10	8.07E-10	1.28E-09	7.15E-10	2.77E-09	9.22E-11	6.69E-12	3.30E-09	2.25E-10	1.26E-08	2.32E-09
⁵⁹ Co	2.77E-04	3.02E-04	2.30E-04	6.42E-04	2.73E-04	3.57E-04	7.19E-04	2.24E-04	6.15E-04	2.59E-04	1.77E-03	1.16E-03
⁵⁸ Ni	4.06E-04	4.57E-04	3.85E-04	9.68E-04	6.60E-04	8.66E-04	1.32E-03	4.12E-04	1.46E-03	5.67E-04	3.31E-03	2.08E-03
⁶⁰ Ni	2.18E-03	1.68E-03	1.65E-03	2.97E-03	2.94E-03	3.29E-03	5.60E-03	1.75E-03	8.50E-03	3.58E-03	1.30E-02	8.49E-03
⁶¹ Ni	2.56E-05	1.72E-05	1.46E-05	4.06E-05	2.50E-05	3.68E-05	6.21E-05	1.94E-05	8.14E-05	3.43E-05	1.57E-04	1.03E-04
⁶² Ni	1.94E-05	1.51E-05	1.24E-05	3.99E-05	1.97E-05	6.66E-05	5.26E-05	1.64E-05	6.26E-05	2.64E-05	1.38E-04	9.04E-05
⁶⁴ Ni	2.14E-15	1.01E-13	1.07E-14	8.67E-13	3.73E-12	7.27E-12	3.59E-12	2.59E-12	1.78E-11	1.78E-11	5.33E-12	9.92E-13
⁶³ Cu	6.24E-06	5.46E-06	4.49E-06	1.53E-05	6.84E-06	9.48E-06	1.90E-05	5.92E-06	2.10E-05	8.84E-06	5.10E-05	3.34E-05
⁶⁵ Cu	1.40E-07	1.23E-07	1.17E-07	4.78E-07	3.64E-07	4.84E-07	1.03E-06	3.21E-07	1.62E-06	6.81E-07	3.10E-06	2.03E-06
⁶⁴ Zn	1.10E-04	9.81E-05	8.47E-05	3.34E-04	1.86E-04	2.49E-04	5.29E-04	1.65E-04	6.57E-04	2.77E-04	1.43E-03	9.37E-04
⁶⁶ Zn	4.49E-07	4.05E-07	3.65E-07	2.53E-06	1.06E-06	2.47E-06	4.19E-06	1.31E-06	5.33E-06	2.25E-06	1.29E-05	8.47E-06
⁶⁷ Zn	1.49E-08	1.59E-08	1.27E-08	1.56E-07	2.36E-08	4.92E-08	1.53E-07	4.78E-08	1.03E-07	4.36E-08	4.35E-07	2.85E-07
⁶⁸ Zn	2.54E-08	3.22E-08	3.43E-08	1.15E-07	1.20E-07	1.32E-07	3.10E-07	9.66E-08	5.03E-07	2.12E-07	1.13E-06	7.40E-07
⁷⁰ Zn	5.95E-16	3.56E-14	6.44E-15	1.08E-13	2.03E-13	2.15E-12	7.54E-13	4.92E-13	2.23E-11	2.23E-11	1.96E-12	3.68E-13
⁶⁹ Ga	7.27E-09	6.01E-09	5.58E-09	2.02E-08	1.95E-08	2.44E-08	4.77E-08	1.49E-08	9.52E-08	4.02E-08	1.40E-07	9.15E-08
⁷¹ Ga	7.45E-15	1.01E-13	1.65E-14	1.49E-12	1.58E-12	3.17E-11	6.77E-12	5.92E-12	1.39E-10	1.39E-10	5.49E-12	1.08E-12
⁷⁰ Ge	7.35E-09	4.76E-09	3.96E-09	2.03E-08	8.99E-09	1.64E-08	2.66E-08	8.27E-09	3.59E-08	1.52E-08	7.31E-08	4.78E-08
⁷² Ge	1.71E-14	7.98E-13	5.75E-13	5.96E-12	2.82E-12	3.08E-11	6.76E-12	3.15E-12	8.47E-11	8.45E-11	3.54E-11	6.59E-12
⁷³ Ge	1.34E-14	1.19E-13	1.10E-13	3.68E-12	5.53E-12	2.78E-11	1.17E-11	8.68E-12	9.33E-11	9.32E-11	2.28E-11	4.28E-12
⁷⁴ Ge	2.49E-15	1.21E-13	4.90E-14	2.02E-13	1.16E-12	8.92E-12	2.57E-12	2.05E-12	3.65E-11	3.64E-11	3.88E-12	7.32E-13

TABLE 13
YIELDS OF UNSTABLE ISOTOPES FOR THE MODELS WITH THE Y_e MODIFICATION.

Species Mass [M_\odot] E_{51}	Yields [M_\odot]											
	13 1	15 1	18 1	20 10	25 5	25 10	30A 20	30B 20	40A 30	40B 30	50A 40	50B 40
^{22}Na	1.51E-07	7.70E-06	1.68E-05	4.65E-05	9.97E-06	7.01E-06	2.70E-05	1.34E-05	1.37E-05	1.19E-05	1.77E-04	9.14E-05
^{26}Al	9.84E-07	1.12E-06	3.33E-06	9.81E-07	1.21E-06	1.37E-06	2.92E-06	1.33E-06	2.13E-05	1.76E-05	5.24E-06	1.26E-06
^{41}Ca	3.54E-07	8.05E-07	1.72E-06	3.73E-06	6.75E-06	6.94E-06	3.66E-06	2.15E-07	2.13E-05	1.20E-06	1.43E-05	2.82E-06
^{44}Ti	9.55E-06	1.19E-05	8.75E-06	1.09E-04	2.86E-05	5.25E-05	1.49E-04	4.63E-05	1.53E-04	6.28E-05	5.37E-04	3.51E-04
^{60}Fe	4.74E-16	7.17E-14	3.78E-15	1.09E-13	1.53E-13	2.37E-12	1.68E-12	1.11E-12	2.40E-11	2.40E-11	7.78E-13	1.45E-13
^{56}Ni	7.00E-02	7.00E-02	7.00E-02	8.27E-02	1.04E-01	1.03E-01	1.60E-01	4.97E-02	2.56E-01	1.08E-01	3.59E-01	2.35E-01
^{57}Ni	7.33E-04	6.88E-04	6.60E-04	1.13E-03	1.26E-03	1.40E-03	2.43E-03	7.56E-04	3.80E-03	1.60E-03	6.09E-03	3.99E-03

TABLE 15
THE EXPLOSION MODELS WITH THE Y_e AND “LOW-DENSITY” MODIFICATIONS.

M_{MS}	E_{51}	$M(^{56}\text{Ni})$	$M(\text{Mg})$	$[\text{Fe}/\text{H}]^{\text{a}}$	$[\text{O}/\text{Fe}]$	$[\text{Mg}/\text{Fe}]$	$M_{\text{cut}}(\text{fin})$	$M_{\text{cut}}(\text{ini})$	$M_{\text{mix}}(\text{out})$	f^{b}	“low-density” factor	The abundance pattern
20	10	0.08	0.16	-3.33	0.50	0.56	1.83	1.52	2.01	0.37	1/2	Fig. 10a
25	5	0.11	0.14	-2.95	0.50	0.35	2.08	1.79	2.38	0.51	1/4	Fig. 10f
25	10	0.10	0.14	-3.25	0.50	0.41	2.67	1.79	2.92	0.22	1/3	Fig. 10b
30A	20	0.16	0.21	-3.31	0.50	0.38	2.97	1.65	3.42	0.25	1/3	Fig. 10c
30B	20	0.05	0.04	-3.86	0.64	0.20	6.50	1.65	6.87	0.07	1/3	Fig. 10c
40A	30	0.28	0.38	-3.22	0.50	0.40	4.80	2.24	5.53	0.22	1/4	Fig. 10d
40B	30	0.12	0.10	-3.59	0.49	0.20	10.09	2.24	10.92	0.10	1/4	Fig. 10d
50A	40	0.37	0.51	-3.20	0.50	0.42	3.18	1.89	3.99	0.39	1/2	Fig. 10e
50B	40	0.26	0.22	-3.36	0.38	0.20	9.80	1.89	12.74	0.27	1/2	Fig. 10e

^a $[\text{Fe}/\text{H}]$ is determined as $[\text{Fe}/\text{H}] \simeq \log_{10}(M(\text{Fe})/E_{51}^{6/7}) - C$. Here we assume that C is a constant value, $C = 1.4$.

^b f is an ejection factor.

NOTE.—Same as Table 1, but for models applied the Y_e and “low-density” modifications described in § 5.

TABLE 17

YIELDS OF STABLE ISOTOPES FOR THE MODELS WITH THE Y_e AND “LOW-DENSITY” MODIFICATIONS.

Species Mass [M_\odot]	Yields [M_\odot]								
	20 10	25 5	25 10	30A 20	30B 20	40A 30	40B 30	50A 40	50B 40
p	8.77E+00	1.06E+01	1.06E+01	1.17E+01	1.17E+01	1.40E+01	1.40E+01	1.63E+01	1.63E+01
d	8.66E-17	2.10E-16	2.17E-16	4.19E-14	4.19E-14	4.43E-12	4.43E-12	1.23E-15	1.23E-15
³ He	4.76E-05	2.11E-04	2.11E-04	2.06E-04	2.06E-04	2.56E-05	2.56E-05	2.86E-05	2.86E-05
⁴ He	5.98E+00	8.07E+00	8.06E+00	9.64E+00	9.55E+00	1.21E+01	1.20E+01	1.57E+01	1.57E+01
⁶ Li	1.22E-22	3.06E-20	7.78E-20	1.37E-16	1.37E-16	1.47E-14	1.47E-14	2.00E-18	2.00E-18
⁷ Li	2.79E-10	5.68E-09	5.68E-09	2.36E-08	2.36E-08	3.50E-11	3.50E-11	8.78E-12	8.78E-12
⁹ Be	1.16E-20	3.12E-17	2.90E-17	6.90E-18	6.90E-18	6.87E-16	6.87E-16	9.43E-17	9.43E-17
¹⁰ B	2.59E-19	1.95E-15	3.81E-15	5.17E-16	5.17E-16	2.20E-14	2.20E-14	9.04E-18	4.50E-18
¹¹ B	9.41E-16	7.26E-15	5.42E-13	3.94E-14	3.44E-14	6.67E-13	6.65E-13	1.13E-14	3.13E-15
¹² C	1.95E-01	2.91E-01	2.77E-01	3.25E-01	2.90E-01	4.26E-01	4.15E-01	1.61E+00	1.24E+00
¹³ C	9.95E-09	3.83E-08	7.78E-08	4.32E-08	4.14E-08	1.05E-07	1.04E-07	4.37E-07	3.75E-07
¹⁴ N	5.43E-05	5.91E-04	5.93E-04	4.07E-05	4.05E-05	8.90E-06	8.70E-06	4.37E-04	4.37E-04
¹⁵ N	3.27E-08	1.77E-07	1.78E-07	2.13E-07	1.05E-07	7.01E-07	6.98E-07	3.05E-07	9.60E-08
¹⁶ O	2.05E+00	2.79E+00	2.50E+00	4.03E+00	1.54E+00	6.96E+00	2.85E+00	9.07E+00	4.80E+00
¹⁷ O	7.06E-08	1.49E-06	1.49E-06	4.74E-08	3.59E-08	5.24E-09	3.71E-09	8.60E-06	8.57E-06
¹⁸ O	2.34E-08	5.27E-07	3.90E-07	2.71E-07	2.70E-07	3.01E-07	3.00E-07	6.80E-06	6.79E-06
¹⁹ F	2.01E-09	1.49E-09	1.42E-09	7.54E-09	5.99E-09	2.97E-08	2.94E-08	9.35E-09	4.56E-09
²⁰ Ne	7.61E-01	4.24E-01	3.05E-01	5.58E-01	2.86E-01	3.06E-01	2.70E-01	2.48E+00	1.43E+00
²¹ Ne	3.44E-05	9.09E-06	7.92E-06	3.66E-05	2.67E-05	1.31E-05	1.13E-05	2.35E-04	1.31E-04
²² Ne	5.61E-05	1.45E-05	9.07E-06	3.94E-05	2.30E-05	6.34E-06	5.16E-06	2.15E-04	1.25E-04
²³ Na	2.33E-03	7.58E-04	4.70E-04	7.75E-04	3.92E-04	1.31E-04	7.59E-05	4.24E-03	2.32E-03
²⁴ Mg	1.62E-01	1.35E-01	1.38E-01	2.09E-01	3.80E-02	3.79E-01	1.01E-01	5.12E-01	2.18E-01
²⁵ Mg	1.05E-04	3.47E-05	3.41E-05	1.36E-04	8.47E-05	2.97E-04	1.20E-04	2.96E-04	1.41E-04
²⁶ Mg	2.09E-04	4.74E-05	4.12E-05	8.67E-05	3.03E-05	8.55E-05	2.49E-05	2.34E-04	1.16E-04
²⁶ Al	5.29E-06	4.59E-06	4.35E-06	1.17E-05	3.51E-06	2.02E-05	8.02E-06	1.41E-05	8.44E-06
²⁷ Al	1.48E-03	8.44E-04	8.72E-04	1.58E-03	1.91E-04	8.56E-03	1.12E-03	2.98E-03	1.01E-03
²⁸ Si	9.31E-02	2.83E-01	1.96E-01	2.52E-01	3.31E-02	4.69E-01	9.11E-02	4.21E-01	1.48E-01
²⁹ Si	2.69E-04	3.71E-04	4.48E-04	7.86E-04	5.88E-05	2.27E-03	2.37E-04	7.59E-04	2.16E-04
³⁰ Si	1.20E-04	7.69E-05	6.95E-05	2.05E-04	1.90E-05	3.29E-03	3.60E-04	2.28E-04	8.25E-05
³¹ P	8.11E-05	9.14E-05	6.23E-05	1.58E-04	1.53E-05	9.93E-04	1.16E-04	2.19E-04	7.74E-05
³² S	3.91E-02	1.21E-01	7.70E-02	1.03E-01	1.77E-02	1.77E-01	4.24E-02	2.01E-01	7.70E-02
³³ S	1.44E-04	2.45E-04	1.76E-04	2.55E-04	1.92E-05	5.77E-04	5.79E-05	5.59E-04	1.58E-04
³⁴ S	1.61E-04	3.50E-04	5.51E-05	5.32E-04	4.36E-05	1.98E-03	2.00E-04	4.74E-04	1.57E-04
³⁶ S	7.55E-10	1.39E-10	6.81E-11	1.23E-09	9.11E-11	5.07E-08	4.88E-09	6.52E-11	1.78E-11
³⁵ Cl	4.57E-05	6.31E-05	2.78E-05	9.85E-05	1.47E-05	1.93E-04	3.76E-05	1.61E-04	8.00E-05
³⁷ Cl	2.21E-05	4.01E-05	2.24E-05	4.52E-05	6.46E-06	7.46E-05	1.59E-05	9.19E-05	2.76E-05
³⁶ Ar	6.53E-03	1.82E-02	1.24E-02	1.82E-02	3.56E-03	2.95E-02	8.45E-03	3.33E-02	1.40E-02
³⁸ Ar	7.42E-05	4.06E-04	2.64E-05	4.97E-04	3.75E-05	5.92E-04	6.04E-05	6.26E-04	1.74E-04
⁴⁰ Ar	3.64E-11	1.44E-11	2.59E-12	2.12E-11	2.17E-12	2.45E-10	2.47E-11	5.33E-12	1.44E-12
³⁹ K	1.69E-05	6.74E-05	1.22E-05	9.09E-05	8.93E-06	9.57E-05	1.41E-05	1.14E-04	4.14E-05
⁴⁰ K	4.18E-09	7.13E-09	8.73E-10	5.14E-09	3.66E-10	9.05E-09	8.66E-10	5.80E-09	1.57E-09
⁴¹ K	3.41E-06	1.06E-05	3.71E-06	7.99E-06	6.40E-07	1.30E-05	1.41E-06	1.62E-05	4.52E-06
⁴⁰ Ca	4.73E-03	1.34E-02	1.01E-02	1.62E-02	3.41E-03	2.70E-02	8.62E-03	2.40E-02	1.18E-02
⁴² Ca	1.70E-06	8.77E-06	5.14E-07	1.63E-05	1.16E-06	1.47E-05	1.40E-06	2.05E-05	5.57E-06
⁴³ Ca	4.60E-07	2.69E-07	2.02E-07	5.68E-07	1.57E-07	6.15E-07	2.58E-07	9.35E-07	6.54E-07
⁴⁴ Ca	2.05E-04	1.68E-04	1.51E-04	4.93E-04	1.37E-04	8.70E-04	3.69E-04	1.26E-03	8.82E-04
⁴⁶ Ca	1.12E-11	5.12E-12	8.54E-12	2.78E-12	9.64E-13	1.69E-11	9.43E-12	1.55E-12	4.20E-13
⁴⁸ Ca	2.53E-15	1.03E-11	7.92E-12	4.12E-13	4.02E-13	1.71E-12	1.71E-12	3.57E-14	9.67E-15
⁴⁵ Sc	3.20E-06	2.66E-06	3.03E-06	1.13E-05	3.11E-06	1.94E-05	8.13E-06	5.44E-06	3.61E-06
⁴⁶ Ti	8.04E-06	8.24E-06	3.69E-06	1.71E-05	3.07E-06	1.49E-05	4.41E-06	2.69E-05	1.44E-05
⁴⁷ Ti	1.42E-05	1.01E-05	8.39E-06	1.98E-05	5.51E-06	2.25E-05	9.55E-06	5.79E-05	4.07E-05
⁴⁸ Ti	2.30E-04	2.53E-04	2.13E-04	5.35E-04	1.49E-04	1.03E-03	4.39E-04	1.29E-03	9.07E-04
⁴⁹ Ti	1.71E-05	1.86E-05	1.71E-05	5.02E-05	1.39E-05	9.38E-05	3.98E-05	5.62E-05	3.93E-05
⁵⁰ Ti	5.55E-13	1.75E-12	3.58E-12	1.93E-12	8.27E-13	7.21E-12	2.65E-12	1.69E-12	4.57E-13
⁵⁰ V	1.49E-11	9.90E-11	1.07E-11	1.17E-10	9.31E-12	1.05E-10	1.23E-11	1.44E-10	3.89E-11
⁵¹ V	4.18E-05	3.70E-05	2.84E-05	6.22E-05	1.72E-05	8.21E-05	3.48E-05	1.31E-04	9.20E-05

TABLE 17—*Continued*

Species Mass [M_{\odot}] E_{51}	Yields [M_{\odot}]								
	20 10	25 5	25 10	30A 20	30B 20	40A 30	40B 30	50A 40	50B 40
⁵⁰ Cr	2.08E-05	4.53E-05	2.01E-05	7.01E-05	1.30E-05	7.56E-05	2.71E-05	7.67E-05	4.10E-05
⁵² Cr	8.68E-04	1.57E-03	1.33E-03	1.87E-03	5.20E-04	4.58E-03	1.95E-03	3.99E-03	2.81E-03
⁵³ Cr	4.44E-05	1.13E-04	9.41E-05	1.21E-04	3.25E-05	2.77E-04	1.17E-04	1.79E-04	1.24E-04
⁵⁴ Cr	2.90E-10	9.47E-09	9.93E-11	1.93E-08	1.37E-09	3.51E-09	3.43E-10	1.59E-08	4.29E-09
⁵⁵ Mn	9.23E-05	2.87E-04	2.26E-04	3.33E-04	8.60E-05	6.30E-04	2.65E-04	3.98E-04	2.68E-04
⁵⁴ Fe	5.65E-04	2.42E-03	1.47E-03	2.94E-03	6.02E-04	3.70E-03	1.42E-03	2.83E-03	1.69E-03
⁵⁶ Fe	8.41E-02	1.13E-01	1.01E-01	1.62E-01	4.51E-02	2.81E-01	1.20E-01	3.71E-01	2.61E-01
⁵⁷ Fe	1.27E-03	1.46E-03	1.38E-03	2.67E-03	7.43E-04	4.27E-03	1.82E-03	6.23E-03	4.38E-03
⁵⁸ Fe	3.22E-10	2.92E-09	1.73E-10	9.60E-09	6.86E-10	2.97E-09	2.99E-10	6.81E-09	1.84E-09
⁵⁹ Co	9.29E-04	9.93E-04	8.51E-04	1.56E-03	4.36E-04	2.19E-03	9.33E-04	3.27E-03	2.30E-03
⁵⁸ Ni	1.54E-03	1.79E-03	1.65E-03	3.39E-03	9.28E-04	5.04E-03	2.12E-03	6.20E-03	4.31E-03
⁶⁰ Ni	3.51E-03	3.60E-03	3.30E-03	7.41E-03	2.07E-03	1.06E-02	4.53E-03	1.59E-02	1.12E-02
⁶¹ Ni	4.93E-05	4.33E-05	3.71E-05	8.34E-05	2.33E-05	1.22E-04	5.20E-05	1.92E-04	1.35E-04
⁶² Ni	5.51E-05	4.85E-05	4.03E-05	8.84E-05	2.47E-05	1.31E-04	5.59E-05	2.04E-04	1.44E-04
⁶⁴ Ni	4.92E-13	3.38E-12	4.38E-12	4.65E-12	2.08E-12	1.23E-11	1.23E-11	7.15E-12	1.94E-12
⁶³ Cu	2.26E-05	2.06E-05	1.70E-05	3.67E-05	1.02E-05	5.59E-05	2.38E-05	8.75E-05	6.15E-05
⁶⁵ Cu	8.36E-07	8.25E-07	7.88E-07	2.37E-06	6.61E-07	4.23E-06	1.80E-06	5.59E-06	3.93E-06
⁶⁴ Zn	5.76E-04	5.24E-04	4.72E-04	1.21E-03	3.39E-04	1.86E-03	7.93E-04	2.58E-03	1.81E-03
⁶⁶ Zn	7.29E-06	6.25E-06	5.68E-06	1.66E-05	4.62E-06	2.83E-05	1.21E-05	3.56E-05	2.51E-05
⁶⁷ Zn	7.52E-07	6.36E-07	5.66E-07	1.73E-06	4.83E-07	2.94E-06	1.25E-06	2.81E-06	1.98E-06
⁶⁸ Zn	7.55E-08	6.89E-08	5.63E-08	1.33E-07	3.72E-08	1.74E-07	7.40E-08	7.00E-07	4.92E-07
⁷⁰ Zn	1.84E-13	1.53E-13	4.52E-12	1.60E-12	1.13E-12	8.04E-12	8.04E-12	4.72E-12	1.28E-12
⁶⁹ Ga	2.63E-08	1.92E-08	1.75E-08	5.19E-08	1.45E-08	8.18E-08	3.49E-08	1.32E-07	9.25E-08
⁷¹ Ga	7.46E-13	1.23E-12	2.84E-11	2.97E-12	1.72E-12	1.72E-11	1.71E-11	9.27E-12	2.63E-12
⁷⁰ Ge	3.10E-08	2.19E-08	1.81E-08	4.93E-08	1.38E-08	7.30E-08	3.11E-08	1.12E-07	7.87E-08
⁷² Ge	4.43E-12	2.23E-12	1.08E-11	6.56E-12	2.34E-12	6.35E-12	5.98E-12	2.48E-11	6.79E-12
⁷³ Ge	1.15E-12	1.52E-12	2.39E-11	6.92E-12	3.62E-12	3.00E-11	2.97E-11	1.47E-11	4.18E-12
⁷⁴ Ge	1.27E-12	7.00E-13	5.45E-12	2.57E-12	1.84E-12	1.54E-11	1.54E-11	3.97E-12	1.11E-12

TABLE 19

YIELDS OF UNSTABLE ISOTOPES FOR THE MODELS WITH THE Y_{e} AND “LOW-DENSITY” MODIFICATIONS.

Species Mass [M_{\odot}] E_{51}	Yields [M_{\odot}]								
	20 10	25 5	25 10	30A 20	30B 20	40A 30	40B 30	50A 40	50B 40
²² Na	4.74E-05	1.09E-05	6.81E-06	3.00E-05	1.54E-05	4.11E-06	3.33E-06	1.82E-04	1.06E-04
²⁶ Al	8.17E-07	9.13E-07	1.04E-06	2.57E-06	9.78E-07	4.26E-06	1.22E-06	7.45E-06	3.74E-06
⁴¹ Ca	3.40E-06	1.06E-05	3.69E-06	7.94E-06	6.26E-07	1.30E-05	1.37E-06	1.62E-05	4.52E-06
⁴⁴ Ti	2.05E-04	1.68E-04	1.51E-04	4.93E-04	1.37E-04	8.70E-04	3.69E-04	1.26E-03	8.82E-04
⁶⁰ Fe	2.45E-13	2.25E-13	9.60E-13	5.11E-13	2.34E-13	2.74E-12	2.74E-12	1.69E-12	4.60E-13
⁵⁶ Ni	8.41E-02	1.12E-01	1.01E-01	1.62E-01	4.51E-02	2.81E-01	1.20E-01	3.71E-01	2.61E-01
⁵⁷ Ni	1.27E-03	1.46E-03	1.38E-03	2.66E-03	7.43E-04	4.27E-03	1.81E-03	6.22E-03	4.37E-03

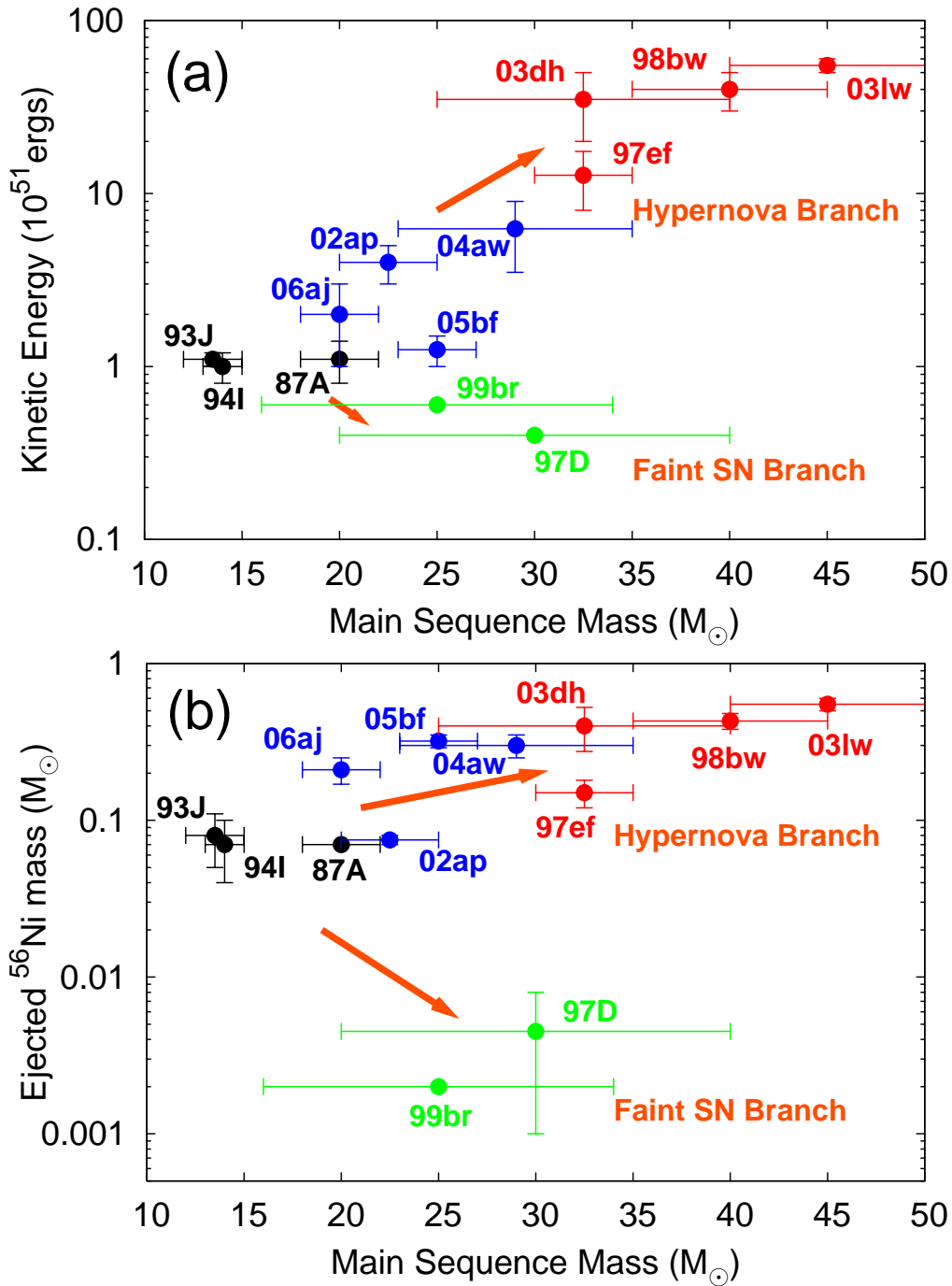


Fig. 1.— (a) The explosion energy and (b) the ejected ^{56}Ni mass as a function of the main sequence mass of the progenitor for core-collapse SNe (SN 1987A, Shigeyama & Nomoto 1990, Blinnikov et al. 2000; SN 1993J, Nomoto et al. 1993, Shigeyama et al. 1994; SN 1994I, Nomoto et al. 1994, Iwamoto et al. 1994, Sauer et al. 2006; SN 1997D, Turatto et al. 1998, Zampieri et al. 2003; SN 1997ef, Iwamoto et al. 2000, Mazzali et al. 2000; SN 1998bw, Iwamoto et al. 1998, Nakamura et al. 2001a; SN 1999br, Zampieri et al. 2003; SN 2002ap, Mazzali et al. 2002, Tomita et al. 2006; SN 2003dh, Mazzali et al. 2003, Deng et al. 2005; SN 2003lw, Mazzali et al. 2006a; SN 2004aw, Taubenberger et al. 2006; SN 2005bf, Tominaga et al. 2005; SN 2006aj, Mazzali et al. 2006b).

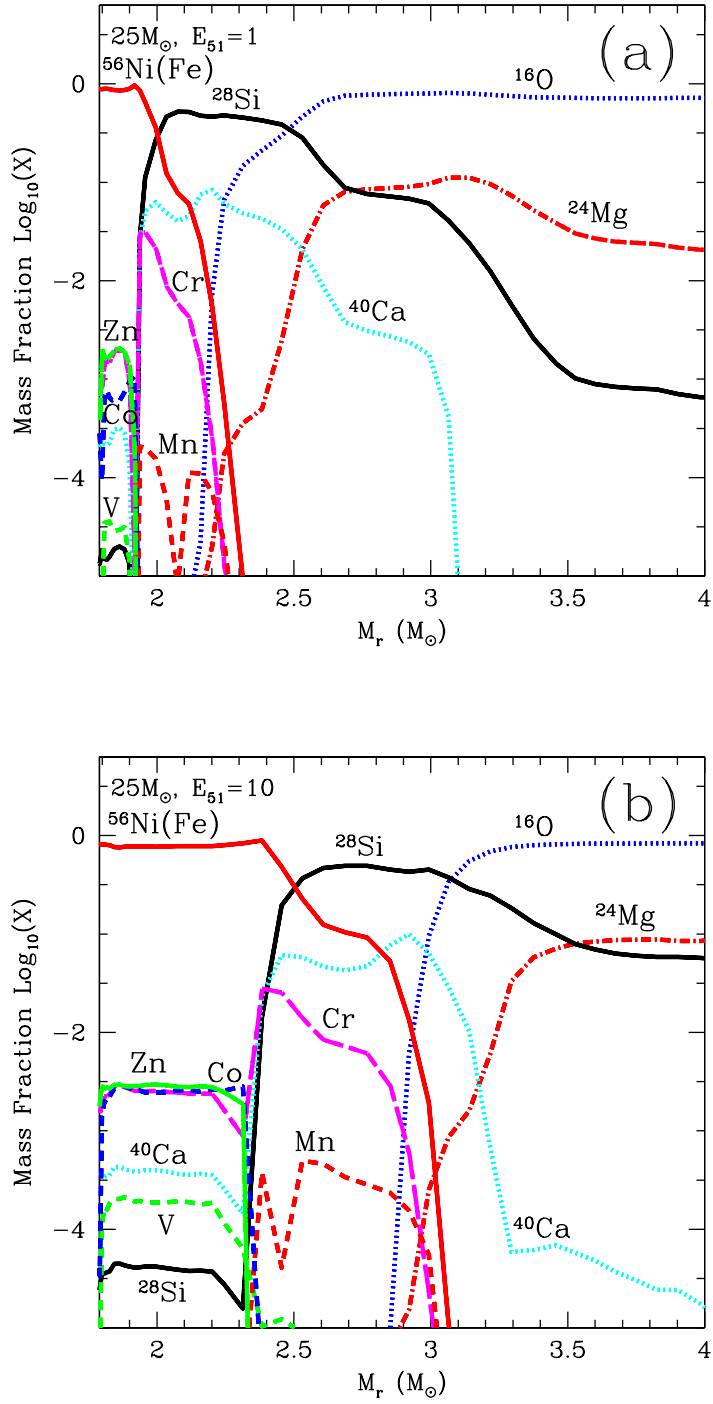


Fig. 2.— Abundance distribution against the enclosed mass M_r after the explosion of Pop III $25 M_{\odot}$ stars with (a) $E_{51} = 1$ and (b) $E_{51} = 10$.

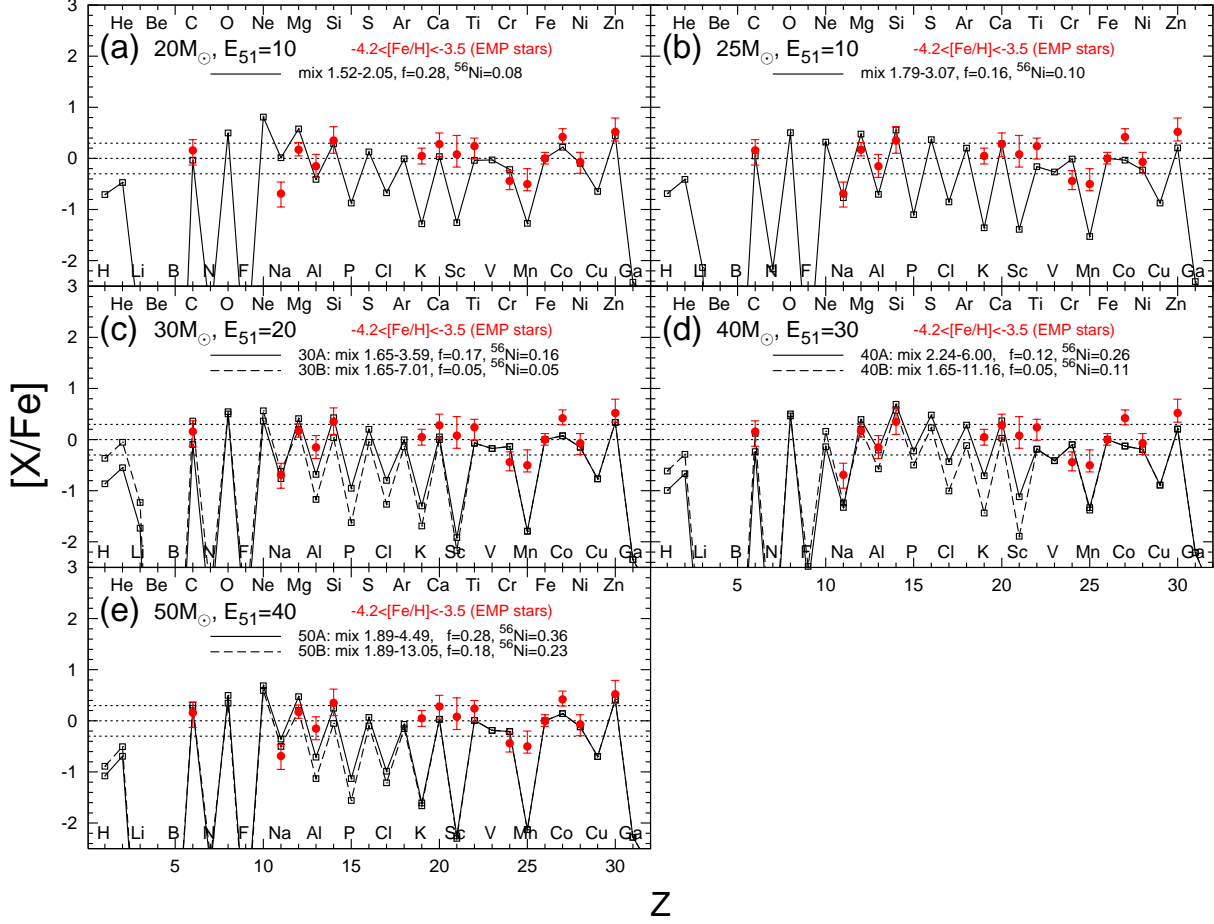


Fig. 3.— The comparison between the abundance pattern of the EMP stars given by CA04 (*filled circles with error bars*) and the theoretical individual HN yields (case A: *solid line*, case B: *dashed line*) with the mixing-fallback model. The parameters are shown in the figures and in Table 1. Figures show the comparisons with (a) $M_{\text{MS}} = 20M_{\odot}$, $E_{51} = 10$, (b) $M_{\text{MS}} = 25M_{\odot}$, $E_{51} = 10$, (c) $M_{\text{MS}} = 30M_{\odot}$, $E_{51} = 20$, (d) $M_{\text{MS}} = 40M_{\odot}$, $E_{51} = 30$, and (e) $M_{\text{MS}} = 50M_{\odot}$, $E_{51} = 40$.

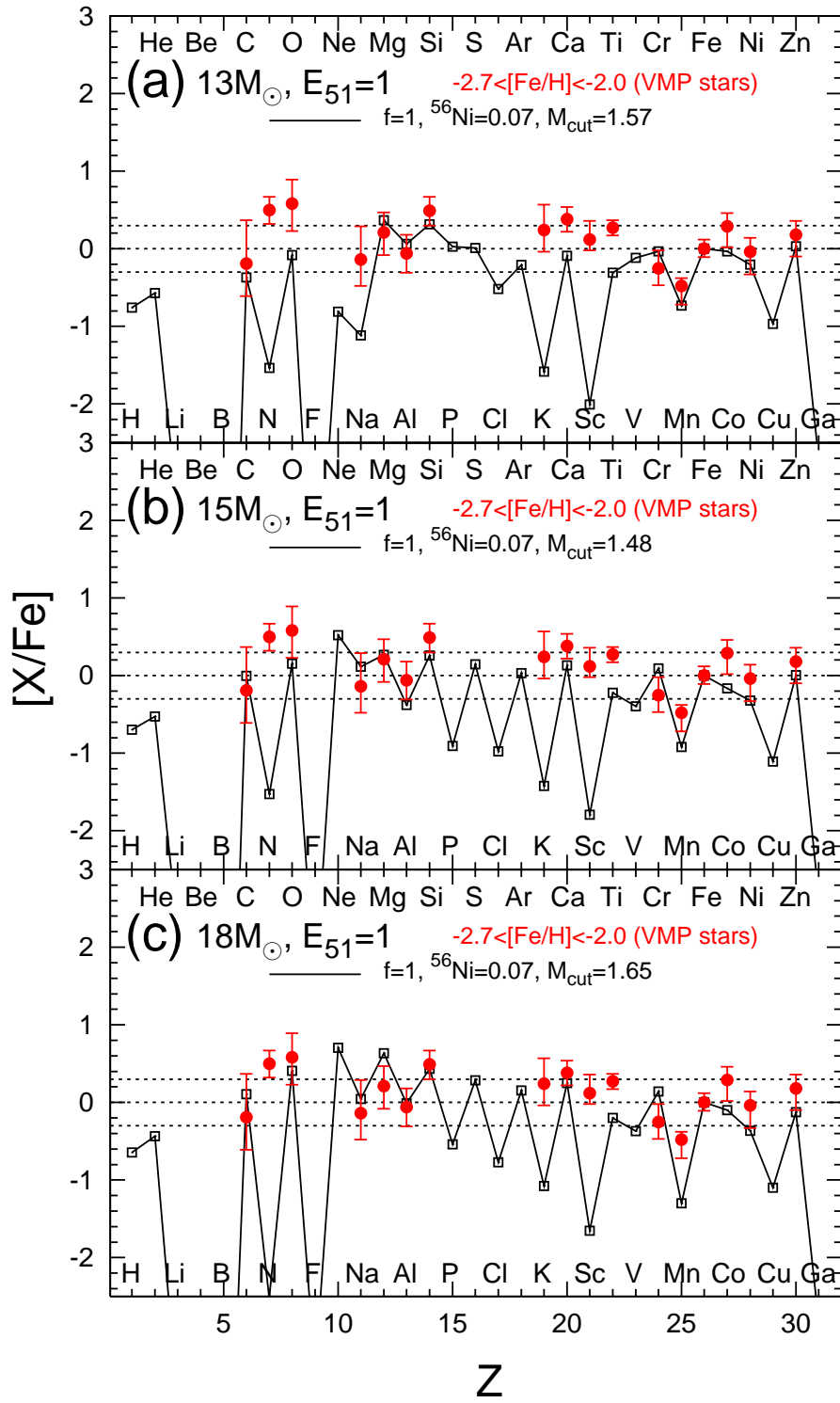


Fig. 4.— The comparison between the abundance pattern of the VMP stars given by CA04 (*filled circles with error bars*) and the theoretical individual normal SN yields (*solid line*). Figures show the comparisons with (a) $M_{\text{MS}} = 13M_{\odot}$, $E_{51} = 1$, (b) $M_{\text{MS}} = 15M_{\odot}$, $E_{51} = 1$, and (c) $M_{\text{MS}} = 18M_{\odot}$, $E_{51} = 1$.

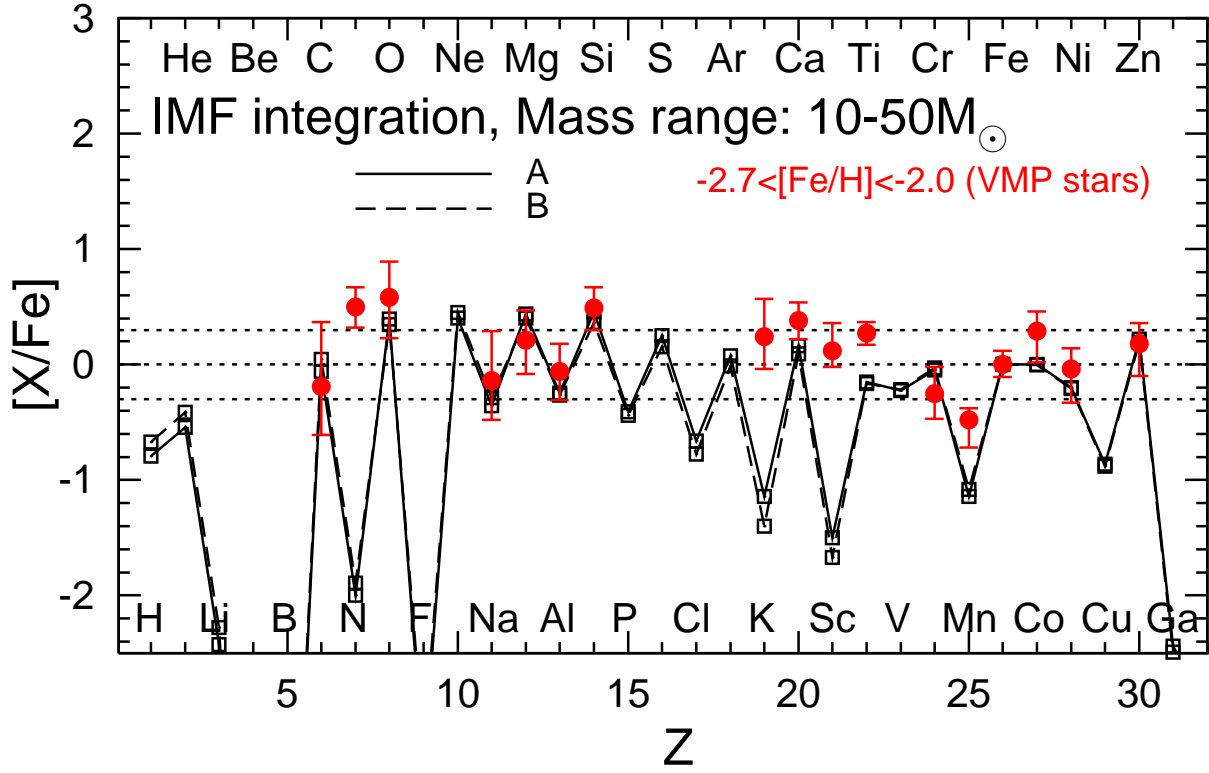


Fig. 5.— Same as Figure 4, but for the IMF-integrated yield of Pop III SNe from $10M_{\odot}$ to $50M_{\odot}$. The mixing-fallback model is applied for HN models, not for normal SN models. In case A (*solid line*), all HN models are determined their mixing-fallback parameters so that $[O/Fe] = 0.5$, but in case B (*dashed line*), massive HN models larger than $M_{\text{MS}} = 30M_{\odot}$ has mixing-fallback parameters so that $[Mg/Fe] = 0.2$.

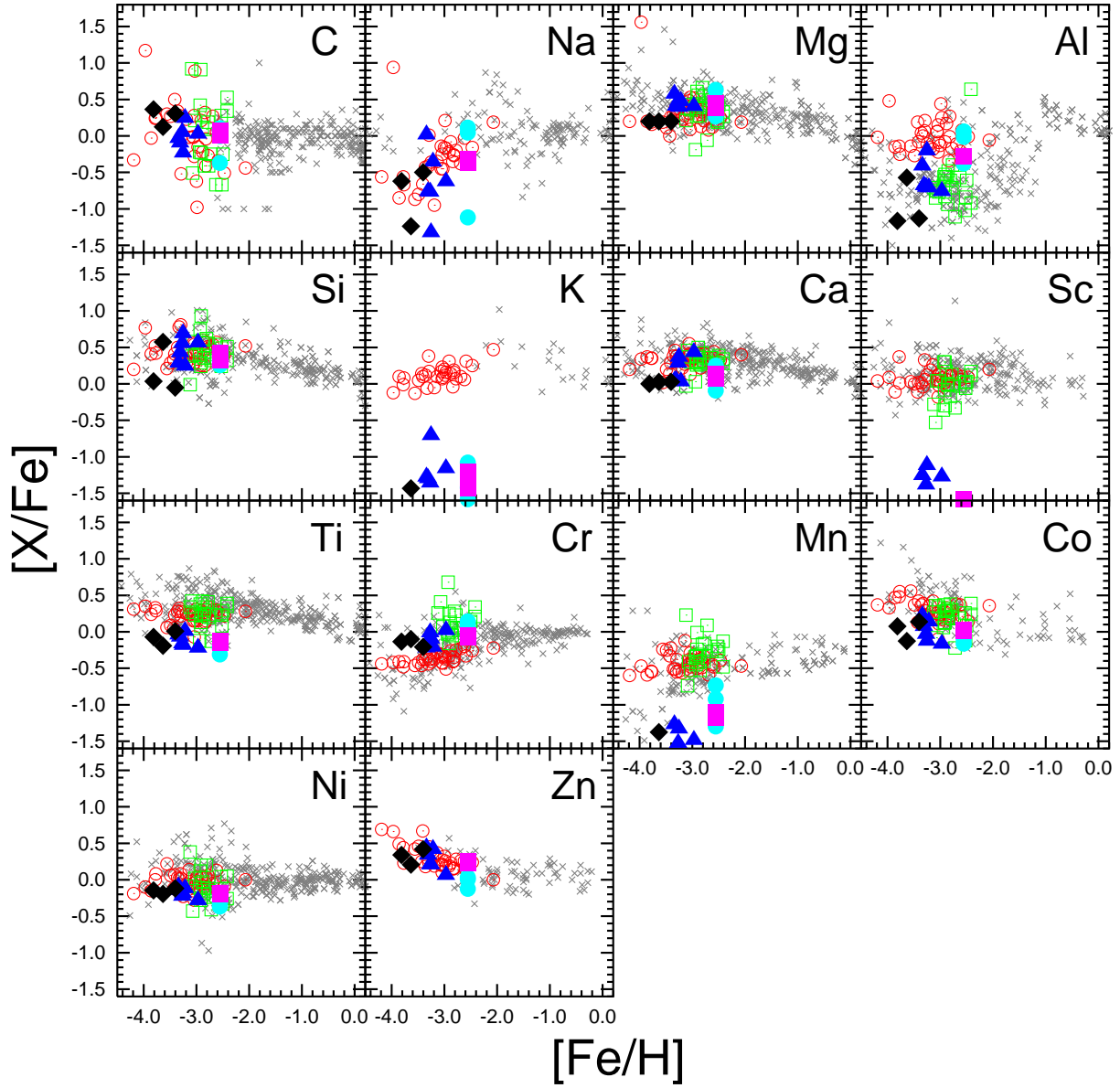


Fig. 6.— The comparison between the $[X/Fe]$ trends of observed stars [the previous studies (e.g., Gratton & Sneden 1991; Sneden et al. 1991; Edvardsson et al. 1993; McWilliam et al. 1995a,b; Ryan et al. 1996; McWilliam 1997; Carretta et al. 2000; Primas et al. 2000; Gratton et al. 2003; Bensby et al. 2003); *cross*, CA04; *open circle*, HO04; *open square*] and those of individual stars models (normal SNe: *filled circle*; HNe with case A: *filled triangle*, HNe with case B: *filled rhombus*) and IMF integration (*filled square*). The parameters are shown in Table 1.

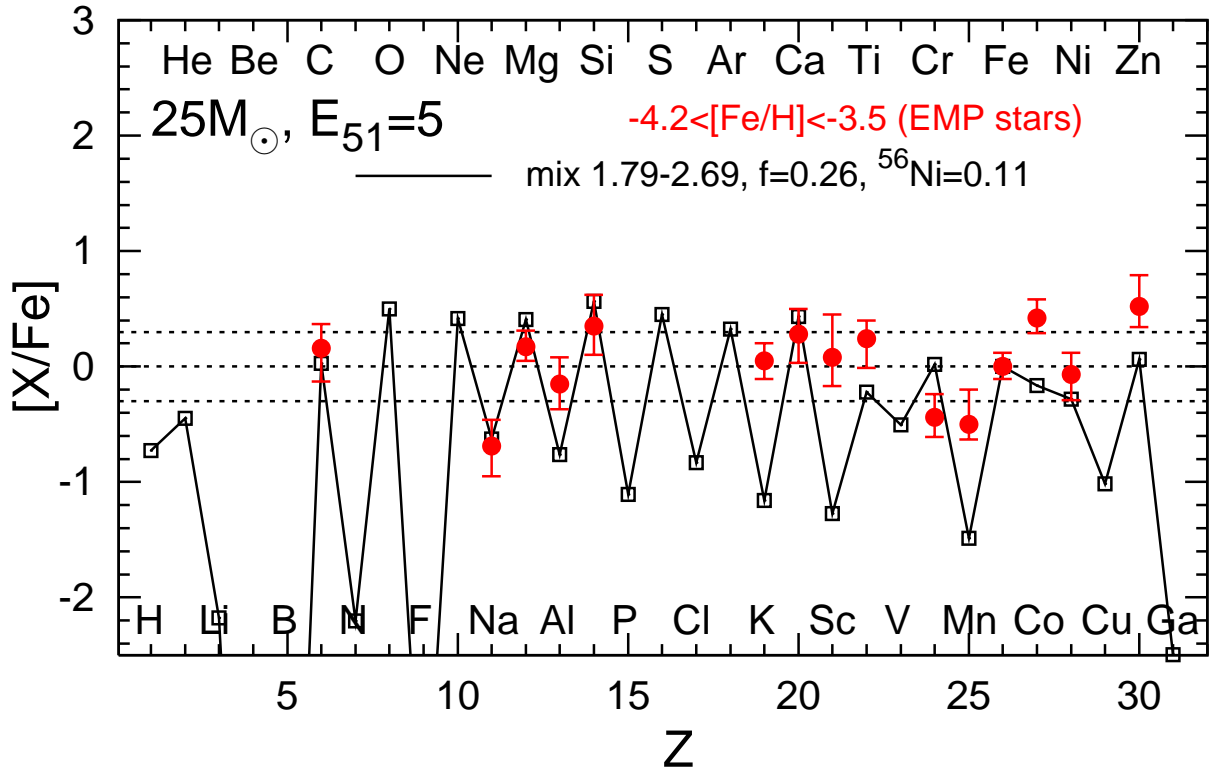


Fig. 7.— Same as Fig. 3, but for $M_{\text{MS}} = 25M_{\odot}$, $E_{51} = 5$.

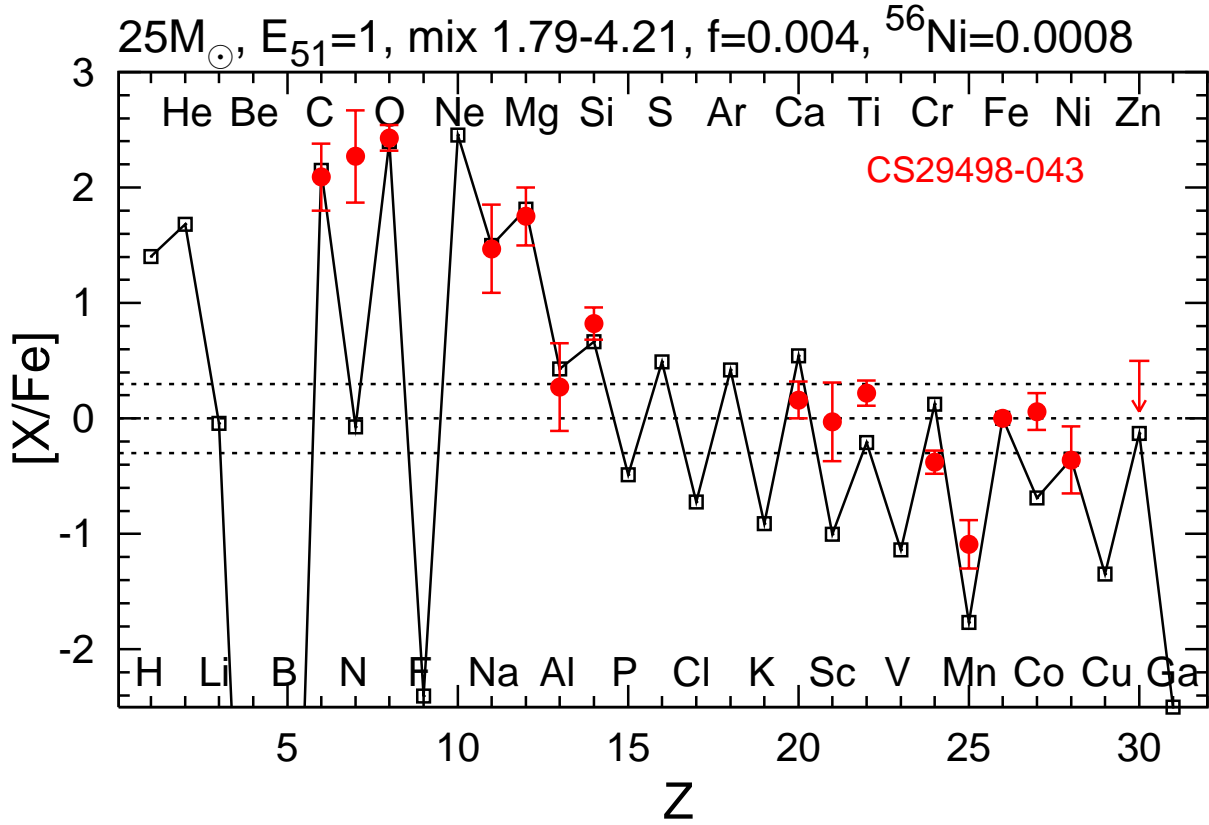
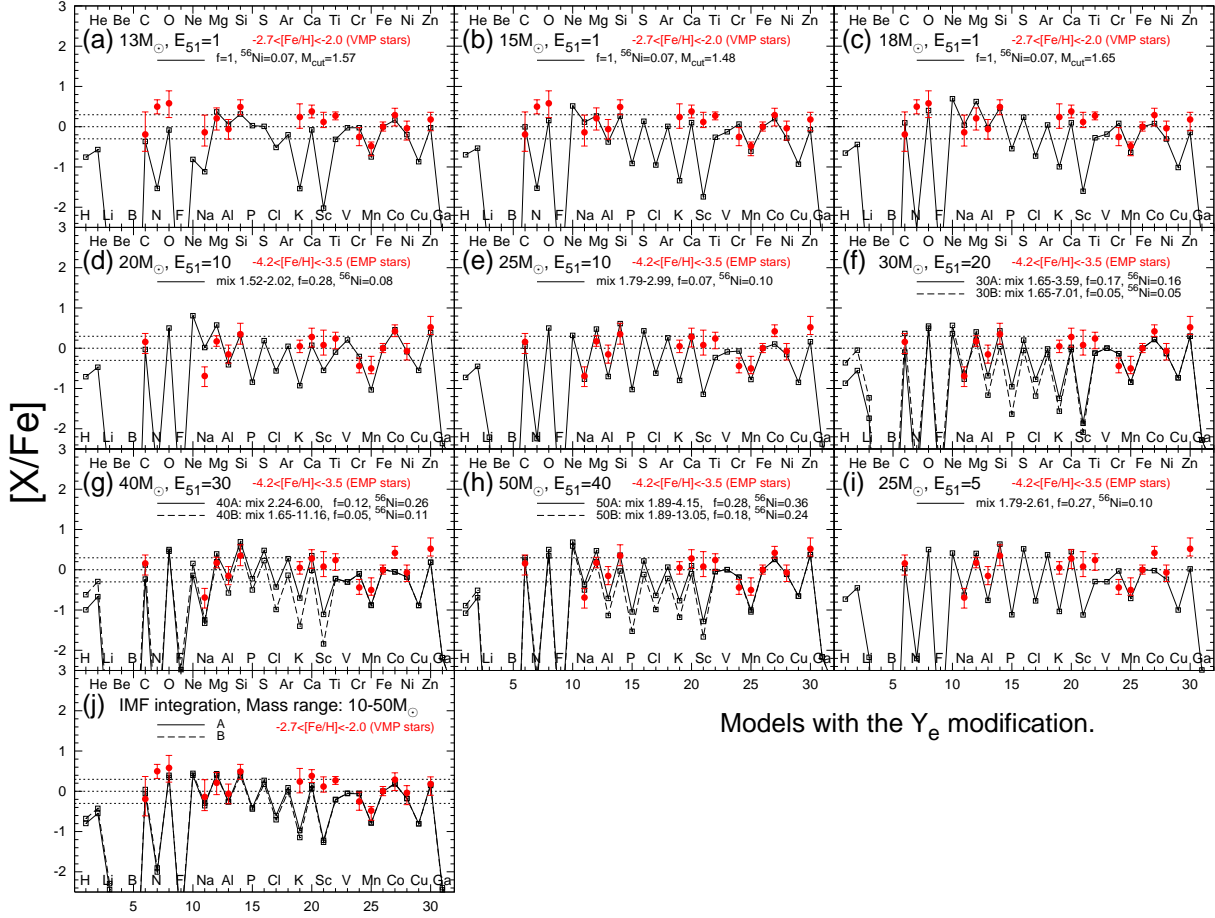


Fig. 8.— The comparison between the abundance pattern of the C-rich EMP star (CS 29498-043: Aoki et al. 2004, *filled circles with error bars*) and the theoretical faint SN yields (25F: *solid line*). The mixing-fallback parameters are determined so as to reproduce the abundance pattern of CS 29498-043.



Z

Fig. 9.— Same as Fig. 3, but models are applied the Y_e modification. Figures (a)-(c) show the comparisons between the abundance pattern of the VMP stars (*filled circles with error bars*) and the normal SN models with the Y_e correction (*solid line*), (a) $M_{\text{MS}} = 13M_{\odot}$, $E_{51} = 1$, (b) $M_{\text{MS}} = 15M_{\odot}$, $E_{51} = 1$, and (c) $M_{\text{MS}} = 18M_{\odot}$, $E_{51} = 1$. Figures (d)-(i) show the comparisons between the abundance pattern of the EMP stars (*filled circles with error bars*) and the HN models with the Y_e modification (case A: *solid line*, case B: *dashed line*), (d) $M_{\text{MS}} = 20M_{\odot}$, $E_{51} = 10$, (e) $M_{\text{MS}} = 25M_{\odot}$, $E_{51} = 10$, (f) $M_{\text{MS}} = 30M_{\odot}$, $E_{51} = 20$, (g) $M_{\text{MS}} = 40M_{\odot}$, $E_{51} = 30$, (h) $M_{\text{MS}} = 50M_{\odot}$, $E_{51} = 40$, and (i) $M_{\text{MS}} = 25M_{\odot}$, $E_{51} = 5$. Figures (j) shows the comparisons between the abundance pattern of the VMP stars (*filled circles with error bars*) and the IMF-integrated yield of Pop III SNe from $10M_{\odot}$ to $50M_{\odot}$ with (a)-(h) models.

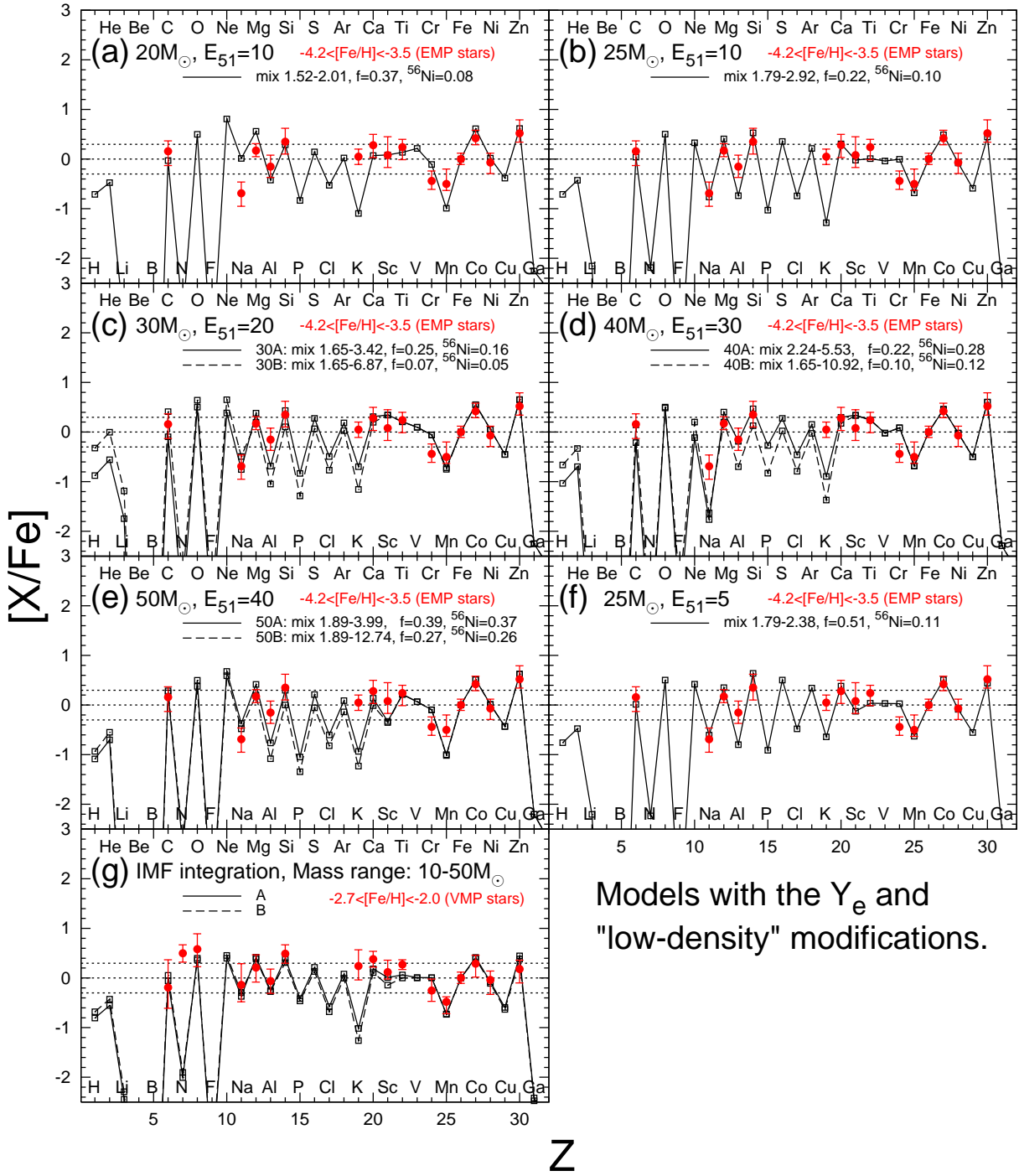


Fig. 10.— Same as Fig. 3, but models are applied the Y_e and “low-density” modifications. Figures (a)-(f) show the comparisons between the abundance pattern of the EMP stars (*filled circles with error bars*) and the HN models with the Y_e and “low-density” modifications (case A: *solid line*, case B: *dashed line*), (a) $M_{\text{MS}} = 20M_{\odot}$, $E_{51} = 10$, (b) $M_{\text{MS}} = 25M_{\odot}$, $E_{51} = 10$, (c) $M_{\text{MS}} = 30M_{\odot}$, $E_{51} = 20$, (d) $M_{\text{MS}} = 40M_{\odot}$, $E_{51} = 30$, (e) $M_{\text{MS}} = 50M_{\odot}$, $E_{51} = 40$, and (f) $M_{\text{MS}} = 25M_{\odot}$, $E_{51} = 5$. Figure (g) shows the comparisons between the abundance pattern of the VMP stars (*filled circles with error bars*) and the IMF-integrated yield of Pop III SNe from $10M_{\odot}$ to $50M_{\odot}$ with normal SN (Figs. 9abc) and (a)-(e) HN models.

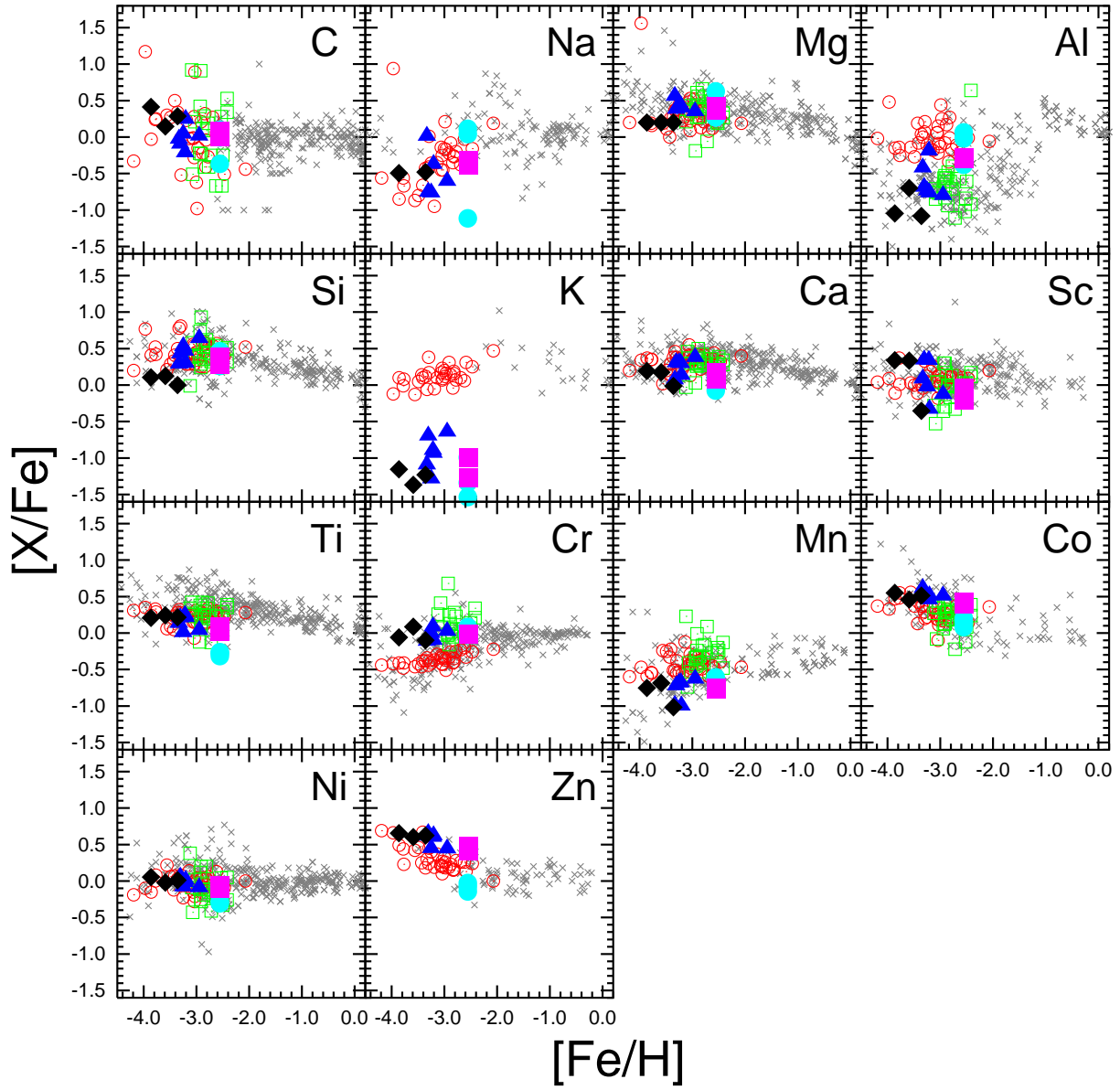


Fig. 11.— Same as Fig. 6, but for the comparisons with models applied the Y_e and “low-density” modifications.

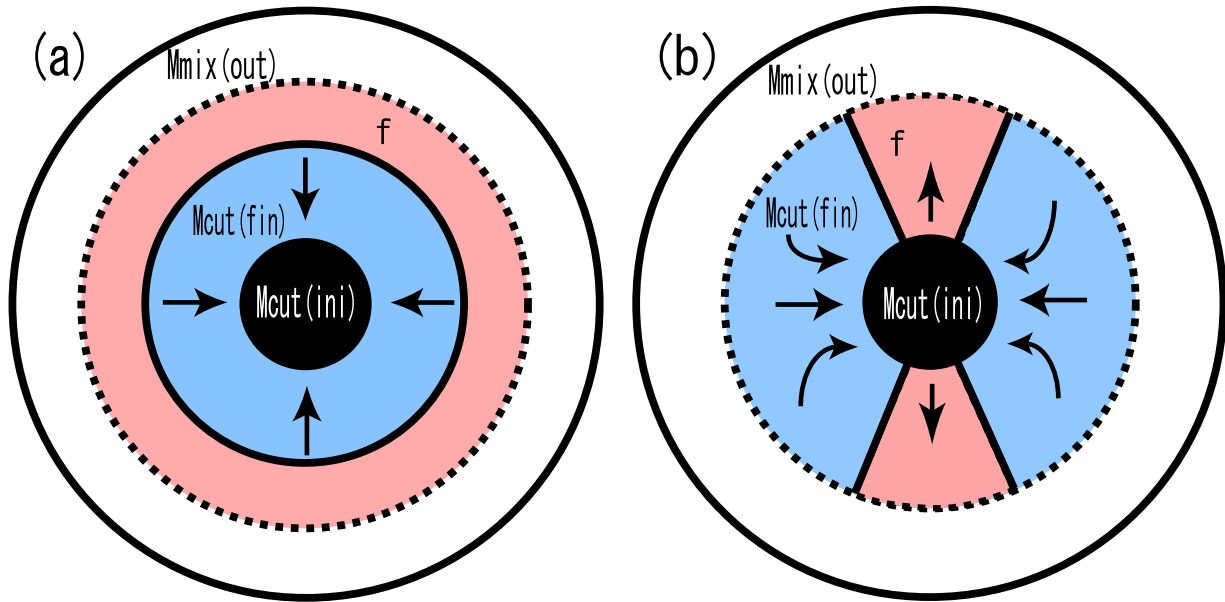


Fig. 12.— The illustration of the mixing-fallback model. The central black region is the initial mass cut, that is, inside the inner boundary of the mixing region, $M_{\text{cut}}(\text{ini})$. The mixing region is enclosed with the dotted line. A fraction f of the materials in the mixing region ejected to the interstellar space. The rest materials, locating in the blue region, fallback into the central remnant. (a) 1-dimensional picture. The materials mixed up to a given radius, and a part of the materials are ejected. (b) 2-dimensional picture. While the all materials in the outer region above $M_{\text{mix}}(\text{out})$, are ejected, the materials in the mixing region may be ejected only along the jet-axis. In the jet-like explosion, the ejection factor f depends on the jet-parameters (e.g., an opening angle and an energy deposition rate).

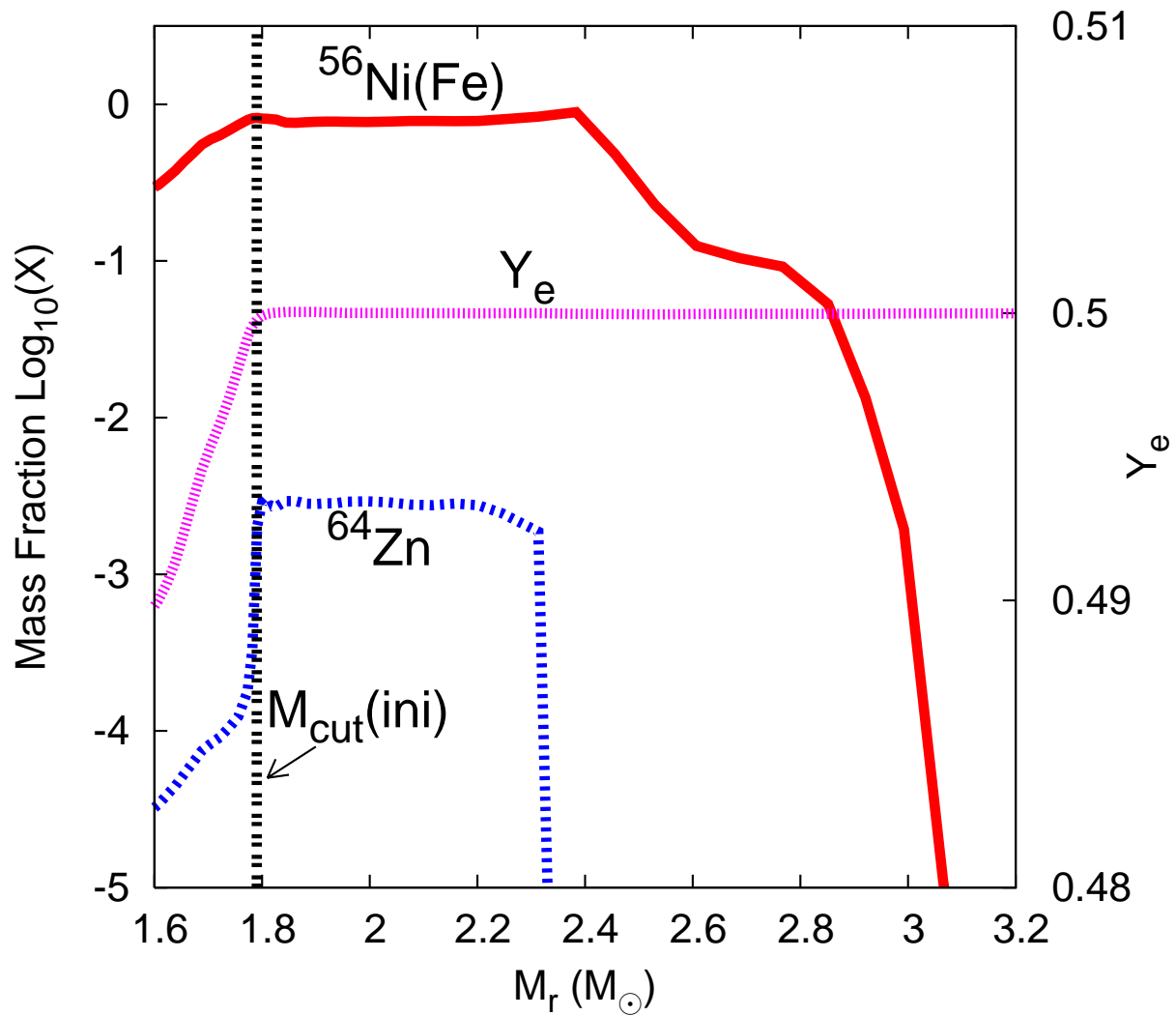


Fig. 13.— The abundance distribution (^{56}Ni ; *solid line*, ^{64}Zn ; *dashed line*) of the $25 M_\odot$, $E_{51} = 10$ model around complete and incomplete Si burning region. In the inner part ($M_r < 1.8 M_\odot$) the Zn/Fe ratio is smaller because of lower Y_e (*dotted line*). $M_{\text{cut}}(\text{ini})$ (*dotted and dashed line*) is where $X(^{64}\text{Zn})$ is smaller, i.e., $Y_e \lesssim 0.5$, as UN05.

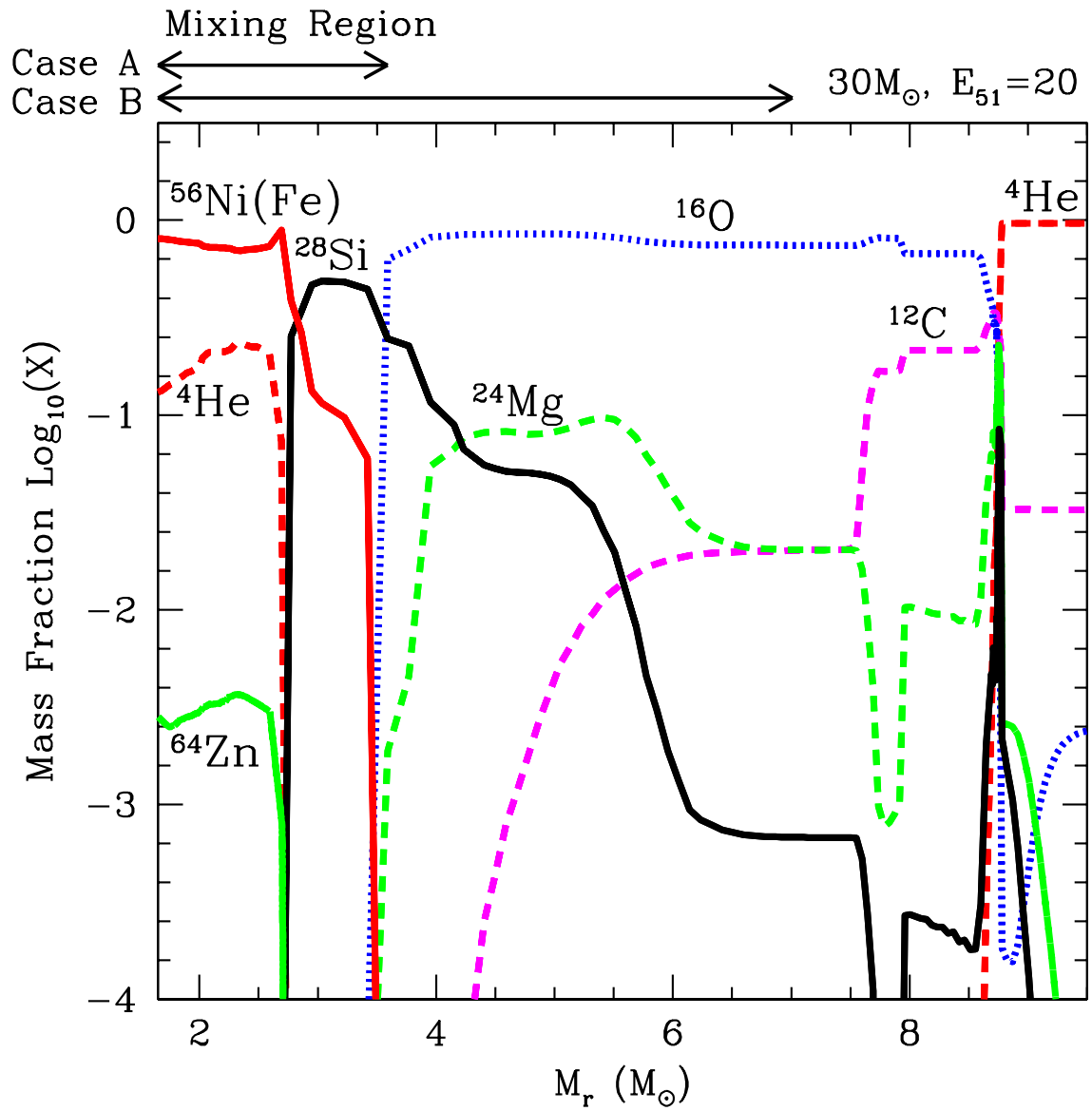


Fig. 14.— The abundance distribution of the $30 M_\odot$, $E_{51} = 20$ model. The mixing regions of cases A and B are illustrated with arrows.